Start-up and Shut-down Water Chemistries in Pressurized Water Reactors

Authors	Iva Betova, Martin Bojinov, Timo Saario
Confidentiality	Public

Report's title	
Start-up and Shut-down Water Chemistries in Pressurized Water Reactors	
Customer, contact person, address	Order reference
SAFIR 2014 –research program	
Project name	Project number/Short name
Water chemistry and plant operating reliability	73786 / WAPA
Author(s)	Pages
Iva Betova, Martin Bojinov, Timo Saario	81/
Keywords	Report identification code
PWR, startup, shutdown, nickel-based alloy, CRUD, modeling	VTT-R-00699-12

Summary

Start-up and shutdown of nuclear power stations are the most crucial operations in which it is important to apply specific chemistry conditions. The associated transients may have an impact on the radiological condition related to maintenance for the following outage, the integrity of materials, the shutdown process duration, the radiochemistry during operation of the next cycle, the chemistry for layup condition during the next outage, etc. CRUD deposition on, and re-dissolution from the fuel cladding surface is an important problem in the primary circuit of light water reactors since it has a large impact on the activity build-up. Effects of fuel cladding material, water chemistry, hydrodynamic conditions and thermal gradients have to be taken into account in order to achieve CRUD control. In the present survey, a detailed description of the shutdown and start-up water chemistry transients and the associated interaction processes between coolant and oxide layers on construction materials is given. Particular attention is paid to the transformation of the corrosion layers and the rate of release of ions to the coolant. In addition, the relationships between CRUD composition, structure and morphology and the axial power anomalies (AOA/CIPS) are described. The main factors influencing AOA – sub-cooled boiling, CRUD formation and boron hideout – are outlined. A comprehensive review of the existing activity accumulation/transport and CRUD deposition/AOA models and associated codes is given, emphasizing the main assumptions, restrictions and predictive abilities. A deterministic model for the growth, restructuring of oxide layers and corrosion release (ANTIOXI) developed by the authors in recent years is presented as a further development of the modeling strategy concerning activity transport. Its application on steam generator construction materials (alloys 600, 690 and 800), as well as its predictive abilities with respect to activity build-up in the primary circuit are briefly outlined. Further steps towards a unified activity transport-CRUD deposition model are proposed.

Confidentiality	Public

Espoo, 25.1.2012
Signatures

Timo Saario	Petri Kinnunen	Pentti Kauppinen
Principal Scientist	Principal Scientist	Technology Manager

VTT's contact address
P.O.Box 1000, FI-02044 VTT, Finland

Distribution (customer and VTT)
Customer 1, VTT 1

Report's title	
Start-up and Shut-down Water Chemistries in Pressurized Water Reactors	
Customer, contact person, address	Order reference
SAFIR 2014 –research program	
Project name	Project number/Short name
Water chemistry and plant operating reliability	73786 / WAPA
Author(s)	Pages
Iva Betova, Martin Bojinov, Timo Saario	81/
Keywords	Report identification code
PWR, startup, shutdown, nickel-based alloy, CRUD, modeling	VTT-R-00699-12

Summary

Start-up and shutdown of nuclear power stations are the most crucial operations in which it is important to apply specific chemistry conditions. The associated transients may have an impact on the radiological condition related to maintenance for the following outage, the integrity of materials, the shutdown process duration, the radiochemistry during operation of the next cycle, the chemistry for layup condition during the next outage, etc. CRUD deposition on, and re-dissolution from the fuel cladding surface is an important problem in the primary circuit of light water reactors since it has a large impact on the activity build-up. Effects of fuel cladding material, water chemistry, hydrodynamic conditions and thermal gradients have to be taken into account in order to achieve CRUD control. In the present survey, a detailed description of the shutdown and start-up water chemistry transients and the associated interaction processes between coolant and oxide layers on construction materials is given. Particular attention is paid to the transformation of the corrosion layers and the rate of release of ions to the coolant. In addition, the relationships between CRUD composition, structure and morphology and the axial power anomalies (AOA/CIPS) are described. The main factors influencing AOA – sub-cooled boiling, CRUD formation and boron hideout – are outlined. A comprehensive review of the existing activity accumulation/transport and CRUD deposition/AOA models and associated codes is given, emphasizing the main assumptions, restrictions and predictive abilities. A deterministic model for the growth, restructuring of oxide layers and corrosion release (ANTIOXI) developed by the authors in recent years is presented as a further development of the modeling strategy concerning activity transport. Its application on steam generator construction materials (alloys 600, 690 and 800), as well as its predictive abilities with respect to activity build-up in the primary circuit are briefly outlined. Further steps towards a unified activity transport-CRUD deposition model are proposed.

Confidentiality	Public

Espoo, 25.1.2012
Signatures

Timo Saario	Petri Kinnunen	Pentti Kauppinen
Principal Scientist	Principal Scientist	Technology Manager

VTT's contact address

P.O.Box 1000, FI-02044 VTT, Finland

Distribution (customer and VTT)

Customer 1, VTT 1

Preface

This literature survey was compiled as part of the project "Water chemistry and plant operating reliability" (WAPA) within the SAFIR 2014 –research programme.

Espoo, 25.1.2012

Authors

Contents

1 Introduction

The chemistry used during normal operation of nuclear power plants is usually clearly understood, defined and controlled. This looks differently under transient conditions. Start-up and shutdown of nuclear power stations are the most crucial situations of such transients, in which it is important to apply specific chemistry conditions. This may have an impact on the radiological condition related to maintenance for the following outage, the integrity of materials, the shutdown process duration, the quantity of liquid and solid wastes related to the purification steps, the radiochemistry during operation of the next cycle, the chemistry for layup condition during the next outage and potentially associated chemical liquid effluents. Concerning the chemistry during start-up there may be a compromise between, time and liquid effluents saving, on one hand, and minimization of impurities to avoid any risk of corrosion, on the other.

CRUD[1] deposition on, and re-dissolution from the fuel cladding surface is an important problem in the primary circuit of light water reactors since it has a large impact on the activity build-up. Effects of fuel cladding material, water chemistry, hydrodynamic conditions and thermal gradients have to be taken into account in order to achieve CRUD control. In that respect, it is paramount to obtain a comprehensive picture of the state-of-the-art in understanding of CRUD deposition and re-dissolution.

2 Goal

The present report is a focused literature study emphasizing the effects of transients on CRUD release and activity build-up. The survey is aimed at supporting the efforts of controlling the activity build-up on primary circuits and impurity bursts/magnetite deposition on the secondary side. A comparison of water chemistry guidelines especially concerning shutdown and start-up practices is also included.

3 Description of the target

At the beginning of the 1990s began a trend to extended cycles and shorter outages for increasing plant availability. In this area, it is of high importance to minimize the outage duration by well-managed shutdown and start-up procedures. Shutdown chemistry issues can often be on the critical path depending on their relative success at reaching their targets due to Corrosion Product (CP) and activity release and removal. A lot of procedures during shutdown and start-up are influencing these goals as well as other like ensuring safety and meet normal chemical conditions within a reasonable timeframe. During a shutdown, significant quantities of corrosion as well as Fission Products (FP) are released and may cause higher general or local radiation areas and refueling water turbidity problems. These additional challenges require high attention of the personnel and presuppose a good

---

[1] According to the U.S. Nuclear Regulatory Commission (NRC) glossary definition, Chalk River Unidentified Deposit (CRUD) is "a colloquial term for corrosion and wear products (rust particles, etc.) that become activated when exposed to radiation".

planning and a grant of time, often even on the critical path, in order to achieve optimal conditions for the shutdown chemistry.

In the primary circuit, there is a need to achieve the shortest possible shutdown duration with limited activity peaks and adequate hydrogen elimination procedures. Another challenge described in the report is to operate the unit without fuel degradation and with limited risk of CRUD Induced Power Shift (CIPS), also named Axial Offset Anomaly (AOA).

The most important areas of improvement with direct cost savings concern the shutdown duration, which is shorter and shorter. The new selection of materials more resistant to corrosion allows a decrease of maintenance activities for non-destructive examinations. In addition, a large effort is being spent on trying to also reduce the shutdown duration by improving chemistry procedures for hydrogen elimination and purification of radio nuclides. Some utilities are using materials with limited nickel content and almost free of cobalt, at least without cobalt base components. This is the first step to decrease quantity of the most radioactive CPs (Co-58 and Co-60). But there are also other ways associated with chemistry practices for reducing the shutdown duration, focusing on efficient and quick hydrogen elimination before opening the vessel for refueling and optimum chemistry conditions during scheduled or forced outages. Their way of actions are directed toward limitation of radioactive compound releases and quicker steps between different gas blanketing as well as limiting the number of these transition phases. In addition, such improvements are also favorable for the materials behavior against thermal stress corrosion.

There are several ways of improving the operation of Nuclear Power Plants (NPP) on the chemistry point of view. On the primary side, after having almost correctly defined the best chemistry for occupational exposure mitigation associated with CPs coming from power operation, the challenge concerns the way of avoiding fuel failure and optimizing the shutdown procedures for saving time and minimizing waste in addition to occupational dose rates during maintenance. The objective of this report and its presentation is to provide a good understanding of the special problems and appropriate good practices for primary side control during shutdown as well as during start-up of Pressurized Water Reactor (PWRs).

4 Bases of chemistry control during start-up and cool-down

A suitable water chemistry program helps a NPP to ensure the integrity of the Reactor Coolant System (RCS) as well as the fuel cladding materials and a satisfactory core performance. An important target regarding primary water chemistry is low radiation fields. This also demands an important contribution from a well-managed shutdown and start-up chemistry, because the releases of activated CPs have significant consequences on radiation fields. Each plant should introduce a program to optimize and control the release and removal of activated corrosion and FPs. The target should be to minimize the deposition of suspended material that may be mobilized during shutdown and start-up.

The main differences between various designs of PWRs in what concerns the shutdown and start-up chemistry are related to the use of different materials for SG tubes and fuel cladding and different surface areas, as well as the number of loops depending on the electrical output of the plant. Start-up and shutdown procedures are different depending on the supplier of the plant, the plant design, the implemented guidelines and last but not least the operator of the plant. However, there are some basic principles that are valid for nearly all the PWRs [1-13]. These principles will be briefly outlined in the present chapter.

4.1 Corrosion product behavior in the RCS

Metallic materials exposed to water in the RCS owe their corrosion resistance to a protective layer of chemically stable metal oxide that is formed in the operating environment. As low as the general corrosion rate of stainless steels and nickel-based alloys that constitute the major part of the primary circuit may be, some oxidation products escape to the water or are dissolved in the water, and are carried through the system.

The process by which released oxidation products migrate from place to place within the RCS involves a complex set of interacting chemical and physical mechanisms that continues to be studied. Nevertheless, the overall outline and the consequences of this process are clear: Some of the released material is deposited on fuel surfaces where it resides long enough to become activated; then, some of this radioactive material migrates to out-of-core locations. Where on the core the material will deposit depends on clad temperature distributions, which drive the precipitation of nickel/iron-based soluble corrosion products from the coolant, and on the degree to which core thermal hydraulics promotes subcooled nucleate boiling [2].

The chemical composition of corrosion product deposits on reactor fuel and on surfaces elsewhere in the RCS is variable, but in a conventional fuel cycle, the major components are non-stoichiometric nickel ferrites with a general formula $Ni_xFe_{3-x}O_4$ on stainless steels, with additional NiO/Ni on nickel-based alloys. If account is taken of the low, but operationally important, cobalt content, the general ferrite formula is $Ni_xCo_yFe_{3-x-y}O_4$, where $x + y = 1$ and $y << x$. Recent studies also indicate that nickel oxide is present at higher than expected levels in the CRUD of high duty cores.

The chemical composition of the corrosion film on steam generator tubing is enriched in Cr, Fe, and Co compared to the base metal and depleted in Ni. Most of the tube oxides originate from the corrosion of the base alloy (0.5-2 mg dm^{-2} month^{-1}) rather than being a result of deposition from the coolant. The representative composition of CRUD relative to oxidized steam generator tubing from PWRs within a conventional fuel cycle is given in Table 1.

Table 1 Representative composition of CRUD on different surfaces [1].

ITEM	STEAM GENERATOR TUBE CRUD	CORE CRUD*
Chemical Composition, %		
Fe	14-22	39-47
Ni	20-30	19-24
Cr	20-38	0.8-2.5
Co	0.24	0.11
Radiochemical Composition, Ci/g parent		
Co-58	0.004-0.05	0.8-1.3
Co-60	2.5-6.0	25-100
μCi/cm^2		
Co-58	2-12	100-500
Co-60	1-5	7-18
Crystallography		
$Ni_xFe_{3-x}O_4$	Probably not present	$0.4 \leq x < 0.9$
Mixed Fe, Cr spinel	Present	Not detected
NiO	Not detected	Sometimes present
Ni	Present	Sometimes present
Surface Concentration, mg/dm^2	11-60	10-350
Density, gm/cm^3	4	1.2

Crystallographic analyses of steam generator tube (primary side) CRUD indicate that the major components are nickel-chromium-iron spinel and metallic nickel with an outer layer of nickel ferrite ($NiFe_2O_4$). The spinel structure is relatively insensitive to changes in the chemistry environment at operating conditions. The chemical form of the core CRUD varies from nickel oxide (NiO) to magnetite (Fe_3O_4) to nickel ferrite. Deposits on the fuel sampled after shutdown have been reported to be primarily non-stoichiometric nickel ferrites ($Ni_xFe_{3-x}O_4$ where $0.4 < x < 0.9$). Cobalt and chromium enter the inverse spinel lattice of nickel ferrite to form $Ni_xCo_yCr_zFe_{3-x-y-z}O_4$; the substitution of nickel by cobalt and iron by chromium is so small that the lattice parameter of the nickel ferrite is not affected. Mixed chrome iron spinels are generally not detected. In contrast, chrome rich spinels were identified as the major species on out-of core surfaces during the early studies. The reasons for this difference are the stability of the chromium spinels and the very low solubility (<0.001 ppb) of chrome in the highly reducing PWR environment during normal operation. In contrast, iron exhibits a significant solubility (of the order of 6 ppb), and nickel has a solubility on the order of 0.1 ppb at normal operating chemistries. This difference leads to the preferential release and transport of iron and nickel from stainless steel and steam generator tubing alloys such as Alloy 600 and 690 as a result of corrosion with a corresponding increase in the chrome concentration in the oxides formed on these surfaces. When metallic nickel or nickel oxide are in the CRUD, the nickel-to-iron ratio is typically greater than 0.5.

Stainless steels in the PWR environment develop a Cr-rich oxide layer containing Fe and Co. After the initial exposure the outer layer crystals nucleate from solution and incorporate much of the iron and cobalt that moved through the inner layer from corrosion of the metal. Surface irregularities act as nucleating sites for the

outer layer crystals. The Co-60 activity deposited on stainless steel piping is ca. 15 times larger than that deposited on nickel-based alloy 600. This is due to the fact that the corrosion layers on the latter are much thinner and the outer layer crystals are much more sparsely distributed on the surface and contain relatively little material originating from the base metal. The activity deposited on steam generator tubing fabricated from Alloy 690 is approximately four times less than that deposited on Alloy 600, resulting in approximately 30-50 times less activity on the 690 compared to stainless steel.

The most significant chemistry parameters that control CRUD composition in PWRs are the pH and the oxygen content. The stability of CRUD deposits and corrosion films is dependent on the redox potential. Traces of oxygen in a large excess of hydrogen can cause a considerable shift in the oxidation-reduction equilibrium of nickel or nickel ferrites. The only place in a PWR circuit where oxygen can exist in large excess of hydrogen is in the cold leg downstream of the CVCS charging line return. Oxygen that reaches the metal surface will control the redox conditions, and thus, the corrosion potential. Oxidizing conditions would lead to increased formation and transport of corrosion products, higher radiation fields, reactivity anomalies, CRUD buildup on fuel, and increased corrosion of fuel rods. Only 1-5 cm^3 kg^{-1} (at Standard Temperature and Pressure, STP) of hydrogen is reported to be sufficient to prevent radiolysis reactions leading to significant levels of peroxide in the core outlet during operation and thus the development of sustained oxidizing conditions.

4.2 Chemistry changes during shutdown

During power operation, the chemistry of the reactor coolant is maintained slightly alkaline and reducing. Low concentrations of lithium hydroxide, a strong base, are adequate to maintain alkalinity in the presence of boric acid, since boric acid is a very weak acid at operating temperatures. Reducing conditions are established by dissolved hydrogen concentrations that are kept high enough to suppress dissolved oxygen to very low levels by radiation-induced reactions. The chemistry of the coolant changes dramatically during plant shutdown and cool-down. Several factors are responsible. First, boric acid becomes a much stronger acid as temperature is lowered, although it is still a relatively weak acid even at room temperature. Second, concentrations of boric acid must be increased to compensate for the hot-to-cold nuclear reactivity increase, and even further to provide a negative reactivity margin at cold shutdown. The two factors cause the pH at cold shutdown to drop to between 4 and 5, which is 2-3 pH units more acid than neutral at room temperature. Additionally, after dissolved hydrogen is removed before reactor head removal for refueling, radiolytically-produced oxidizing species such as hydrogen peroxide and oxygen are no longer consumed, yielding cold shutdown chemistry that is acidic and oxidizing. Hydrogen peroxide is often intentionally added to accelerate selected dissolution processes while the system is closed and the letdown purification system is still operating, which contributes significantly to the acid-oxidizing conditions.

A change from alkaline-reducing conditions to acid-oxidizing conditions, combined with the temperature change itself, constitutes a severe chemical shock to corrosion product deposits that have equilibrated with normal operating chemistry. One consequence is the solubilization of radioactive species, primarily Co-58, from in-core deposits. Crud bursts are another consequence of such a shock. Three critical

issues must be considered when shutdown chemistry practices result in concerns regarding activity release:

- A critical inventory of CRUD must be available to cause a problem.
- Improper shutdown techniques can release this CRUD in particulate form, resulting in deposition on plant surfaces and high radiation levels.
- Release of soluble activity under shutdown conditions is not known to result in high radiation levels after the activity is cleaned up, unless precipitation occurs. High reactor coolant activity levels can result in high radiation levels on components such as heat exchangers, but once the activity is cleaned up radiation levels are generally within normal ranges. In fact, no driving force to incorporate soluble activity into corrosion films during shutdown condition during a relatively short period exists.

In addition, shutdown chemistry has been reported to be influenced by recent modifications of plant operation and core design, as follows:

- Longer fuel cycles, reduced outage times, and higher duty cores are expected to result in increased activation of target material deposited on the core (e.g., the specific activity of Co-58 may increase unless the residence time on the core can be reduced).
- Plants with high duty cores with significant boiling have an additional concern: CRUD accumulation with significant boiling is governed by the mass evaporation rate. For this reason, measures directed at limiting CRUD deposition on the core by controlling solubility (i.e., pH control) may not have the desired result. Cores with significant boiling and new steam generators are expected to have an increased CRUD burden.
- Plants with replacement steam generators may have an increased nickel source term because of the increased surface area of the replacement steam generators and limited passivation prior to operation.
- Increasing evidence suggests that the CRUD deposits on cores contain significant nickel oxide (and perhaps nickel metal) in addition to nickel ferrite. Developing effective shutdown protocols to manage release of the CRUD will require a thermodynamic model of the nature of the CRUD species on the core, with and without boiling.

4.3 Effects of shutdown chemistry changes on corrosion products

4.3.1 Reductive decomposition of nickel ferrites

The main reaction by which non-stoichiometric nickel ferrite is decomposed by dissolved hydrogen is generally written as follows

$$Ni_xFe_{3-x}O_4 + \frac{4}{3}xH_2 \rightarrow \left(1-\frac{x}{3}\right)Fe_3O_4 + xNi^0 + \frac{4}{3}xH_2O \qquad (1)$$
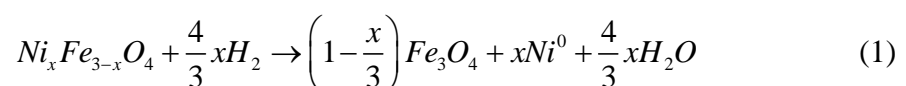
This is a redox reaction in which Ni(II) is reduced to Ni metal at the expense of hydrogen oxidation to water. Additionally, some of the trivalent Fe is most probably reduced to divalent and released to the coolant. Co-58 is associated with Ni and derived from the Ni sites in the CRUD. The rate of reaction (1) does not depend on pH thus it is possible both in acidic and alkaline environments. The extent to which this reaction will occur depends on the availability of hydrogen and temperature. More information on the modeling of the kinetics of this process is given in the chapters below.

There are other reported reactions by which decomposition or dissolution of nickel ferrites can take place in a reducing environment. These reactions, however, are considered secondary (i.e., slower) in nature and do not fit data generated from shutdown chemistry surveillance. As an example, partial dissolution in shutdown scenarios for which acid reducing conditions are prolonged by delayed oxygenation with high boration can occur according to the reaction

$$Ni_xFe_{3-x}O_4 + 2xH^+ + \frac{x}{3}H_2 \rightarrow xNi^{2+} + \left(1-\frac{x}{3}\right)Fe_3O_4 + \frac{4}{3}xH_2O \qquad (2)$$
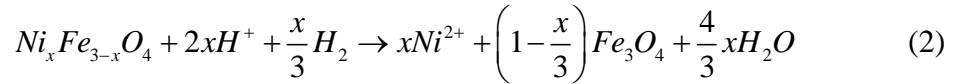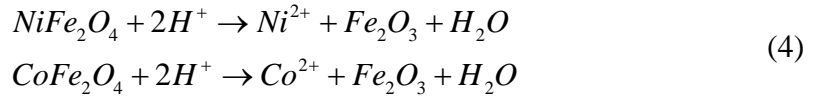
Further, magnetite dissolves as a function of pH, T and hydrogen concentration

$$\frac{1}{3}Fe_3O_4 + (2-b)H^+ + \frac{1}{3}H_2 \rightleftharpoons Fe(OH)_2^{(2-b)+} + \left(\frac{4}{3}-b\right)H_2O \qquad (3)$$
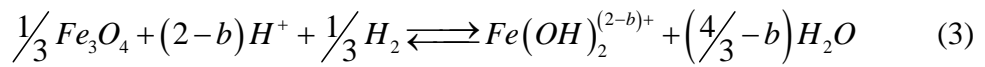
In nickel- and cobalt-containing spinels, this reaction is accompanied by the release of Ni and Co according to the reactions

$$NiFe_2O_4 + 2H^+ \rightarrow Ni^{2+} + Fe_2O_3 + H_2O$$
$$CoFe_2O_4 + 2H^+ \rightarrow Co^{2+} + Fe_2O_3 + H_2O$$
$$(4)$$

Nickel and cobalt can be released from the respective monoxides that have been also reported to be thermodynamically stable at certain acid-reducing conditions:

$$NiO + 2H^+ \rightleftharpoons Ni^{2+} + H_2O$$
$$CoO + 2H^+ \rightleftharpoons Co^{2+} + H_2O$$
$$(5)$$
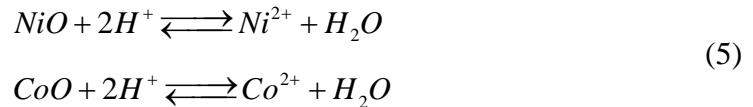
Reaction (3) indicates that the dissolved iron concentration during acid-reducing conditions will increase as a function of the acidity and hydrogen concentration. Since iron can precipitate under oxidizing conditions as Fe(III)-hydroxide, consideration should be given to limiting the hydrogen under acid-reducing conditions if iron levels cannot be reduced before oxidizing conditions are established. Fe(III) hydroxide can co-precipitate CRUD activities, possibly resulting in hot spots or unwanted deposition on plant surfaces. Figure 1 shows approximate limits of stability for nickel ferrites with respect to decomposition by equation(1), as calculated from known and estimated thermodynamic data. High hydrogen concentrations and low temperatures increase the thermodynamic instability of nickel ferrites, but the rate of the decomposition reaction is likely to be slow at or near room temperature. Plant data suggest the most favorable conditions for accomplishing decomposition by reaction (1) are at intermediate temperatures (around 150°C) with levels of dissolved hydrogen near the minimum recommended for normal operating conditions (i.e., >25 cm^3 kg^{-1} STP). Further discussion on the kinetics of this reaction at various conditions can be found in the following chapters.
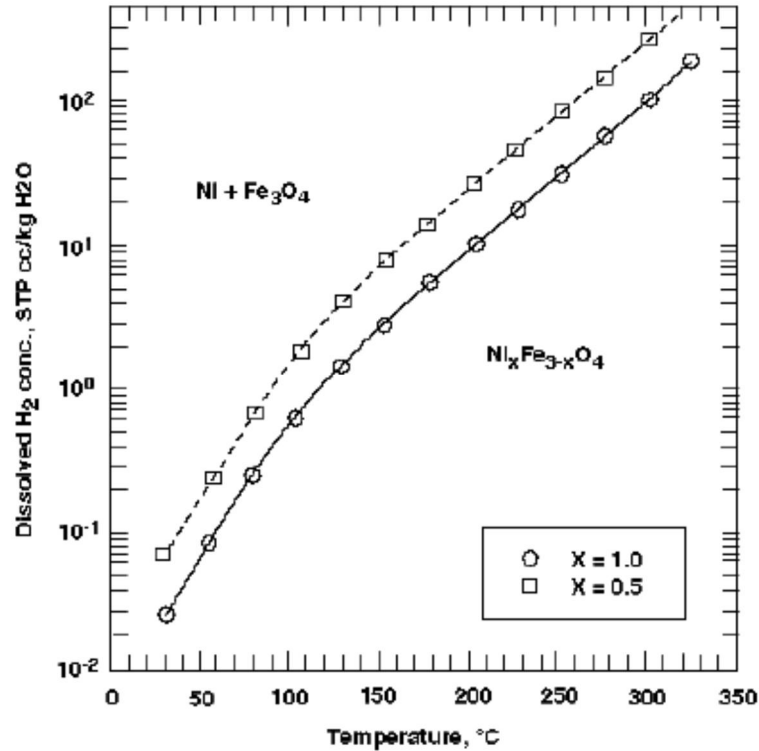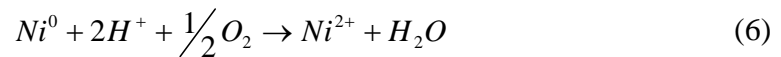
Figure 1 Approximate stability limit of nickel ferrites as depending on temperature and dissolved hydrogen concentration [1].

4.3.2 Oxidation reactions during shutdown

The most important oxidation reaction is oxidative dissolution of nickel metal according to the overall equation

$$Ni^0 + 2H^+ + \tfrac{1}{2}O_2 \rightarrow Ni^{2+} + H_2O \tag{6}$$

Upon intentional addition of hydrogen peroxide to the coolant, the following reaction may be effectively competing with reaction (6)

$$Ni^0 + 2H^+ + H_2O_2 \rightarrow Ni^{2+} + 2H_2O \tag{7}$$
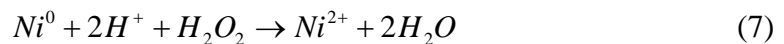
Ni metal can dissolve oxidatively also in acidic conditions with no oxygen and at low hydrogen contents, when the temperature is decreased below about 150-200 °C

$$Ni^0 + 2H^+ \rightarrow Ni^{2+} + H_2 \tag{8}$$

Dissolution of nickel proceeds rapidly in the acid-oxidizing condition of cold shutdown. Nickel metal that was produced by reductive decomposition of nickel ferrites, as per reaction (1), will be dissolved, along with any nickel metal that may have been present in the original CRUD.

Free cobalt metal, if formed, is expected to dissolve in a manner similar to nickel. It is worth noting that iron (II) is insoluble and most probably also unstable under oxidizing conditions at the pH of the boric acid solution (~5), and soluble iron often

shows a rapid decrease (from several hundred µg kg^{-1} to <50 µg kg^{-1}) during cool-down even prior to controlled oxygenation of the RCS with hydrogen peroxide.

Figure 2 shows the pattern of nickel, cobalt, and iron behavior in solution during a simulated shutdown test on nickel cobalt ferrite in 0.2 m H$_3$BO$_3$. Near equilibrium values for solubility were reported for nickel and iron at 275 °C, at the beginning of the test. Cooling to 130 °C in the presence of hydrogen leads to an increase of dissolved nickel, iron, and, cobalt, but not to levels corresponding to equilibrium at that temperature. Addition of hydrogen peroxide then causes an additional significant and continuing increase of dissolved nickel and cobalt. At the same time a major decrease of dissolved iron is observed, which as commented above is attributable to surface oxidation of magnetite to less soluble Fe$_2$O$_3$. Experiments show that the key first step in the overall process is production of nickel metal by reaction (1). When material that has been treated in this way is subsequently exposed to an acid-oxidizing environment, nickel and cobalt are released to solution rapidly and at substantial concentrations.
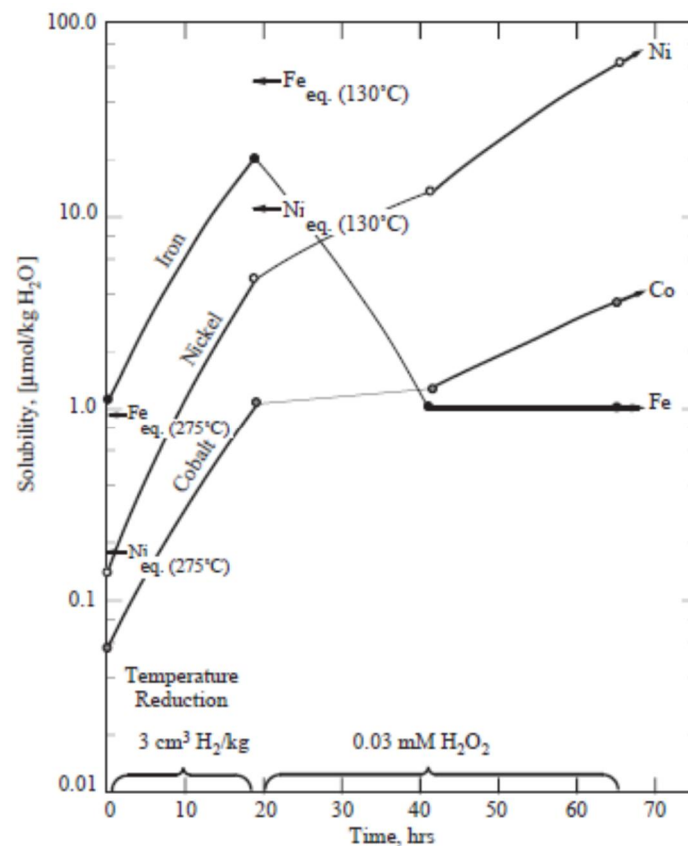
Figure 2 Behavior of nickel ferrite containing cobalt during a schematic shutdown test.

The temperature, power and shutdown chemistry data, such as the content of boron and dissolved hydrogen as function of the first 50 hours of a typical shutdown are shown in Figure 3 [10]. The start time point zero is at the beginning of cooling. The first phase (green part in the figure) is determined by the acid-reducing conditions. At the temperature of 150°C degasification by venting the VCT to replace the remaining hydrogen with a nitrogen atmosphere should begin. The second phase is controlled by an acid-oxidizing condition (orange part in the figure) and is introduced by dosage of hydrogen peroxide at a temperature of about 80°C and dissolved hydrogen < 1 ppm (or equivalently, 11.2 cm^3 kg^{-1} STP). Figure 4 shows

the concentrations of the two types of radio-cobalt, whereas Figure 5 demonstrates the evolution of the Fe and Ni concentrations during the first 50 h of shutdown.

As mentioned above, in the acid-reducing condition phase, nickel compounds will be reduced to metallic nickel and the iron-nickel compounds decompose to magnetite and metallic nickel. A part of iron is dissolved in this phase, which can drag nickel along from iron-nickel compounds. The results indicate that the major part of iron is dissolved at a temperature between 100°C and 150°C, whereby a small amount of nickel from the iron-nickel compounds is dissolved, too. The nickel curve of Figure 5 shows a similar behavior as Co-58 and Co-60.

In the following phase, i.e. in the acid-oxidizing conditions, metallic nickel and Co-58, respectively, as well as the rest of iron (resp. Co-60) from the nickel-iron compounds are dissolved and will be removed by the purification filter. With these measures it was possible to reach the main objectives of the shutdown chemistry, i.e. low dose rate in the water, high translucency of the water and low dose rate on primary components. This would guarantee refueling with low personnel doses.
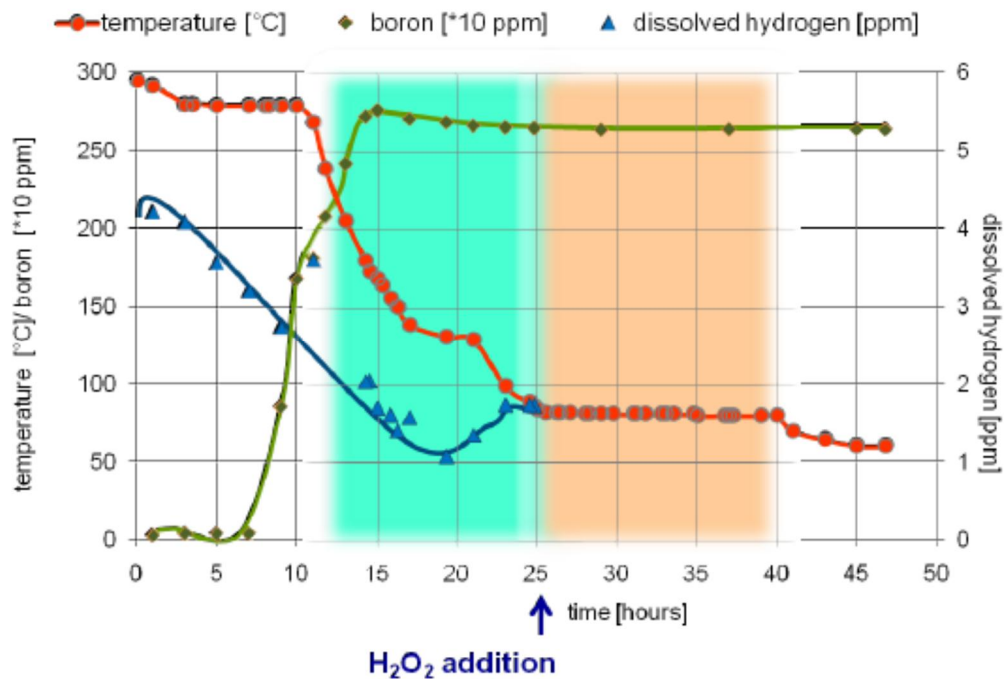
Figure 3 Evolution of main water chemistry parameters during the first 50 h of a typical shutdown.
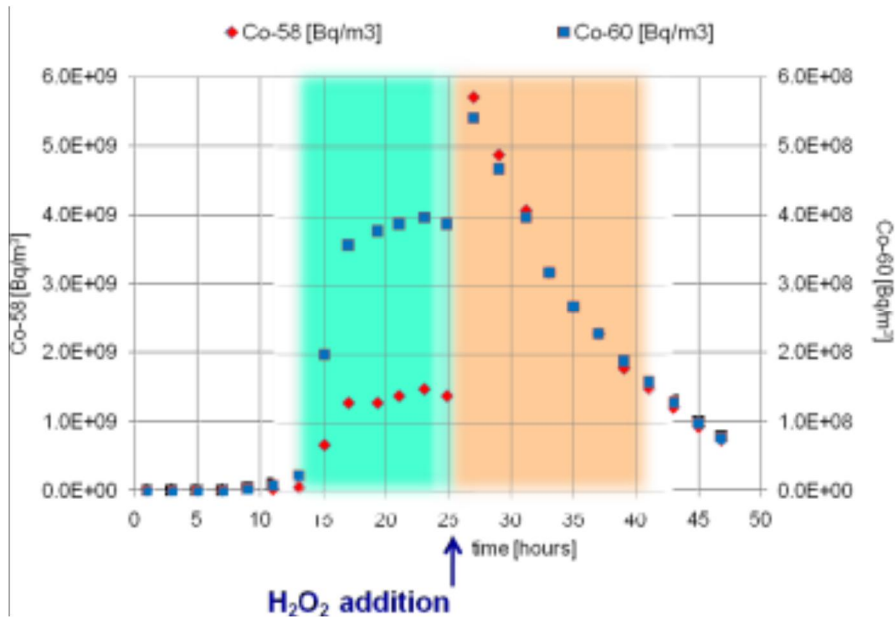
Figure 4 Concentrations of radio-cobalt during the first 50 h of shutdown.
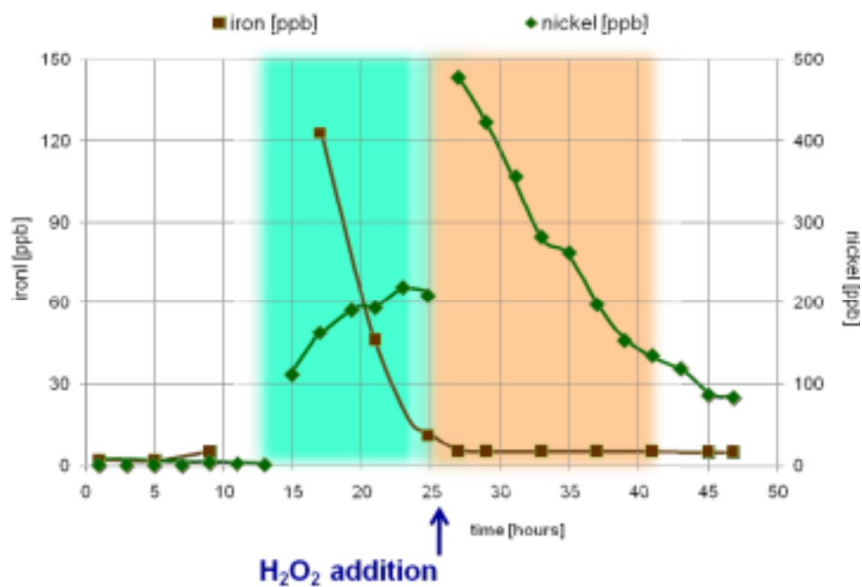
Figure 5 Concentration of Fe and Ni during the first 50 h of shutdown.

4.3.3   Ni and NiO considerations during shutdown

The dual phase shutdown chemistry program consisting of an acid-reducing phase followed by an acid-oxidizing phase is based on the expected behavior of non-stoichiometric nickel ferrite. Recent experience indicates that CRUD on cores, particularly cores with extended duty, may have excess nickel over that in non-stoichiometric nickel ferrite. Although the form of the excess nickel has not been positively identified, it is thought to be mostly nickel oxide, although nickel metal could also be present [14,15,16]. Crud that is enriched in nickel oxide will not respond as well to dual phase shutdown chemistry as non-enriched CRUD. In addition, boiling will produce a more porous CRUD, which may possibly result in a greater likelihood of release during shutdown. During the acid-reducing phase the nickel oxide (and associated cobalt-58) on CRUD surfaces will slowly dissolve, with no additional benefit of acid oxidizing chemistry (nickel metal on

surface deposits will dissolve in acid-oxidizing conditions). Additional studies are required to determine optimum decomposition/dissolution conditions for nickel oxide.

4.3.4 Release of particulate corrosion products

Particulate CRUD release is often observed at the end of an operating cycle. This behavior does not necessarily predict an anomalous shutdown, but increased precautions may be warranted. The following suggestions are offered for better shutdown management with regard to particulate CPs [17]:

• Reduction of pH_T to 6.9 near the end of the operating cycle. This may stabilize CRUD and aid in establishing acid-reducing conditions for the RF.
• Ensure sufficient reactor coolant hydrogen at shutdown to provide a reducing environment during borations with oxygenated boric acid. Aggressive reducing chemistry is not necessary for iron control.
• Pay particular attention to events that cause rapid physical changes (such as flow perturbations) that could impact particulate CRUD release.
• Plants with historical release profiles showing little benefit from acid-reducing chemistry cannot justify maintaining this condition for an excessive time. However, plants whose release profiles show significant soluble release during acid-reducing conditions should consider extended time at these conditions, and establishing acid-reducing chemistry during mid-cycle outages.
• Minimize the RCS volume and maximize the purification flow during forced oxygenation. This is easily accomplished at plants with loop isolation valves. For other plants, RCPs may be secured to effectively reduce RCS volume by reducing flow to SGs/loops. However, plants experiencing significant particulate CRUD releases should consider the impact of deposition on surfaces if pumps are taken out of service too soon.

It can be concluded that CRUD which behaves in a manner consistent with nickel ferrite can be managed during shutdowns with reasonable predictability using the controls recommended by EPRI [1-5]. However, CRUD that is characteristic of nickel oxide or bonaccordite (Ni_2FeBO_5) will require alternative CRUD management techniques. Fuel cleaning during RFs may be a viable supplement to chemical CRUD control measures for plants in which fuel deposits are expected to be physically stable during the shutdown.

5 State-of-the-art of the primary water chemistry during shutdown

5.1 Acid-reducing conditions (phase 1)

Three global shutdown chemistry strategies have been used successfully prior to peroxide treatment:
o High temperature acid-reducing chemistry
o Low temperature acid-reducing conditions
o No acid-reducing conditions.

The success for a particular strategy depends on the composition and inventory of CRUD on the core. Since no clear conclusions have been established that are universally applicable for all situations, each plant should develop a shutdown chemistry control strategy.

A series of recommendations and principles for consideration during development of site-specific shutdown chemistry programs during shutdown evolutions have been summarized presented in Volume 2 of the PWR Primary Water Chemistry Guidelines [1]. The principles reflect general guidance for establishing acid reducing (AR) conditions, minimizing/avoiding precipitation of solubilized species, maximizing cleanup during the evolution, establishing an oxidizing environment to promote solubilization of core deposits at an optimum time, etc. It is recommended in Ref. 7 that utility personnel evaluate and implement these principles, which are summarized below, consistent with plant-specific circumstances:

• The reactor coolant should be borated to the refueling boron concentration as soon as possible within plant constraints to achieve acidic conditions. Rapid boration at elevated temperatures maximizes the time in AR conditions.

• Lithium concentrations may be reduced prior to shutdown to increase the time at acidic conditions. The minimum pH at operating temperature (pH_T) without significant risk of excessive CRUD redistribution is 6.5. Reductions below pH_T 6.9 should be of limited duration. If iodine activity is found to be excessively high, the lithium management program may need to be modified, e.g. as discussed in Revision 5 of the EPRI Guidelines [1].

• Upon shutdown, the lithium concentration in the reactor coolant should be decreased as quickly as plant conditions permit.

• The Li content of the reactor coolant should not be increased during cool-down.

• Hydrogen may be reduced to 15 cm^3 kg^{-1} STP 24 hours prior to a planned shutdown. The time that the RCS chemistry is both acidic and reducing when dissolution of nickel and radio-cobalt are favored for non-stoichiometric nickel ferrite should be maximized. The suggested minimum time in AR conditions is 12 to 16 hours, and added benefits are anticipated if times as long as possible are used consistent with outage schedule.

• If schedule and operations permit, hydrogen should be maintained at greater than 10 cm^3 kg^{-1} STP for at least 16 hours at 120-150 °C to decompose non-stoichiometric nickel ferrite. At present, little is known about the kinetics of nickel ferrite decomposition, but maximum dissolution is expected to occur at approximately 120-150 °C.

• The time with at least one RCP operating should be maximized, unless the plant configuration precludes RCP operation. This is performed to maximize mass flow through the core to enhance dissolution of CPs. Maintaining steady RCP operation can be important when a large particulate release has occurred.

• Letdown purification flow rate should be maximized, and filter and demineralizer removal efficiencies should be high.

- No significant pH increases should be permitted to occur when the Residual Heat Removal (RHR) or decay heat systems are valved into service. Adding hydrazine to the RHR loop to scavenge oxygen is permitted; however, the addition should be made several weeks prior to an outage since the kinetics is slow at ambient conditions, particularly in acidic environments.

The critical parameters and main targets of the optimal shutdown chemistry are summarized in Table 2, whereas the typical initial and final values of the parameters during a shutdown of an average PWR are collected in Table 3.

Table 2 Critical parameters and main targets of the PWR shutdown chemistry.

Parameter / Target	Explanation
pH_T	Important for acid conditions, for decomposition and dissolution; increased acidity promotes dissolution. Solubility of Ni_{met} and NiO increases with decreasing pH under shutdown conditions
Rapid boration	Precondition for low pH_T during cooldown
Delithiation	Supports low pH_T during cooldown
Hydrogen	Necessary for reducing conditions, supports decomposition of ferrite, decomposition of nickel-cobalt ferrite increase at higher hydrogen
Hydrogen peroxide	Is used to remove residual hydrogen and is needed for oxygenation to dissolve nickel, iron, cobalt, accelerates the dissolution process of Ni_{met}
Temperature	Decomposition of Ni-Co ferrite increases at lower temperature; Ni solubility increases when temperature decreases
RCP operation	A RCP should be operated as long as possible to remove particulate releases. It should be noted that the flow in loops without running pumps is backwards, leading to a possible deposition of CRUD
Fresh mixed bed filter	Supports acid conditions by removal of lithium

Table 3 Example of initial and final parameter values in the primary coolant during shutdown of a PWR.

	Initial	Final
Pressure (bar)	155	Atmospheric
Temperature (°C)	≈ 300	≤ 60
Boron (mg/kg)	< 2000 to ≈ 10	≥ 2000
Lithium (mg/kg)	2.2 to $0.5^{(*)}$ ($pH_{300\,°C} \leq 7.2$)	≈ 0
O_2 (µg/kg)	<10	>8000
H_2 (Ncm³/kg)	$25-35^{(*)}$	≈ 0

5.2 Acid-oxidizing conditions (phase 2)

Accordingly, the main action principles concerning phase 2 of the shutdown are summarized below:

- Acid oxidizing conditions should be established and maintained to solubilize radio-cobalt and nickel.

- Cleanup should continue until fission and activation products are reduced to limits specified in plant procedures.
- Dissolved hydrogen should be reduced to <5 cm^3 kg^{-1} (STP) prior to opening the RCS. Ensuring hydrogen has been reduced to this level supports the prevention of combustible/explosive mixtures in containment.

Oxygenation of the primary coolant is performed so as to prevent the risks of materials corrosion, avoid the formation of hazardous H_2/O_2 mixtures and control the release of the CRUDs from the core. Since 1993 the standard procedure is a forced oxygenation by injection of H_2O_2, when $T_{RCS} \leq 80°C$. An alternative method is also allowed, by introducing air in the VCT, if $T_{RCS} \leq 120°C$. With H_2O_2 injection, the primary coolant is generally oxygenated in less than 30 minutes $([O_2]_{dissolved} > 1\text{-}3$ mg $kg^{-1})$. The VCT is swept with air, as soon as possible, in order to sustain the O_2 concentration in the coolant.

There are some particular outages for which it is not planned to open the RCS. These are generally mid-cycle outages, planned or unplanned, which are likely to last from a few days to a couple of months. The chemistry of the primary coolant should be adjusted depending on the final operational mode. In general, it is advisable to keep the solubility of CPs as low as possible, so that all the activity remains confined in the reactor area, thereby preventing the risks of out-of-core contamination. This is done by injecting H_2 and Li in the coolant and enabling an efficient purification rate. Typical concentrations targeted are $[H_2] > 15$ cm^3 kg^{-1} (STP) and $[Li] > 2$ mg kg^{-1}, or adjusted according to the Boron/Lithium coordination. The current EdF guidelines, for example, do not recommend applying acid-oxidizing conditions to the coolant, if the outage lasts more than 3 days [12]. Therefore, the primary coolant may remain several days and weeks in alkaline and reducing conditions, if needed. There are however 2 limitations to this approach:

- It is recommended to perform an oxygenation of the coolant if the plant is to stay more than 3 weeks with H_2 and Li conditioning, especially if $T_{RCS} \leq 80°C$.
- It is recommended that the chemical degassing procedure be ready on the plant, in order to enable a quick removal of H_2 if needed, at low temperature and pressure of the RCS.

If the plant operated less than 6 months prior to the outage, it is considered that the CP source term (mainly Co-58 and Co-60) will be reasonably low. Table 4 shows several recommended operating modes and the corresponding chemistry, in order to minimize the risks of recontamination of the RCS. The preference decreases from state 1 to state 4.

If the plant operated for more than 6 months before shutdown and its SG tubes are "passivated", the recontamination risks are considered as negligible with respect to Co-58. The "passivated" SG tubes are those fabricated of alloy 690TT after approximately half a dozen cycles, when the Co-58 peaks observed after the oxygenation are less than 50 GBq per tube. For the plants with the so-called "passivated" SG tubes, the recommendations are the same as for plants operating less than 6 months. If the SG tubes are not "passivated", the Co-58 source term is considered as non-negligible, as well as the recontamination risks during shutdown. Therefore, only 2 favorite states are recommended, which are supposed to lead to the lowest recontamination risks (Table 5).

Table 4 Recommended operational modes for shutdown after power operation of less than 6 months.

1	Hot shutdown, higher temperature	$T_{RCS} \geq 286\ °C$ $15 < H_2 < 50$ N cm³/kg Li according to B conc.
2	Cold shutdown with oxygenation	$T_{RCS} < 80\ °C$ $O_2 > 1$ mg/kg
3	Cold shutdown without oxygenation	$T_{RCS} < 80\ °C$ $25 < H_2 < 50$ N cm³/kg Li > 2 mg/kg
4	PZR biphasic, medium temperature	$T_{RCS} \geq 170\ °C$ $15 < H_2 < 50$ N cm³/kg Li > 2 mg/kg

Table 5 Recommended operational modes for shutdown after power operation of more than 6 months.

1	Hot shutdown, higher temperature	$T_{RCS} \geq 286\ °C$ $15 < H_2 < 50$ N cm³/kg Li according to B conc.
2	Cold shutdown with oxygenation	$T_{RCS} < 80\ °C$ $O_2 > 1$ mg/kg

6 State-of-the-art of the primary water chemistry during start-up

6.1 Corrosion product behavior during heat-up

Section 4.3 described the complex behavior of corrosion products during the changing chemistry of cool-down. During startup, these chemistry changes occur in reverse with much less dramatic effects. It is known that the solubility of cobalt, nickel and iron are significantly lower at operating temperatures than at shutdown temperatures. If soluble corrosion products are not removed from the coolant prior to operating conditions, these species will deposit in the system because of decreased solubility at elevated temperatures. It is difficult to quantify the impact of removal of corrosion products on radiation fields based on current field data, since many factors contribute to radiation fields and the location of the removed activity is difficult to determine. The recommendations in the EPRI guidelines to achieve low corrosion product concentrations prior to heat-up are based on the following:

- Maintaining low soluble nickel concentrations prior to resuming power operation is consistent with the common industry practice of maintaining low coolant activity (i.e., continued purification flow and effective ion exchange).
- The fate of nickel on startup involves uncertainty since thermodynamic effects determine the chemical form as a function of oxidation-reduction potential and pH at temperature, but kinetic effects may be controlling. Dissolution processes during startups are controlled by kinetics rather than by thermodynamic equilibrium, while near 300 °C concentrations tend to be near the solubility limit. Dissolved nickel rapidly disappears from the

reactor coolant on heat-up, and the concern is that specific cleanup steps may be warranted in some cases. Nickel management during startup can be practiced for both AOA considerations and for CRUD management considerations.

6.2   Overview of the start-up guidelines

The main issues of the start-up procedure, as far as chemistry is concerned, are the following:

- o   The removal of residual O_2.
- o   The purification during N_2H_4 injection.
- o   The best time to add H_2 and Li in the coolant.

According to e.g. the French guidelines [12], there are three possibilities of oxygen removal:

- Vacuum fill of the RCS. - it is preferable to refill the RCS under low pressure (typically 0.2 bar), in order to reduce the volume of air captured in the upper regions, i.e. mostly in the SG tube bundles.
- Physical degassing of O_2 ("stripping") – this process should be enhanced as much as possible during start-up. This could be done by venting the gaseous phase of the VCT with N_2, while sustaining a sufficient flow rate from the CVCS letdown line into the VCT.
- Chemical scavenging of O_2 - Hydrazine is injected in the coolant in order to react with the dissolved O_2, according to:

$$N_2H_4 + O_2 \rightarrow N_2 + 2H_2O \qquad (9)$$

In principle, the volume of N_2H_4 solution to inject may be calculated precisely from the oxygen amount in the coolant and the stoichiometry of the reaction above.

The injection of N_2H_4 is allowed only when at least one RCP operates. The first injection generally occurs when T_{RCS} lies in the range 60 to 80 °C. It is recommended to inject the hydrazine with the minimum number of injections, 1 or 2 if possible. The filter beds are by-passed before injecting the hydrazine ($T_{RCS}< 80$ °C). They are usually connected later in the start-up procedure, during hot shutdown, once the concentrations of N_2H_4 and NH_3 are below a certain limit, usually around 0.5 mg/kg. Depending on the plant procedure and operational constraints, the coolant purification may be off for several days, sometimes until criticality is reached. This leads to consider the opportunity to purify the coolant during hydrazine injection. The purification of the coolant during O_2 scavenging and heating was implemented recently, for start-ups following a steam generator replacement.

According to the EPRI guidelines [1], removal of residual dissolved oxygen from reactor coolant prior to or during heat-up can be accomplished by VCT hydrogen addition. Hydrogen is delivered to the RCS via CVCS charging system in a mode similar to that during normal power operation. Precautions, however, need to be taken to ensure that explosive mixtures of hydrogen and oxygen are not created during the evolution. The residual reactor core gamma flux is sufficient to drive the hydrogen/oxygen reaction [2]. This reaction rate is rapid and independent of temperature. The rate of reduction in RCS dissolved oxygen is a function of charging flow rate and dissolved hydrogen concentration. Maximized letdown and charging flow rates decrease hydrogen delivery time to the RCS, thus reducing the time required to complete oxygen removal.

Hydrogen addition at startup for oxygen removal, like hydrazine, should be used only after mechanical methods have been completed and should not be considered as the principal means for RCS oxygen reduction. Reactor coolant pump loop sweeps, reactor head venting and VCT purging with nitrogen must first be completed. Precaution must be taken to ensure that oxygen concentrations are minimal to prevent explosive mixtures from being formed in the VCT or the pressurizer. While the pressurizer is maintained solid, the coolant dissolved oxygen concentration is <100 ppb and after the equilibrium VCT gas space oxygen concentration has been reduced by mechanical means, the VCT gas space can then be converted from a nitrogen to a hydrogen atmosphere.

Li should be injected later in the process, for instance during hot shutdown ($T \geq$ 290 °C), before criticality. It is preferable to avoid the presence of residual Li in the RHRS, since it may have a detrimental effect on the next shutdown, after its connection. The technical specifications require that H_2 must be added before the reactor becomes critical. In general, there are no particular reasons for anticipating the injection. However, one exception is concerning the first start-up after a SGR. The presence of hydrogen may improve the passivation of the SG tubes during the Hot Functional Test (HFT). If nickel release is desired, hydrogen should be added before Li.

6.3   Start-up chemistry practices

The main features of a typical start-up procedure for EdF PWRs will be outlined in the following (Figure 6). At first, the RCS is filled with aerated water under normal pressure or low pressure (0.2 bar). As far as possible, the RCS will be filled under vacuum. Physical degassing using the VCT (under N_2) is used as much as possible. Then the RCS is pressurized and the RCP are started. Before heating, the following condition is fulfilled: [Co-58] < 7 GBq per tube, [total-γ] < 14 GBq per tube. Despite the vacuum fill, the amount of O_2 captured in the SG tubes and then dissolved after starting the RCP, is not negligible (Figure 7). Calculations show that O_2 concentrations in the range 11 to 13 mg/kg may be reached in the coolant, whereas equilibrium with air leads to concentrations around 7-8 mg kg^{-1} in O_2.

Next, the volume of hydrazine that has been evaluated is injected a variable number of times. The O_2 weight and the corresponding N_2H_4 volume, need to be evaluated by summing-up two contributions: i) the initial O_2 amount coming from the refill with aerated water, and ii) the additional O_2 coming from the air trapped in the SG and dissolved after the RCPs were started. The second term may be evaluated from the measurement of residual air performed by the operators during pressurization, before starting the RCPs. The first injection generally occurs when T_{RCS} lies in the range 60 to 80°C. In principle, the kinetics should be favored at a higher temperature, according to the kinetic expression for the rate of reaction(9):

$$\frac{d[O_2]}{dt} = k_0 e^{-E_a/RT} [N_2H_4]^a [O_2]^b \qquad (10)$$

According to some reports [12], the activation energy of the reaction (E_a) is of the order of 160 kJ mol^{-1}, and the partial orders of the reaction with respect to hydrazine and oxygen concentrations are $a=b=0.5$. However, other investigations

[18] have resulted in lower activation energies of the order of 60 kJ mol^{-1} and partial reaction orders of $a=1$ and $b=0.5$.

In addition, other operational constraints must be considered. In particular, the RHRS operating time must be limited at $T_{RCS} > 90°C$, in order to mitigate the thermal fatigue risks. Therefore, the $[O_2]<0.1$ mg kg^{-1} limit is generally met at $T_{RCS} < 90°C$, in order to avoid any hold point between this temperature and 120°C.
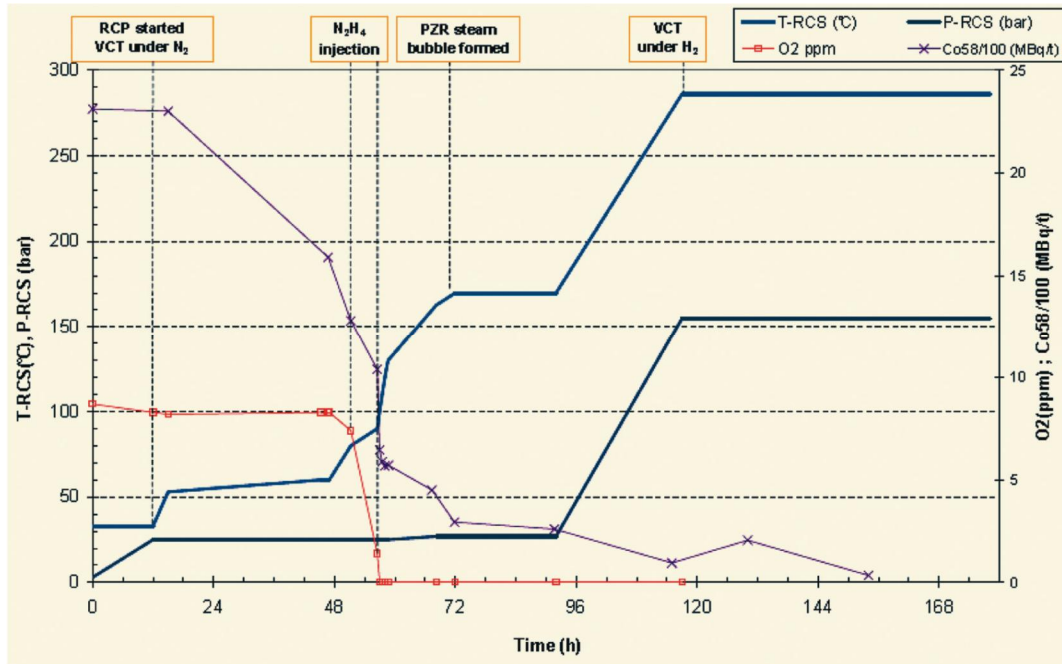
Figure 6 Typical start-up procedure of a French PWR.

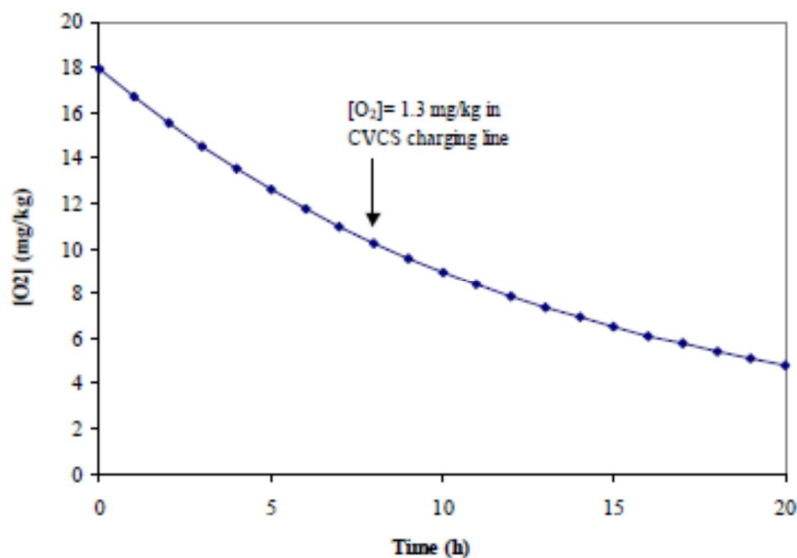*Figure 7 Physical removal of oxygen in the VCT with 2 bar of N$_2$-2%(v/v)O$_2$.*

As an example, Figure 8 shows the evolution of oxygen concentration with time during four consecutive injections of N$_2$H$_4$. The concentration drops almost instantaneously after the injection and then levels off when no more hydrazine is available to react. The removal of dissolved O$_2$ was done between 80 and 87°C in

this particular case, and it took almost 7h 30min to reach the $[O_2]<0.1$ mg kg^{-1} limit.
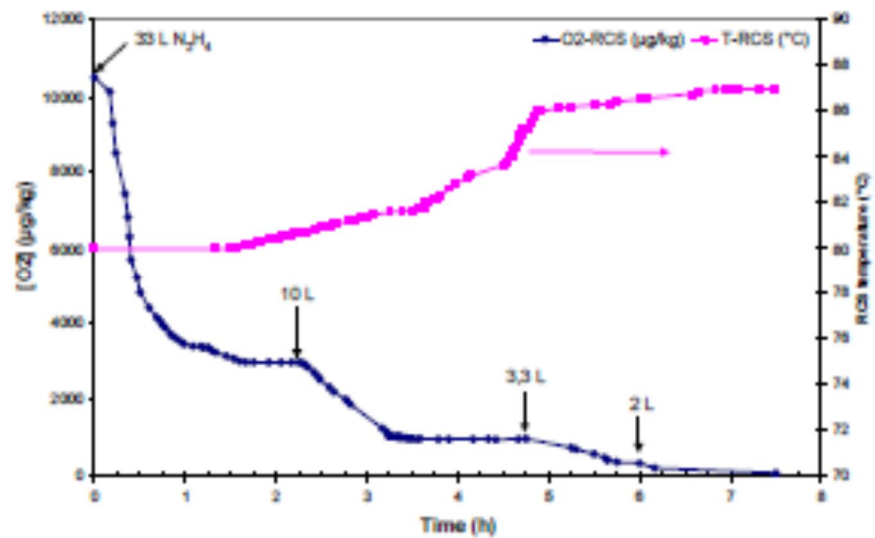

Figure 8 Example of O2 variation in RCS, as a function of time and N_2H_4 injections.

Following degassing operations, including the vacuum application in the RCS and removing any residual oxygen contained in the reactor, careful attention is paid to controlling CPs in solution, which are likely to precipitate with the rise of the reactor temperature. They must therefore be removed by purification at high flow rate, for as long as the start-up schedule allows. To do this, the removal of nickel and its activation product, Co-58, will be monitored: the expected value for total nickel should be < 100 μg kg^{-1}, when the temperature of the reactor coolant is below 120 °C. Hydrogen is also dissolved in the reactor coolant, together with injecting the right quantity of lithium hydroxide needed to obtain the $pH_{300 °C}$ value according to the total B concentration required, as soon as nominal operating conditions are achieved (hot shutdown condition).

Neder et al. [13] reported filed experience with oxygen removal during plant start-up operation. Reducing conditions at higher temperatures are indispensable to avoid specific type of corrosion (e.g. SCC) of the stainless steel components of the primary side. Therefore, all water chemistry guidelines are requiring oxygen removal from the primary coolant during the plant heat-up. Whereas all other water chemistry guidelines require the oxygen removal to be performed during the plant heating-up at 80 °C with coolant oxygen concentration of $[O_2] \leq 100$ μg kg, this oxygen removal criterion, according to VGB guidelines, is at ≤ 170 °C with the same limit. The basis to select higher temperature in the VGB guidelines for oxygen removal is the plant chemistry measurements performed to study the reaction kinetic of the Hydrazine/Oxygen reaction for chemical oxygen removal under PWR plant heat-up conditions. The main motivation to perform these measurements was to find out the optimum temperature range for oxygen removal by hydrazine. Accordingly, hydrazine addition to the coolant for oxygen removal at lower temperatures like 80 °C would result in an unnecessary loading of the ion resins of the coolant purification system by hydrazine in the CVCS, which increases the nuclear waste. A summary of the oxygen removal according to the VGB guidelines is presented in Figure 9.
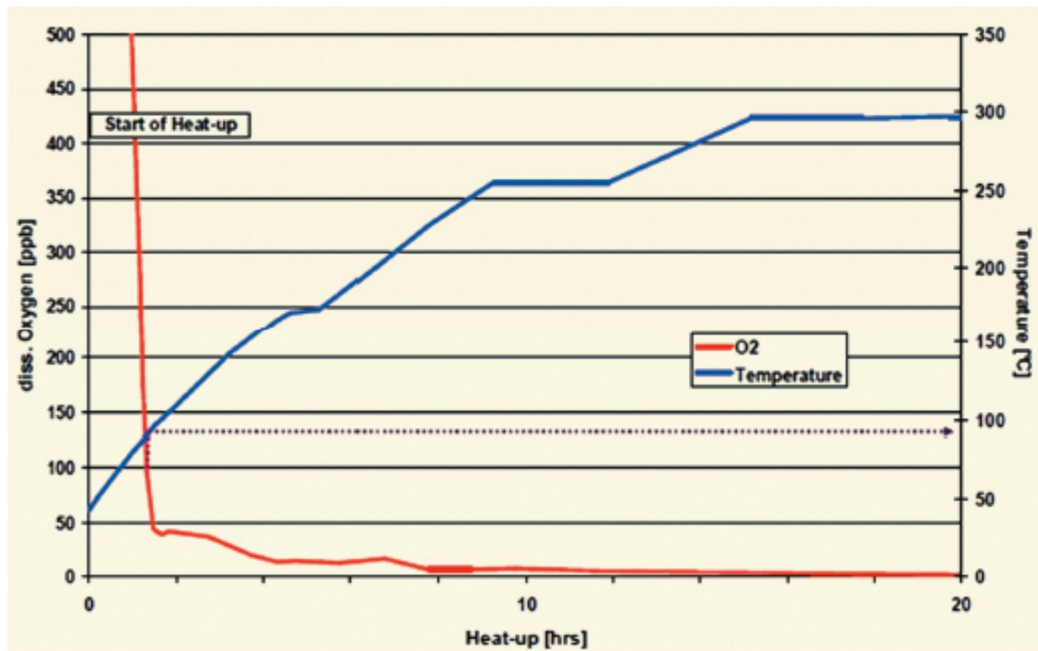
Figure 9 Oxygen removal according to the VGB guidelines.

After RHR is secured for the last time, lithium hydroxide is added to raise the pH above pH neutral and hydrogen is subsequently placed on the VCT. This philosophy allows for a transition from acid–oxidizing to alkaline–reducing environment as quickly as possible and begins the stabilization of CRUD and filmed surfaces as quickly as possible. This approach is based on the concept that further decomposition of CRUD would result in a small fraction of the released nickel being removed unless the start-up was delayed and corrosion potential (ECP) control consistent with nickel solubility, just below the hydrogen evolution line. In the absence of this provision, which is prohibited by start-up schedule, CRUD decomposition would primarily result in an RCS inventory of "tramp" nickel metal that would be highly susceptible to oxidation, transport and redistribution on the core feed fuel assemblies during the beginning of the next cycle as shown through a diagnostic multi-variable analysis.

7 Effect of transients on CRUD formation and associated thermal conduction anomalies

7.1 Introduction

The axial offset (AO) of a PWR plant is the integrated power output in the top half of the core minus the integrated power over the bottom of the core, all divided by the total power output

$$AO = \frac{(P_t - P_b)}{(P_t + P_b)} \times 100, \% \qquad (11)$$

When a PWR is operational this parameter is measured and compared with predictions from a computer code [19]. For most plants these comparisons are good but in recent years, for some plants operating at high power, this has not been the case. This AO anomaly (AOA) results from a shift in power output

towards the bottom of the core as a result of a fall in the neutron flux in the upper core regions. This can have safety implications which could lead to a down rating of the plant and subsequent economic losses. At least 18 plants in the U.S. have suffered from AOA along with units in France, Korea and Belgium. The effect of AOA on axial power distribution is illustrated in Figure 10.
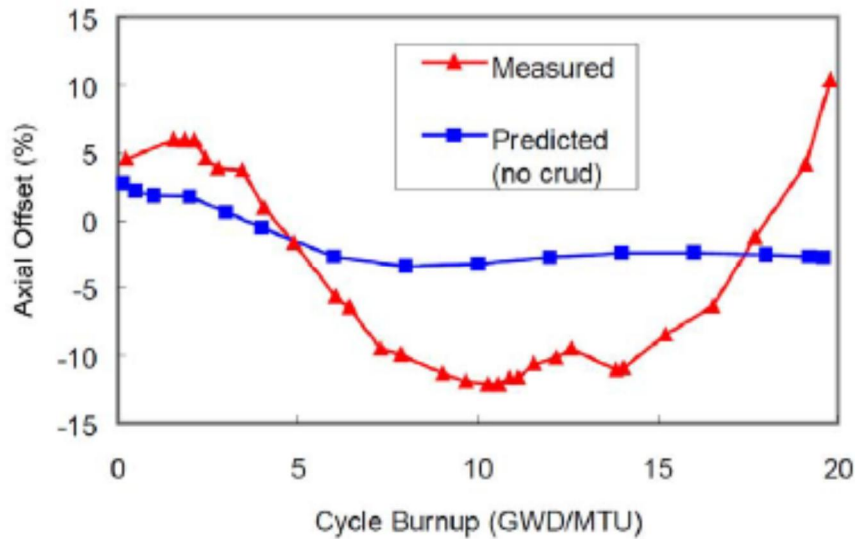

Figure 10 Example of an Axial Offset Anomaly.

It has been reported that the cause of AOA is due to CRUD build-up on the fuel in the top half of the core as a result of increased sub-cooled nucleate boiling in this region. The take-up of boron in this deposit gives increased local boron concentrations that lead to the observed drop in the neutron flux. In general, there are three conditions that are believed necessary for AOA to occur: soluble boron in the coolant, corrosion products in the coolant, and sub-cooled nucleate boiling at fuel rod surfaces. These conditions are illustrated in Figure 11.
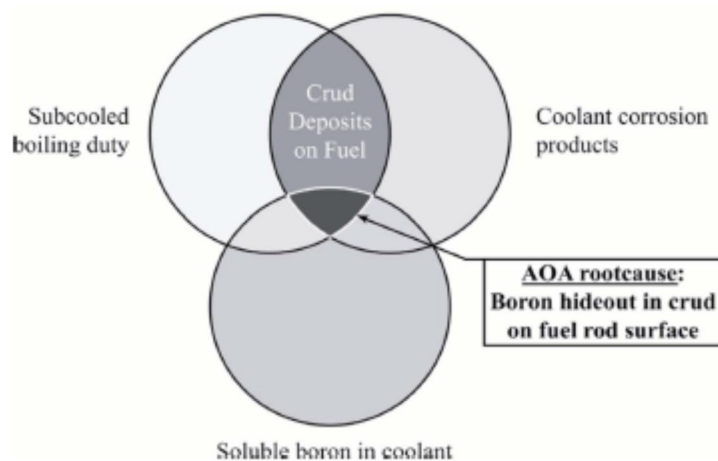
Figure 11 Factors that contribute to AOA.

While it is now fairly clear that this is the mechanism for AOA, many details are not clear. Questions about the relative importance of plant operational parameters, such as boron, lithium and hydrogen concentration still remain, as are questions about the nature of the boron within the deposit and by how much it is concentrated. The temperature, pH and oxidizing conditions within the CRUD are

also unclear and these may have consequences for fuel performance. In order to suggest the best mitigation strategy it is important to understand AOA further and have answers to all of these questions.

The present survey discusses both aspects of the phenomena; the CRUD deposition process and the chemistry that takes place within this CRUD once it is formed. Special attention is paid to the effect of transients on the behavior of CRUD and their influence on the balance of corrosion products and activity accumulation in the RCS inventory.

7.2   Critical factors that contribute to AOA

7.2.1   Sub-nucleate boiling (SNB)

The basic mechanism of sub-cooled nucleate boiling (SNB) on clean surfaces is fairly well understood [19]. Boiling on surfaces covered by CRUD are more complex and not as well understood, although the same basic principles can be applied. In a PWR, the coolant at the inlet to the core is highly sub-cooled, typically by 32-38 °C. Forced convection is the dominant heat transfer mechanism from the fuel cladding to the coolant. Heating the coolant at very high heat flux (e.g., high assembly peaking) increases the coolant temperature as the coolant flows up the core. Maintaining this high heat flux will eventually bring the cladding wall temperature (the temperature at the interface between the coolant and the solid surface of the heat source) to slightly above the saturation temperature. The liquid adjacent to the wall is then superheated, although the bulk coolant temperature (the average of the coolant temperature taken across the flow channel at that elevation) is still sub-cooled. Bubbles will begin to form at certain preferential sites on the cladding surface called nucleation sites. These are minor surface imperfections such as scratches or grinding marks that provide indentations on the surface where the coolant can reach a slightly higher temperature. Bubbles tend to form at these locations first, hence the term nucleate boiling. This process is shown schematically in Figure 12. Liquid water adjacent to the fuel rod surface is heated by the energy from the fuel rod and evaporates into the bubble. Simultaneously, steam is condensing back into liquid at other points on the bubble's surface. A given bubble will grow at a faster or slower rate depending on the relative rates of evaporation and condensation.

In a PWR, the heat flux that will cause nucleate boiling is primarily a function of the coolant temperature; the lower the coolant temperature, the greater the heat flux required to start nucleate boiling and vice-versa. Nucleate boiling is a much more efficient means of heat transfer from the cladding surface than forced convection. The evaporation of liquid water into steam transfers large amounts of heat with very little temperature difference. The heat transfer coefficient in nucleate boiling can be many times greater than in forced convection. Therefore, in nucleate boiling, the same amount of heat generated in the fuel rod can be transferred to the coolant with a much smaller temperature difference than in forced convection. The heat flux in the nucleate boiling regime cannot be increased indefinitely. At some critical heat flux, the bubbles coalesce into a steam blanket over the surface, causing a large rise in the cladding wall temperature (heated surface).
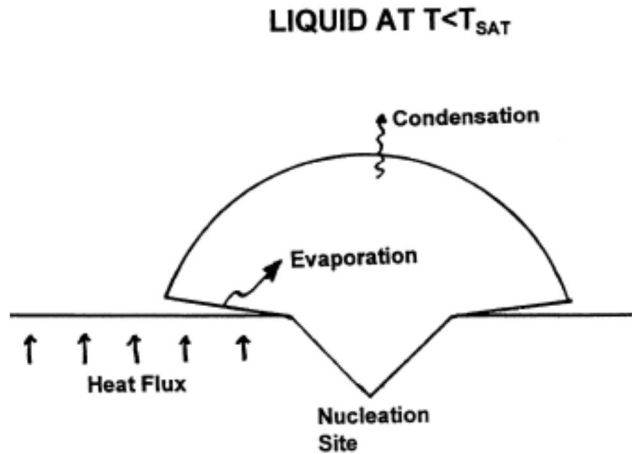
LIQUID AT T<T$_{SAT}$

Figure 12 Schematic of Sub-cooled Nucleate Boiling.

Quantification of SNB was not a core design consideration until AOA became a significant fuel performance issue. A 3D thermal-hydraulic analysis of the steaming rate, S_R was developed to characterize the SNB condition of a core [19]. Only the relatively high power fuel assemblies in a PWR will exhibit SNB (i.e., S_R greater than 0), and these will not exhibit SNB in the lower half of the assembly. At any given location within the core, the value of S_R will also vary with burn-up as the power distribution changes. Therefore, calculations at a number of burn-up steps throughout a cycle are necessary to adequately characterize the amount of SNB in a given plant. In terms of thermal hydraulic parameters (void fraction, quality etc.), investigators [19] found that S_R correlated best with the surface corrosion product deposition rate. This phenomenon can be explained by the fact that boiling causes more super-saturation of dissolved corrosion products at base of bubbles and the growth of nickel ferrite in this area is accelerated. Increased mass flow due to boiling transports more particles to the surface where they are entrained within the CRUD. Shallow boiling chimneys start to build. This process is illustrated in Figure 13.
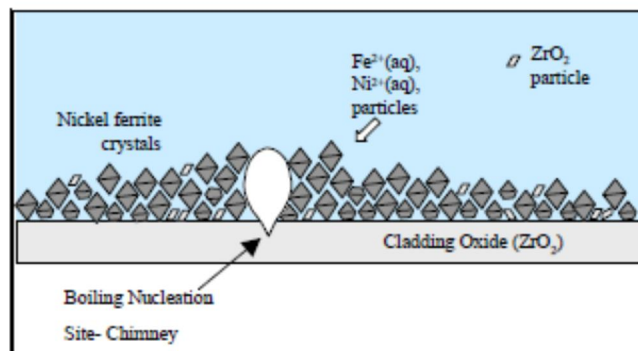
Figure 13 A possible mechanism by which sub-cooled boiling accelerates deposit growth.

7.2.2 Role of CRUD

Crud deposited on the fuel clad serves as the substrate for concentrating boron that leads to the AOA phenomenon. Thus, some discussion of its origin and characteristics are warranted for an appreciation of the key role CRUD plays. From a system-wide perspective, the reactor coolant system represents a forced-convective and non-isothermal system in which corrosion product transport, in

either soluble or particulate form, is dictated by release and deposition mechanisms [20]. Parameters that influence soluble species release and deposition are principally temperature, pH and local electrochemical potential. The local electrochemical potential is driven by the coolant hydrogen concentration. Ref. 20 points to coolant hydraulic conditions (flow rate) as having a small but not insignificant impact on corrosion and transport processes. Overall, the tendency for release and deposition will depend on the primary circuit location. While the durations are typically short, corrosion product transport can also be significantly impacted by system perturbations (e.g. power transients, pH transients).

7.2.2.1 CRUD sources from non-fuel surfaces

The main source of corrosion products that deposit on fuel surfaces is from the corrosion of steam generator (SG) tubes. The SGs comprise approximately 65-75% of the RCS surface area in PWRs. The main SG tube materials used in PWRs today are Alloy 600, Alloy 690, and Alloy 800. The nominal composition of these alloys is given in Table 6. The lower nickel content in Alloy 690 and Alloy 800, along with higher chromium levels is believed responsible for the increased corrosion resistance [19]. The data also suggest that the use of Alloy 800 in German high duty plants has contributed, at least in part, to an absence of fuel CRUD and lack of AOA in these units [19]. As described in the next section, AOA CRUD deposits tend to be nickel-rich.

Table 6 Nominal composition of nickel-based alloys and Alloy 800 (weight-%).

Material	C	Co	Cr	Cu	Fe	Mn	Ni	S	Si	Other
Alloy 600	<0.15	0.018	16	≤0.5	8	0.83	bal.	0.015	≤0.5	Al 0.23 Ti 0.25
Alloy 690	<0.05	0.011	30	≤0.5	9	0.31	bal.	0.006	≤0.5	Al 0.18 Ti 0.29
Alloy 800	0.022	0.014	20.5	0.07	44	0.75	32.5	0.0005	0.6	Al 0.28 Ti 0.44

A distinction should be made between the *corrosion rate* of the materials described above and *corrosion product release rate*. *Corrosion* of materials is a process where the exposed surface of an alloy to primary coolant is transformed to an oxide that is more thermodynamically stable. As the corrosion process continues, everything else being equal, the rate of corrosion slows down. Therefore, the corrosion rate of SG tubes is higher in Cycle 1 (and still higher in the early portion of this cycle) than in subsequent cycles. Over time, the change in corrosion rate will become indiscernible from one cycle to the next, again assuming all conditions remain the same. *Corrosion product release* accompanies the corrosion process and occurs by transport of transition metal ions through the protective oxides followed by dissolution as they enter the coolant, in which they will exist in ionic or particulate form. The rate at which the metal ion enters the coolant is in general dependent on the diffusion coefficient for the particular metal and the oxide thickness and composition, as well as how close to saturation the respective metal is in the coolant [21]. Direct attrition of solid deposits can also result in corrosion product release. Numerous investigations focus on the thickness and composition of the oxide films on Alloys 600 and 690 which are widely used as construction materials in primary PWR coolants [22-35]. Table 7 presents a summary of the oxide film thicknesses on alloys 600 and 690 formed in

different environments compatible with the primary PWR coolant conditions. Thicker films (ca. 1000 nm) are reported for films formed on the inner side of Alloy 600 tubes after 20 000 h of in-reactor exposure only [24]. The thickness of the films on Alloy 600 in lithiated water at short exposure times increases significantly (from 10 to 60 nm) when the temperature is increased from 200 to 250 °C [22]. Another important fact is that the films on Alloy 690 are usually reported to be thinner than those on Alloy 600, the difference becoming significant only for long exposure times. This means that increasing the Cr content in the alloy does substantially impede the growth of the oxide in primary PWR conditions only for long exposure periods.

Table 7. Summary of oxide thicknesses for nickel-based alloys in primary PWR conditions.

Material	Tempe-rature °C	Time / h	Water chemistry	pH	Oxygen/ Hydrogen content	Thick-ness / nm	Ref
Alloy600	360	250-1000	1200 ppm B 2 ppm Li	n.q.	1 psi H_2	< 100	[22]
Alloy 600	150-200 250 300 350	72	0.01M H_3BO_3 0.001 M LiOH	8.1	1.58 ppm H_2	10 60 80 150	[23]
Alloy 600 Ni-5%Cr Ni-30%Cr	360	100 h	pure water	7	16 cm^3/kg H_2	23 24 25	[24]
Alloy 600	330	1300 2950	1200 ppm B 2.2 ppm Li	n.q.	25 cm^3/kg H_2, < 5 ppb O_2	40 55	[25]
Alloy 600 tube ID tube OD	330	20,000	700 ppm B 1 ppm Li	n.q.	18-26 cm^3/kg H_2	1000 400	[26]
Alloy 690 tube ID tube OD	330	20,000	700 ppm B 1 ppm Li	n.q.	18-26 cm^3/kg H_2	120 60	[26]
Alloy 600	325-350	<100 >100	1000 ppm B 2 ppm Li	n.q.	25-30 cm^3/kg H_2	<20 50	[27, 29]
Alloy 690	325-350	<100 >100	1000 ppm B 2 ppm Li	n.q.	25-30 cm^3/kg H_2	18 37	[27, 29]
Alloy 600	325	400	1200 ppm B 2 ppm Li	n.q.	35 cm^3/kg H_2	20	[30]
Alloy 690	325	400	1200 ppm B 2 ppm Li	n.q.	35 cm^3/kg H_2	40	[30]
Alloy 690	325	144 2160	1000 ppm B 2 ppm Li	n.q.	33 cm^3/kg H_2	33 50	[30]
Alloy 690	325	24 144 2160	1000 ppm B 2 ppm Li	pH_{325} 7.3	< 5 ppb O_2 30 cm^3/kg H_2	30 40 60	[32]
Alloy 800	220 350	2000 360	n.q.	pH_{RT} 10.5	3-10 cm^3/kg H_2	140-150 150	[36]
Alloy 800	325	50 400	1000 ppm B 2 ppm Li	n.q.	25-30 cm^3/kg H_2	50 150	[37]

Figure 14 presents a typical compositional depth profile of the oxide formed on Alloy 690 in primary PWR coolant conditions [26-32]. The duplex nature of the film with a relatively thin Ni-rich outer layer and a thicker Cr-rich inner layer is evident from the figure. Regarding the kinetics of the evolution of film composition with exposure time, it has been reported that at short exposure times the films contain essentially Cr_2O_3, whereas $Ni(OH)_2$ and NiO are

formed for longer exposure times or in the presence of higher content of NaOH. The effect of temperature on the surface film composition in lithiated water is such that substantial Cr enrichment is observed in the temperature range 250-300 °C only, nickel being the main cationic constituent of the films for temperatures below 250 and above 300 °C [22].
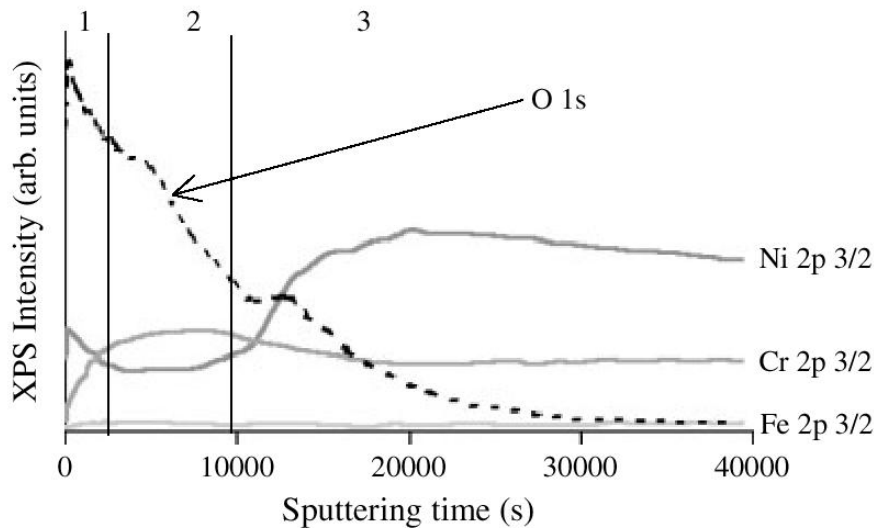

Figure 14 XPS depth profile of the film formed on Alloy 690 in a simulated PWR primary coolant conditions at 325 °C [29].

The extent of Cr enrichment in the inner layer has been reported to be a sensitive function of the water chemistry, i.e. of the concentration of lithium and boron in the coolant [25] and also the dissolved hydrogen content [27]. Furthermore, the films formed on Alloy 600 and Ni-30%Cr-9%Fe in pure hydrogenated water at 360 °C are reported to consist essentially of Cr_2O_3 [23], i.e. the solution pH seems to be another important factor in determining the in-depth composition of the films on nickel-based alloys. Another important finding regarding especially Alloy 690 is that the outer layer formed on this alloy in primary PWR coolant is not porous and no intergranular voids or channels have been detected, i.e. the microstructure of the film does not correspond to the usual duplex scale microstructure as found on stainless steels [30,31]. On the other hand, on Alloy 600 exposed during 300 h in simulated primary coolant at 360 °C under electrochemical conditions corresponding to the NiO/Ni equilibrium potential, a non-compact external oxide scale was evidenced while an inner thin continuous layer rich in Cr was observed [32]. Consequently, a Cr-depleted zone just in the underlying alloy was found [32]. In-situ Raman spectroscopy of the oxide formed on Alloy 600 in similar conditions has demonstrated that NiO is the main phase at low hydrogen concentrations (1 cm^3kg^{-1}(STP), 290-350 °C). At higher dissolved hydrogen concentrations, CrOOH (at 250-290°C) and $NiCr_2O_4$ (at 320-350 °C) have been evidenced [33]. The predominance of NiO at low hydrogen contents and Cr(III) oxide at very high hydrogen contents has been also demonstrated by XPS [34]. A mixed spinel-like Ni-Cr phase containing a certain amount of Fe was stipulated as the main constituent of the oxide at intermediate hydrogen contents.

Ziemniak and Castelli [38] and Ziemniak et al. [39] expanded on previous work in the area of thermodynamic mixing in binary spinels and concluded that although the spinel solid phase was dictated by the temperature, pH, and dissolved hydrogen concentration in the coolant, actual stoichiometry of the films was

defined by a solvus of immiscibility in the mixing of spinel binaries of normal and inverse spinels. In a nickel binary system of nickel ferrite–nickel chromite [39], the stable solvus phases at reactor temperatures (ca. 300 °C) occur at a nickel fraction of n = 0.2 and n = 0.7. This is illustrated in Figure 15. Using the data in the figure, one can illustrate the growth of the corrosion films on a nickel-based alloy such as Alloy 600 or 690. Upon exposure to hot primary reactor chemistry, the alloy begins to corrode and the chromium-rich (or chromite) sublayer begins to form first. This is probably due to the fact that chromium has a very low solubility in primary reactor coolant conditions (on the order of parts per trillion). Thus, virtually all of the chromium is left behind in the corrosion film. As increasingly more of the alloy corrodes and iron enters the film, the mole fraction of chromium is diluted until it reaches the upper solvus value (n=0.7) at the reactor coolant temperature. At this point, no more iron can enter the chromite sublayer and the iron-rich ferrite surface layer begins to form. This layer is believed to be a recrystallization layer and as such is very loosely adherent. This concept has been corroborated by recent results of Ziemniak and Hanson [40,41] for alloy 600 in high-temperature hydrogenated water with or without the addition of Zn. On the other hand, more recent results on Alloy 690 tend to indicate that the innermost layer of oxide in contact with the alloy substrate is Cr_2O_3 [42-45].
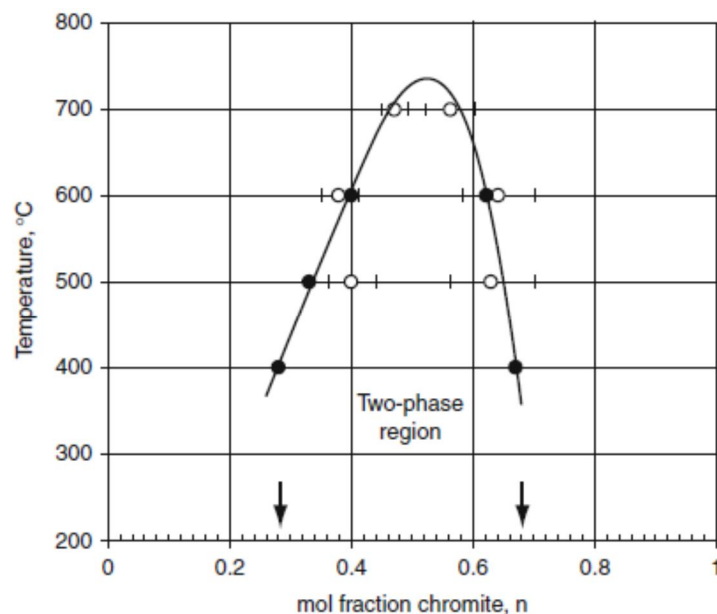

Figure 15 Solvus of immiscibility in the $NiFe_2O_4$ - $NiCr_2O_4$ spinel binary.

Concerning corrosion release, extensive data on Alloy-690 at 325 and 285 °C indicated that, at constant pH, a change of release occurs in the 20 to 500 ppm B range and in the 50 to 200 ppm B range, respectively, with higher releases at high boron concentration [46]. A test with potassium, instead of lithium, confirmed that the observed change is due to boron and not to lithium. The kinetic results at both temperatures demonstrate that there is a boron concentration effect with a temperature dependent threshold for which the release generally does not increase anymore (an example at 325 °C is presented in Figure 16. Additional data for Alloy-600 at 300 °C indicated a change of release in the 500 to 1000 ppm B range. This may be the same concentration effect, but with a different threshold due to a different test temperature. Characterization of the corrosion layers depicted a duplex microstructure with a non-continuous outer oxide and an inner homogeneous oxide. The outer layer was found to be enriched in nickel, the inner

layer with chromium, and iron is depleted in both. Boron was always located in the external scale and lithium in the inner oxide. At the oxide/alloy interface, there is Ni-enrichment, Cr-depletion and Fe-stability. The thickness of the different corrosion layers were reported to result from the test duration rather than the water chemistry [46].
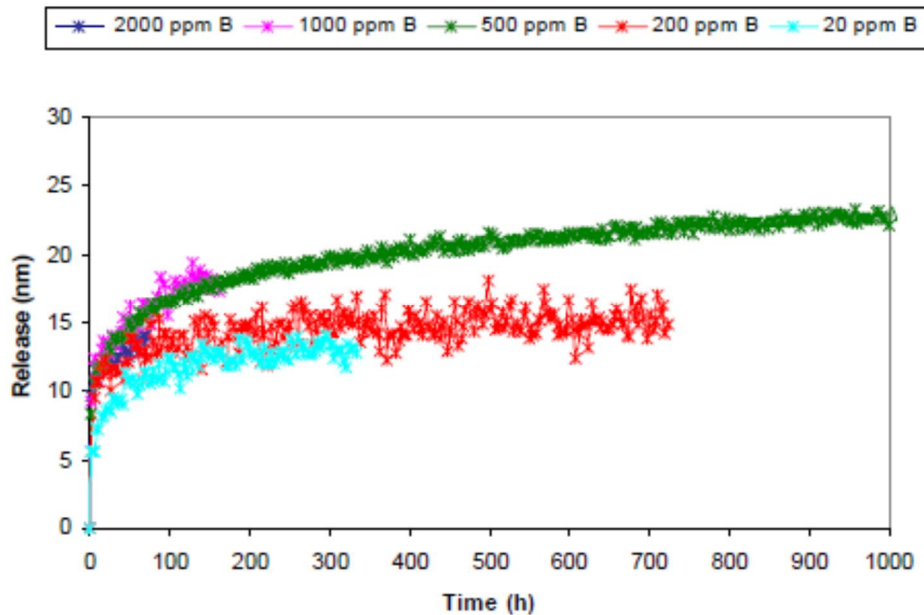

Figure 16 Influence of B concentration at constant pH on the corrosion release from Alloy 690 at 325 °C.

7.2.2.2 Crud Source from Fuel Surfaces

In most AOA cases, flux depressions have been measured on high-powered feed assemblies. CRUD deposition and AOA are a function of SNB which is typically highest in the feed assemblies. CRUD carryover from once and twice burned re-insert fuel is not a new concept, but has been evaluated more thoroughly over the past several years as a contributing source of CRUD for AOA affected feed assemblies. It has been demonstrated that CRUD on reinsert fuel can become a source of CRUD to fresh fuel during subsequent operating cycles. Whether or not reload assemblies will "give up" nickel and iron in the next cycle depends largely on the relative power of that assembly during the subsequent cycle(s) of operation.

The solubility of the metal species will depend largely on the local temperature, pH, and hydrogen concentration. Because PWR reactor coolant sample systems were not designed with quantitative corrosion product sampling in mind, theoretical models have been devised to calculate the solubilities of the relevant transition metals circulating in the coolant. As discussed here, the calculated solubilities can vary from model to model, thus emphasizing the limitations plant chemists face when evaluating high temperature corrosion product transport data from the reactor coolant.

The coolant chemistry parameter considered to have the major impact on these processes is pH_T, the pH at the coolant temperature. It is established by the relative concentrations of lithium and boron and the local temperature. Although

ammonia can be present at significant concentrations in the primary coolant, it does not ionize significantly at operating temperatures and thus does not significantly affect pH_T. In the range of current interest for PWR systems (pH_T of approximately 7.0 to 7.4) assessments of available laboratory data for Alloy 600 and stainless steels indicate that the effect of pH_T on corrosion and release rates is not particularly significant. However, pH has a significant impact on the tendency for precipitation of corrosion products from the coolant onto the fuel surfaces as a result of its effect on the solubility of iron and nickel. The maximum solubility of iron is limited to that in equilibrium with the major stable iron bearing solid phase in the primary system, i.e., nickel iron spinel. The solubility of iron in equilibrium with $NiFe_2O_4$ is shown as a function of pH_{300} in Figure 17 for coolant temperatures between 290 and 325 °C. The solubility cannot exceed its equilibrium value; however, it can be less than this value if there is a removal process from the primary coolant, e.g., precipitation on the hotter fuel surfaces.
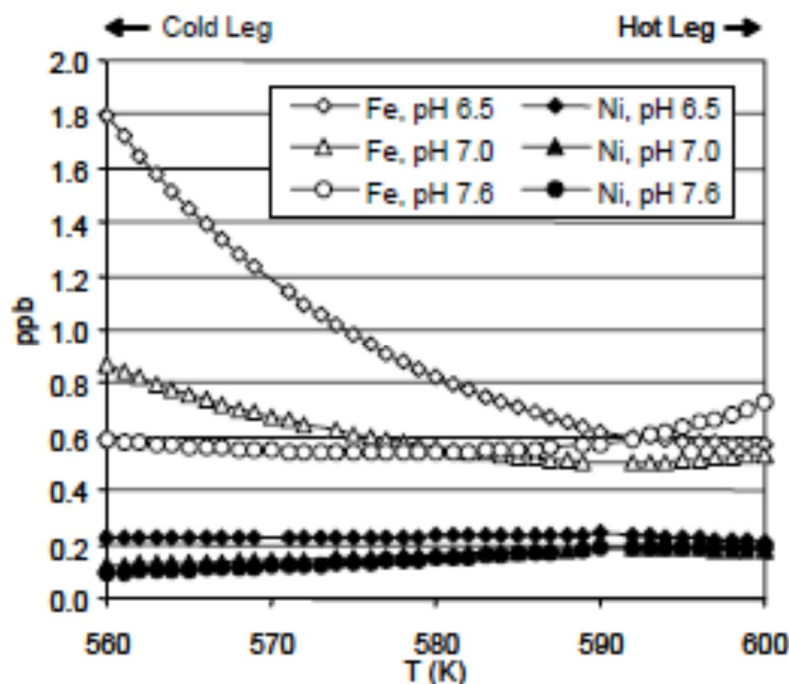

Figure 17 Variation of Fe and Ni solubility from core inlet as a function of pH_{300} as a function of temperature (650 ppm B, 25 cm^3kg^{-1} STP of dissolved hydrogen).

The precipitation of spinel is expected on the fuel surfaces and in the coolant if the pH_T is less than approximately 7.4. If precipitation occurs, the solubility at the core outlet will decrease resulting in release from the steam generator tubing and piping surfaces. If the rate of deposition increases, as is expected as the core boiling duty increases, the solubility of iron at the core outlet will decrease further thereby further increasing the iron release rate from the out-of-core surfaces. In the absence of precipitation, the coolant concentration will come to equilibrium near the solubility limit of iron. Similar but more complicated phenomena govern the behavior of nickel because the stable solid phase of nickel can vary around the system. This complicates the prediction of nickel behavior in the core, i.e., if boiling depletes the hydrogen concentration within the fuel deposit, the stable phase in the bulk coolant at a given core axial position could be Ni whereas the stable phase in the deposit could be NiO. The variation in predicted NiO solubility with coolant pH_T and temperature is also shown in Figure 17. Note that in the range of interest, pH_T has a minimal effect on NiO solubility. It is again

emphasized that thermodynamic calculations for predicting circulating corrosion product concentrations and the use of Pourbaix diagrams for predicting oxide stabilities at reactor operating temperatures have inherent uncertainties. Additionally, they do not account for any radiation effects present in the reactor. Yet, they do offer theoretical insight into what may be occurring and can be used to corroborate plant measurements.

The main CRUD characteristics as derived from such measurements can be summarized as follows:

• CRUD mass is roughly proportional to the degree of SNB.

• The nickel-to-iron ratio in CRUD tends to increase with assembly height for high SNB cores. This is also true for ratios of the activation products of nickel and iron, e.g. 58Co/59Fe and 58Co/54Mn. Two potential explanations for this observation are offered; i) CRUD tended to be thicker in the upper spans where SNB is high. As the CRUD thickens, it concentrates soluble species such as boron and lithium. If pH rises within the deposit due to concentrating lithium, the solubility of iron rises and can preclude precipitation of iron-based deposits and/or dissolve existing iron within the deposit. Since nickel solubility is essentially independent of pH at clad surface temperatures, it will remain deposited on the clad, thus raising the observed nickel-to-iron ratio. ii) Alternatively, the observed high nickel-to-iron ratio in high SNB deposits may merely be due to the presence of a less soluble nickel deposit under shutdown chemistry environments, resulting in the high measured ratios.

• Porosities within CRUD are in some cases lower near the clad and higher near the coolant interface. In others, the porosity is uniform across the CRUD deposit. Low porosity deposits accelerate the concentration process of soluble species within the deposit.

• Metallic nickel (Ni°) is typically absent in thicker deposits on rods undergoing significant SNB, while Ni° has been measured in thinner deposits from low power feed rods and from twice and thrice burned rods. NiO is more prevalent in deposits undergoing SNB.

• Thin CRUD has more chromium than thicker CRUD.

• Thick CRUD from rods undergoing significant SNB can have fully substituted nickel ferrite (Fe^{2+} is absent), whereas thinner CRUD contains partially substituted nickel ferrite (contains both Fe^{2+} and Fe^{3+}).

Several of the above observations suggest the local chemistry environment within thick deposits from rods undergoing significant SNB is different than the bulk coolant. Some possibilities that could create this shift in local chemistry are considered:

- Elevated pH from concentrating Li within the deposit,
- Due to hydrogen stripping within the deposit, radiolytically-produced oxidizing species form in small but sufficient concentration to change the ECP within the deposit, and hence deposit composition
- Concentrating boron within a deposit raises the local alpha dose via the ^{10}B (n,α) ^{7}Li reaction, which in turn, interacts with water generating higher hydrogen peroxide levels. These effects likewise change the ECP within the deposit, and hence deposit composition.

In the same way that zinc replaces cobalt on ex-core surface it can be assumed that this substitution can also take place in the CRUD. The issue is to determine if the "new zinc-CRUD" is better or worse than the "typical CRUD". From scraping

investigations, significant modifications of the distribution, structure and composition of the CRUD introduced by zinc injection have been observed. The "new zinc CRUD" seems to exhibit the following characteristics:
• It is distributed uniformly along the assemblies contrary to non zinc deposits which are mostly localized in heated regions.
• Its structure is formed by very small particles and there is no evidence of an increase of density in PWR environments.
• The zinc fraction is about 2-7%.

Based on these data, the "zinc CRUD" has been considered as "benign" [47,48]. It has been recognized that the reduced corrosion rate in the long-term can reduce fuel CRUD and its possible consequences such as AOA. Hence, there are also significant attempts to implement Zn injection as regard of first barrier integrity and power availability of unit's operation, especially as preventive/mitigation action of future fuel management evolutions.

The possibility of zinc precipitation in fuel CRUD is a major concern for any zinc injection program. Under typical PWR conditions, the solubility studies [49,50] show that zinc injection does not cause ZnO precipitation on surfaces of primary circuit, in the absence of a concentration mechanism such as SNB and zinc complexation. Therefore, zinc deposition rate is primarily driven by the SNB rate of the core and process of zinc complexation. The SNB mechanism, particularly in conjunction with thick oxide films and CRUD layers, can cause an increase in the soluble concentration into the pores of the deposit in the boiling area. In fact, the SNB -process provides a mechanism for circulating corrosion products to concentrate and deposit on the cladding surface. Once porous CRUD deposits are present, the boiling process also favors the increase in the concentration of any impurity or contaminant in the coolant within the CRUD layer. While zinc species like zincite (ZnO) and willemite (Zn_2SiO_4) are soluble in the bulk coolant [50], vaporization conditions of the coolant in SNB regions has the possibility to create localized areas where deposition can occur. These potential risks are more significant for plants with high boiling levels (high-duty cores).

7.2.3 Boron hideout

Neutron calculations show that excess boron hideout on the upper half of the fuel is needed to induce AOA. Figure 18 shows the amount of boron as a function of cycle burn-up required to induce the AOA shown in Figure 10. If this amount of B were fully released from the CRUD, a change in the RCS boron concentration of about 5 ppm would occur.

Analytical studies of mass transfer in porous materials overlaying boiling surfaces indicate that concentrations of solute can build within CRUD. Once a sufficient CRUD thickness is achieved, the ratio of surface to bulk concentrations of a soluble chemical species can increase as an exponential function of the surface boiling heat flux. Thus, sub-cooled nucleate boiling duty can result in CRUD deposition containing coolant additives, such as lithium and boron. On one hand, it is suggested the most likely boron hideout process is via lithium meta-borate ($LiBO_2$) precipitation within the deposit. As $LiBO_2$ has retrograde solubility with respect to temperature (i.e. solubility drops as temperature is increased and vise versa), this hypothesis is supported by observations of reactor coolant lithium return during power reductions in plants symptomatic of AOA. Plants with AOA cycles have also

observed hideout of lithium after return to full power (raised temperature and resumption of SNB). An example of that is given in Figure 19. However, the requisite concentration factors believed necessary to precipitate $LiBO_2$ were found to be difficult to achieve. On the other hand, bonaccordite (Ni_2FeBO_5) has been observed in at least one PWR CRUD deposit and while not specifically analyzed, may have been present in another deposit based on the similarities of the two CRUDs. While it is speculated that bonaccordite is likely to form under the severest in-situ conditions, the presence of boron in this oxide certainly must contribute to the observed AOA in these cases. A scheme of CRUD containing bonaccordite for a plant experiencing severe AOA is shown in Figure 20, left [51].
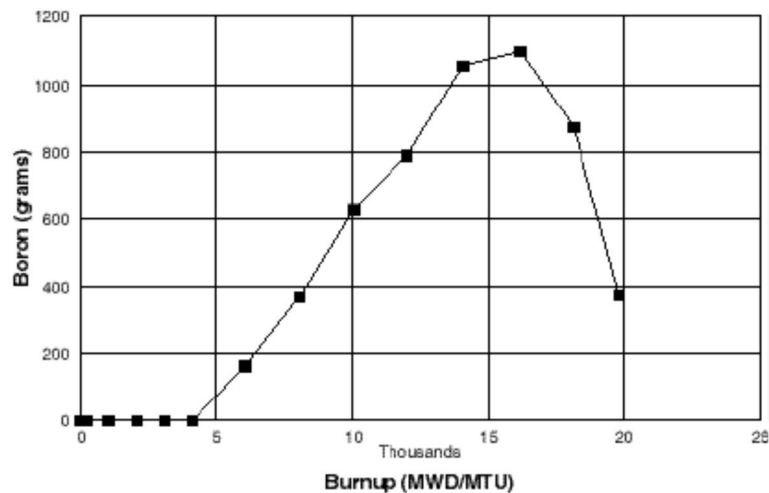

Figure 18 Boron Required to Deposit on the Top Half of the Core to Account for the Observed Axial Offset Deviation Shown in Figure 10.
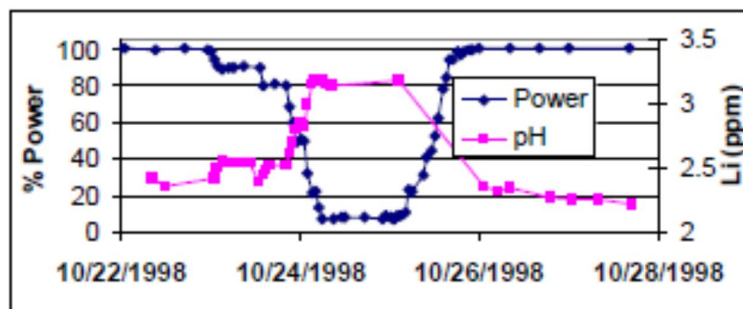

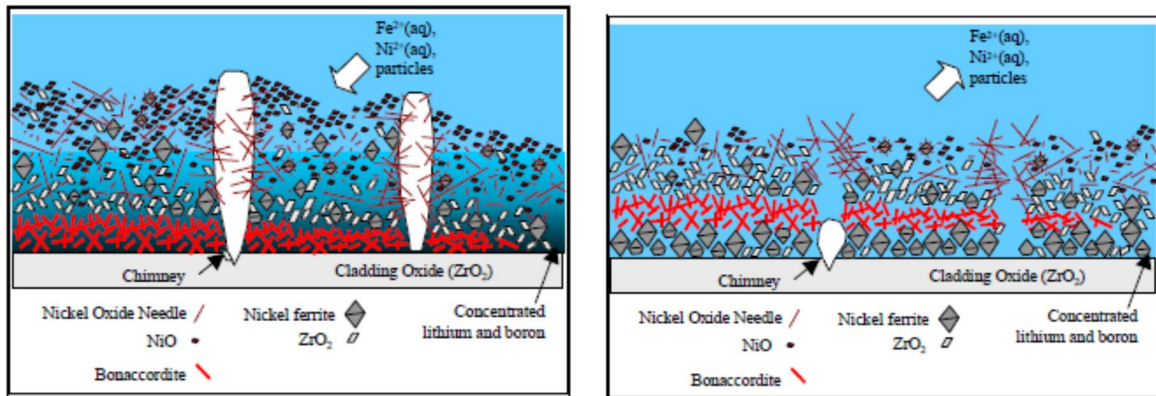*Figure 19 Example of Li behavior during a power transient.*

Figure 20 (left) CRUD structure with severe AOA, (right) transformation of the CRUD after temperature reduction in a subsequent cycle.

On the other hand, the effect of the coolant temperature decrease due to the power output reduction in a subsequent cycle was reported to have a strong impact on CRUD (Figure 20, right). The temperature change initiated an escalating particulate release from the core. The changes in the microstructure can be explained by the disappearance of the concentrated lithium borate solution with reduced boiling. Nickel ferrite was favored in the new environment and grew under old deposits. The zirconium oxide content of deposits increased as the nickel oxide and bonaccordite species dissolved. However, nickel oxide and bonaccordite dissolved only very slowly, and much of the original structure was conserved.

In the PWR core, the formation of Ni_2FeBO_5 can start early in the fuel cycle, in the presence of a high power density especially on high span first feed assemblies, high Ni and Fe species transport at high Ni/Fe mass ratios, and high concentrations of B and Li near the fuel surface [51-54]. Conditions leading to the accumulation of Ni and Fe oxides at Ni/Fe mass ratios larger than 2 may lead to accumulation of large amounts of Ni_2FeBO_5 on fuel. Such adverse conditions should be avoided in high boiling duty cores. It is proposed that neutron capture reactions $10B(n,\alpha)7Li$ may play a decisive role in modifying the microchemistry of water in metal oxide deposits on high-duty reactor fuel. The heat and alkaline/ oxidizing conditions produced by 10B-n reactions in fuel CRUD are needed to promote the transformation of $NiO/NiFe_2O_4$ to Ni_2FeBO_5. Elevation of the pH level, resulting both from concentration due to under-deposit boiling and nuclear production of 7Li from n-10B reactions near CRUD pores, most likely plays a significant role in the formation of Ni_2FeBO_5. Such reactions can produce significant amount of lithium, thus providing – in addition to boiling concentration mechanism – aggressive alkaline conditions in the fuel CRUD layers. The production of lithium in neutron capture $10B(n,\alpha)7Li$ reactions and their effects on local pH and temperature should be taken into account in further development of models of Axial Offset Anomaly of neutron flux in PWRs.

8 State-of-the-art of the CRUD deposition modeling

8.1 Introduction

As pressurized water reactors (PWRs) have increased cycle lengths and undergone power up-rates, some reactors have experienced increased deposits on the fuel cladding. These deposits arise from deposition of corrosion products released from reactor coolant system (RCS) surfaces onto fuel cladding and as mentioned in the previous chapter, are referred to as CRUD. While difficult to characterize directly because of the impacts of plant shutdown chemistry on their form, CRUD scrapes from the fuel and high temperature water sampling has shown that PWR CRUD is composed mostly of Ni-Fe-Cr oxides and reach thicknesses up to 75 μm. The CRUD is rather porous, and during the onset of sub-cooled nucleate boiling, boron and lithium may concentrate within the CRUD. Boron is a neutron absorber, and the increased boron mass within the CRUD has impacts on the neutronics. The CRUD deposits can cause shifts in the core neutron flux, referred to as axial offset anomaly (AOA) or CRUD induced power shift (CIPS). Plants that exceed acceptable limits are forced to reduce power or shut down [55].

The modeling of CRUD formation is directly related to the modeling of accumulated radiation on the wet surfaces of the structures of the primary loop of a PWR, due to the activation and mass transport of dissolved corrosion products in the primary coolant. The term activity transport refers to the accumulation of radioactivity on the interior surfaces of the primary loop structures of a PWR that are in contact with the primary coolant, due to the activation of dissolved corrosion products in the primary coolant. An overview of the physical process behind this phenomenon is given below [56].

- The inner surfaces of the structures of the primary loop, such as the interior of the piping and steam generators, corrode as a consequence of their contact with the primary coolant.
- The corrosion layers are dissolved into the primary coolant. The dissolution of the corrosion products is considered to be described by an equilibrium electrochemical and chemical system formed by primary loop structures and the primary coolant.
- The dissolved corrosion products, now aqueous species of the elements found in the corrosion layers on the wetted surfaces of the primary loop structures, travel with the primary coolant through the reactor core, where some of them will absorb a neutron.
- The absorption process is also called neutron activation, and changes the atomic weight of the isotope in question. This change in atomic weight may cause the struck isotope to become unstable, and hence radioactive.
- The normal and radioactive isotopes travel with the primary coolant out of the core and, through a change in saturation concentration of the isotope, deposit on the interior walls of the primary loop structures.

Clearly, as this chain of processes is repeated the amount of radioactive nuclides on the wetted surfaces of the primary loop structures will increase, leading to a build-up of radiation fields in that area of the plant. This process is schematically illustrated in Figure 21.
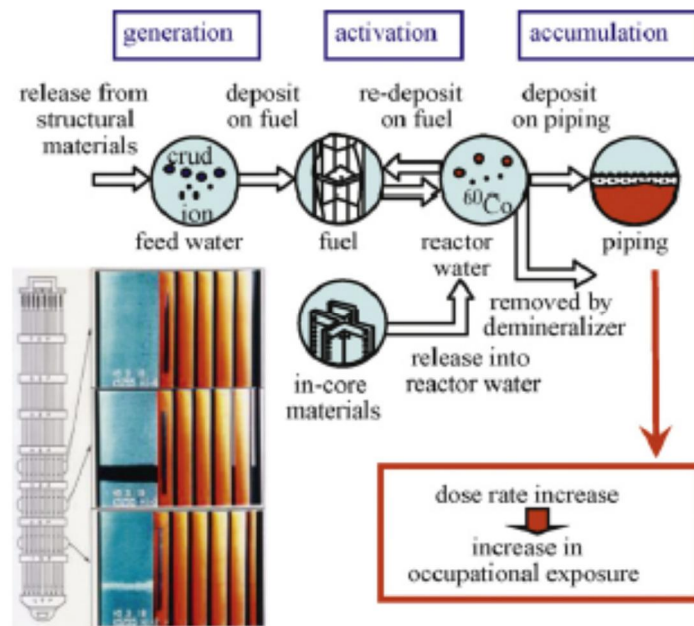
Figure 21 Corrosion product behavior – generation, activation and accumulation.

In the following sections, a review of existing models for activity accumulation will be presented with special emphasis on their ability to predict CRUD deposition and behavior.

8.2 Review of existing models for activity accumulation

8.2.1 CPAIR-P model

Mirza et al. proposed a computer simulation model to describe the corrosion product activity in the primary coolant of pressurized water reactors [57-61]. The most recent modifications include the ability to simulate flow rate transients and account for linearly and non-linearly accelerating corrosion during the fuel cycle. The original model is based on five physical processes: the production of activated CRUD products due to their passing through the neutron flux in the core, the removal of activated isotopes due to purification of the water, the removal of activated isotopes from the primary coolant due to deposition on the interior surfaces of the primary loop structures, leakage of coolant from the primary loop, and radioactive decay of these isotopes. At first, uniform time independent corrosion has been assumed, whereas in later versions, linearly and non-linearly increasing corrosion has been also included. The concentration gradients are assumed to be zero at a given point along the primary loop, which signifies the effects of local concentration gradients have been ignored. Finally, the precipitation of CRUD and activated species onto the interior wetted surfaces of the primary coolant loop structures is assumed to occur in the same proportion as the species are found in the primary coolant. Figure 22 is a diagram of the many possible paths of how the generation and removal of activated corrosion products may occur in the primary coolant of a typical PWR according to this model.

A major feature of this approach is the mass balance approach to quantifying the number of nuclides, precursor and activated, by describing the source and loss terms. While these terms certainly represent physical processes occurring, the

mechanisms for predicting these rates are not present. All of these rates are taken as empirical or previously calculated results, and are not derived from any sort of first principles in the code itself. Even with this disadvantage, the code has merit in its consideration of many physical processes.

8.2.2 ACE-II

The ACE-II code was developed to predict the residual radiation fields in the components of Japanese style PWRs. The code is also largely empirical in nature [62,63]. The process of activity transport and diffusion of activated isotopes into the construction materials is described by the following sequence of physical phenomena:

- Inner and outer oxides form on the wetted surfaces of the primary loop components due to corrosion
- The corrosion is released into the primary coolant by dissolution and erosion of the outer oxide layer.
- The dissolved and particulate corrosion products in the primary coolant are activated as they travel through the intense radiation fields in the core.
- The particulate and dissolved corrosion products, both non-activated and activated are precipitated onto the wetted surfaced of the primary loop components, resulting in a buildup of CRUD.
- Activated isotopes in the CRUD diffuse into the outer layer oxides, and then into the inner layer oxides, and eventually into the construction materials themselves by isotopic exchange.
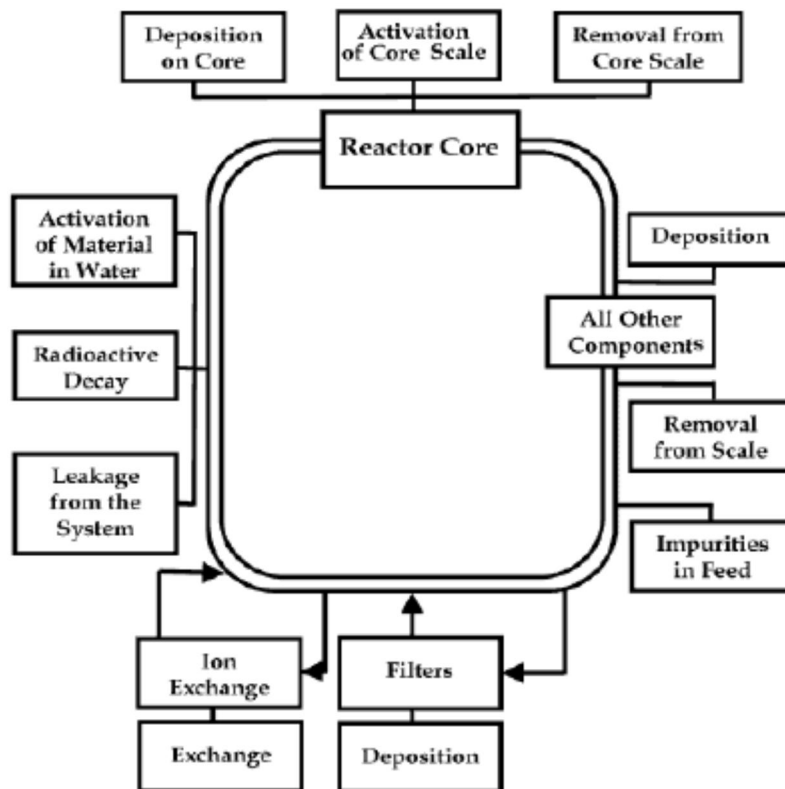

Figure 22 Diagram of situations that can lead to the generation and removal of activated corrosion products in the primary coolant of a typical PWR [57].

The code also identifies that the corrosion products released from the core are to be activated before they are released, providing a source of activated corrosion products that do not occur by activation after being released into the coolant. The corrosion products accounted for are Co-58 and Co-60, with precursor isotopes of iron, nickel, and cobalt. The code uses solubility to describe mass transfer. It either calculates or uses experimentally determined solubility for NiO, Ni and $NiFe_2O_4$. Cobalt's solubility is not calculated; instead the movement of cobalt is determined by the movement of the nickel ferrite. All of the above listed processes are quantified through empirical measurements. None of the processes are quantified by fundamental principles, making the code difficult to adapt to different styles of nuclear power plants; however, for the Japanese PWRs, the code works well [10]. The volume mesh for the code considers many segments of the primary loop, which allows for detailed calculation of radiation field buildup in a given area. Figure 23 shows a diagram of the processes described by the ACE-II code for a given element.
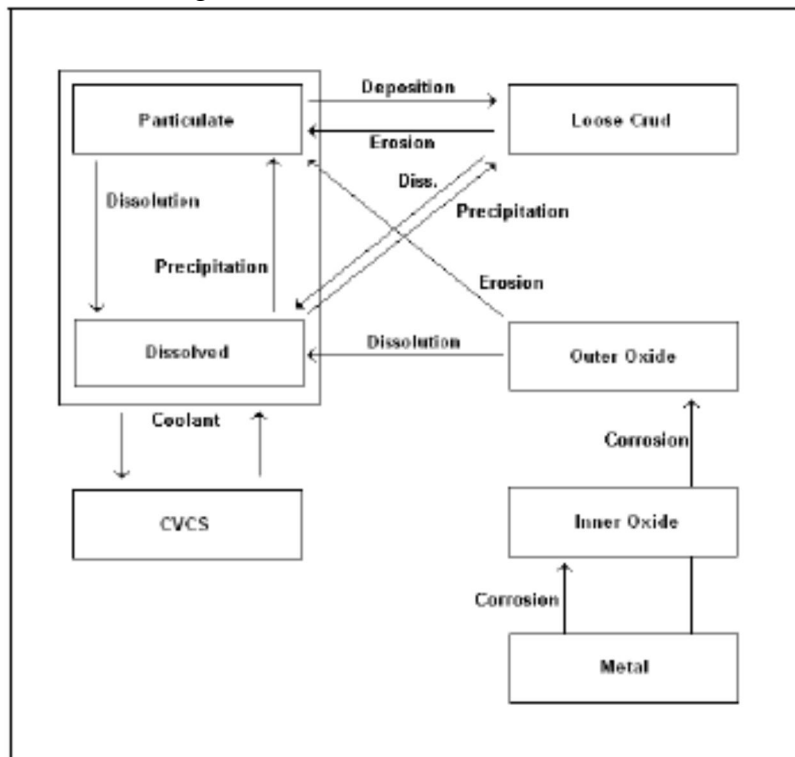

Figure 23 Diagram of the mass transport processes modeled in the ACE-II approach.

8.2.3 MIGA-RT code

The activity transport code MIGA-RT originated in Bulgaria and has been used to make predictions about radiation fields in PWR and VVER type reactors [64]. The most recent versions of this code focus on the use of particulate forms of corrosion products to predict the accumulation of radiation around the primary heat transfer loop. This approach was taken from previous work in which an analytical model to calculate mass transfer coefficients for particulate corrosion products has been advanced [65]. The mass transfer of particles is assumed to be dependent upon the interior surface conditions of the coolant pipes and sticking probabilities. While the emphasis in this model is on particle deposition, the model still includes the effects of soluble corrosion products in the primary coolant. The dissolved corrosion products are quantified by using a parabolic rate law for the first fuel cycle, and a constant release rate for subsequent cycles.

Particulate forms of the corrosion products are assumed to be released into the coolant by erosion of the corrosion films on the wetted surfaces due to the primary coolant flow. The elemental solubility of iron and nickel and the ratio of these elements in the construction materials of the primary loop determine the release rates of the corrosion products. These products are magnetite, nickel ferrite, sub-stoichiometric nickel ferrite, metallic nickel, and nickel oxide. The activated isotopes considered by MIGA-RT are Co-58 and Co-60; they are characterized in the primary coolant in the same manner as their precursor isotopes. The change in time is simulated by changing the water chemistry conditions as appropriate for the duration of a normal fuel cycle [63].

8.2.4 PACTOLE models

The Pactole series of codes are considered to be one of the the most developed and advanced series of activity transport codes [66]. The Pactole-2 version of the code used analytical solutions for many of its calculations, while the version Pactole-3 employed numerical methods and object oriented languages to perform the calculations. This code has been under development in France for nearly 20 years, and is also considered by the authors to contain all of the necessary and relevant mechanisms for predicting activity transport. Pactole works from the assumption that corrosion layers on the internal surfaces of the primary loop components release corrosion products directly into the primary coolant.

Both the inner and outer oxide layers are considered to be composed of the same species, namely oxides of the elements found in the base metal. The thickness of the inner layer is used to determine the rate of release of dissolved ions into the coolant, while the thickness of the outer oxide layer, beyond a critical thickness, is used to determine the rate of erosion of particulate corrosion products into the coolant. Pactole-3 will also include the effects of dissolution kinetics on reaction rates as new parameter for determining the rate of release of ions into the coolant. The mass transfer of magnetite is solved completely in this model, and is used to determine the mass transfer of other ferrites, including manganese ferrite, cobalt ferrite, and nickel ferrite. Precipitation of any of these ferrites is determined to occur when their concentration in the bulk coolant exceeds their saturation concentration in a given section of the primary loop. According to the model, precipitation can occur at any point around the primary loop, including both in-core and out-of-core areas. The water chemistry of the primary coolant, in this model, is assumed to be dominated by the addition of boron and lithium to the system for the purposes of pH control. Other deposition methods, besides precipitation due to concentration gradients of dissolved species, are considered to occur as well; precipitation of particulate corrosion products can occur by turbulent diffusion, thermophoresis, and gravitational settling.

Ten activated nuclides are modeled in the Pactole series of codes. They are isotopes of iron, nickel, manganese, chromium, cobalt, and zirconium created by neutron activation from both thermal and fast neutrons. Permanent radiation field growth due to isotopic exchange with both the base metal and inner oxide layers is also accounted for in this model. In terms of program mechanics, the Pactole codes incorporate a fixed water chemistry system, meaning the system conserves mass. The primary loop is divided into seventy sections -eight for the CVCS system, four for each steam generator, forty-two are included in the core, while the rest of the sections are other supporting structures of the primary loop. The

PACTOLE V 3.0 code is based on a control volume approach, the primary circuit is represented by an arrangement of several volumes in which transient mass balance equations are solved:

$$\frac{\partial m_i}{\partial t}+\left(m_s-m_e\right)=\sum_{source} J_m-\sum_{sink} J_m \qquad (12)$$

where m_i is the mass of the ith isotope in a considered medium defined as a form for the corrosion products, t is the time, m_s-m_e is the convective term (balance between input and output) and except for nuclear reaction, which are mass production/loss within the considered medium, J_m is an exchange mass rate between two different media. Seven different media are taken into account in a control volume and depicted in Figure 24 below. The transfer mechanisms, which are modeled in the mass balance equations, between all the considered media, are summarized in Figure 25.
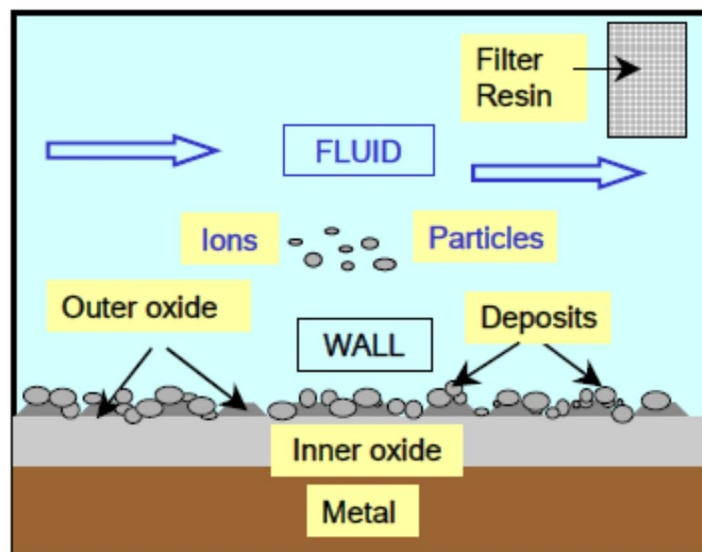

Figure 24 Media in a Control Volume for a PACTOLE representation.
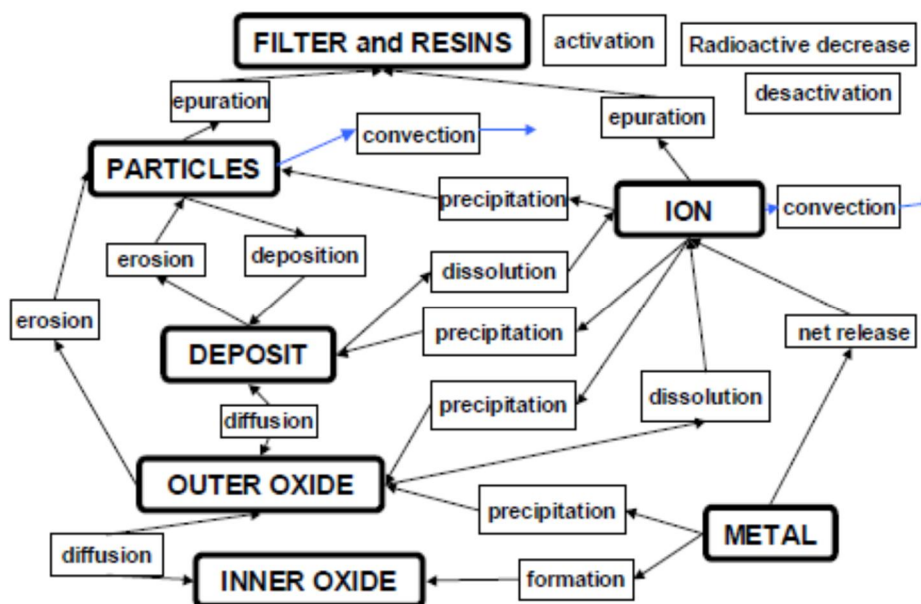

Figure 25 Transfer processes between media in a control volume.

The corrosion and release processes are formulated in the mass balance equations as functions of their time production rates that now enable to describe the consequences of material surface treatments on the corrosion and release processes and, so that, on the primary circuit contamination. The corrosion kinetics and the release kinetics can be measured for different alloys with different fabrication processes using, for instance, the CORELE or BOREAL loops [68]. In the proposed modeling, corrosion is the process by which the base metal becomes oxidized. This oxidation leads to several mass transfer processes, which are: generation of an inner oxide, generation of an outer oxide and release of metallic ions directly in the fluid. These transfers are shown in Figure 26. In the PACTOLE V3 code, corrosion and release mass transfers are, respectively, directly dependent of a corrosion and of a release velocity, which are defined by the user.
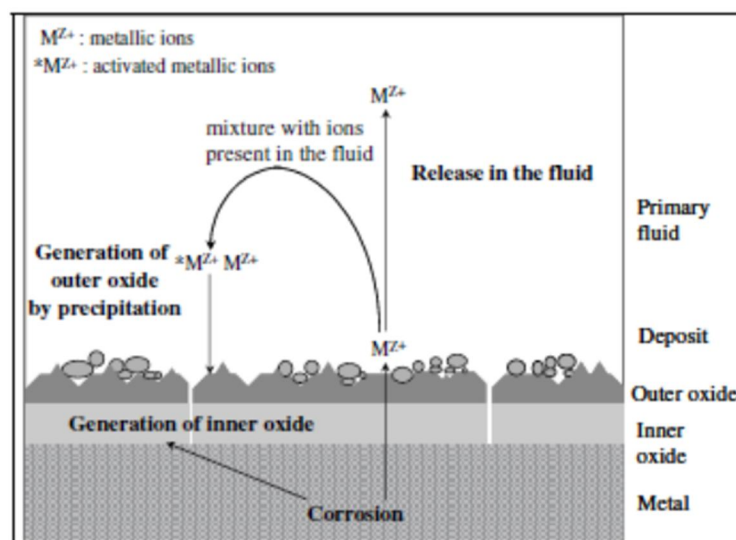

Figure 26 PACTOLE local modeling for inner and outer oxide generations and ion release

Major improvements have been achieved in the V3.0 PACTOLE code version for the data processing architecture and numerical analysis for solving transient equations [69]. This new architecture will allow the PACTOLE code of being an integration tool for the complex physics involved in contamination transfer studies. Some physical models have been already modified (among them corrosion and release rates), but there are still both existing models to improve and new models to implement. The making of a willful work program for improving the physical models and the data is under way. The chemistry module is being improved for the PACTOLE V3.1 code. A new approach for oxide determination and equilibrium concentration calculation has been developed by CEA. This model, based on a survey of oxides thermodynamic behavior, is aimed at predicting in a more accurate way the equilibrium concentration values.

Other important steps in the PACTOLE code development for version 3.1 were as follows:

- Improvement of the corrosion/release mechanism. Based on the present empirical mathematical expression, the impact of macroscopic parameters such as solubility or temperature is thought to be accounted for.
- Addition of a specific module for shutdown. In the present model, only reducing conditions can be treated: a real simulation of oxygenation phase

is therefore impossible at this point. Due, for a large part, to the lack of available data, an important effort is devoted to the data collection of oxide characteristics in oxidizing conditions.

8.2.5 Activity build-up model of Macdonald and co-workers

The review of codes in this chapter has demonstrated the diversity present in existing approaches to modeling activity transport in PWRs. The various approaches emphasized different processes which they consider important. Most models considered the mass transport of dissolved ions and particulate corrosion products, while one, MIGA-RT, looked between these two states and described the formation and deposition of colloids. The primary variation between codes is the area of detail present in each model. For example, Mirza et al. [57] chose to identify and quantify many sources and deposits of mass transfer, while PACTOLE focused on the microscopic model of the surface-coolant interface to describe the release of corrosion products into the coolant [69].

A common feature of many of the codes is the use of various empirically determined constants. This feature precludes them from being applied to primary circuits other than the ones they have been specifically designed to model, because the necessary constants may not be applicable to different loops or the data may not be available. In this respect, the purpose of Macdonald et al. [56] was to take previously developed modeling techniques for activity transport and use them in a model not dominated by empirical constants. More specifically, the goal was to create a model that predicts the extent of activity transport from the physical properties of the primary coolant circuit, such as the temperature, chemical characteristics, hydrodynamic properties, and, most importantly, the electrochemical properties. The calculation of the ECP, at a given position along the primary loop of a PWR, is the basis of the model proposed by Macdonald and co-workers. In the primary loop of a PWR, this quantity is significant because of its variance with position in the loop, due to changes in thermal-hydraulic parameters, temperature, pH, and the local concentration of electro-active species. The ECP is a function of these values, thus, they must be known in order to calculate it. The thermal-hydraulic parameters and temperature were adopted from TRACE, the Nuclear Regulatory Commission's accident safety code. The local pH, as a function of temperature, and the local concentration of electro-active species is calculated by considering a system of chemical reactions involving the primary species responsible for determining pH, namely boron and lithium hydroxide. Quantifying the local concentrations of electro-active species is performed by first identifying the important species, and then determining their rates of production and consumption. Finally, the ECP is calculated using a Mixed Potential Model (MPM) [70,71].

Figure 27 gives a graphical representation of the nodes according to the model of Macdonald et al. [56]. Each section of the loop is considered to be comprised of only one material. The flow is assumed to be constant, over a node, and only in the axial direction of the node.

The dissolution/precipitation of corrosion products into/out of the primary coolant is determined by chemical and electrochemical processes. The saturation point, or surface concentration, of the corrosion products in the primary coolant is determined by considering the chemical and electrochemical reactions that reduce

the species found in the passive corrosion films into aqueous ions. The approach used to calculate this was presented by Urquidi-Macdonald and D. D. Macdonald for the release of magnetite into the primary coolant of PWRs, in order to describe the mass transport of magnetite around the primary coolant loop [70]. Their approach has been broadened to include other species likely to be found in the primary coolant. These species are listed on the left hand side of Table 8, and were chosen because of the corrosion film composition.
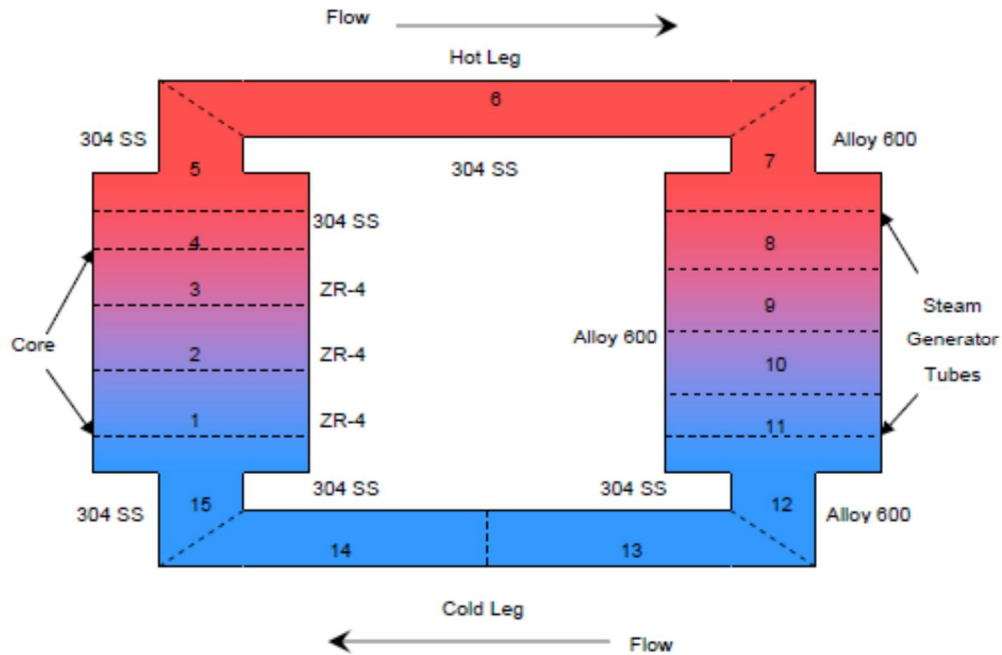

Figure 27 Graphical View of Primary Loop nodalization according to the model.

Table 8 Corrosion products found in the primary loop and the aqueous species used to determine surface concentration at the coolant-metal interface.

Corrosion Products	Aqueous Species
Fe_3O_4	$M(OH)_i^{(2-i)+}$
Fe_2O_3	$M = Fe, Cr, Ni, Co$
Cr_2O_3 $\Rightarrow$	
ZrO_2	$M(OH)_i^{(3-i)+}$
NiO	$M = Fe, Cr, Co$
CoO $\Rightarrow$	
Ni	$M(OH)_i^{(4-i)+}$
Co	$M = Zr$

Special consideration has been taken in this model to accurately describe the rate of dissolution during cold shutdown due to scheduled outages, such as refueling. The special consideration was derived from a limitation of the MPM model for the calculation of ECP [56].Currently, no measurements to derive values for the radiolysis constants during times of PWR cold shutdown are available. Because of this, Macdonald et al. [56] decided that until the predictions of the ECP code can be validated against experimentally measured values for times at cold shutdown, the hydrogen equilibrium potential should be used instead of the predicted corrosion potential.

Further, the concentration of an ion in the bulk of the coolant is calculated from the equilibrium values at the surface by examining the difference between surface and the bulk concentrations, and hence, determining rates of dissolution or precipitation. Precipitation is assumed to occur at the location where the bulk concentration is greater than the local equilibrium concentration of the coolant-metal interface. Then the rate of release/deposition of certain species in a defined node is given by

$$R_{ij} = D_{ij} \frac{\partial c_{ij}}{\partial x} A_j = \frac{D_{ij} Sh_j A_j C}{L_j} \left(c_{s,ij} - c_{b,ij} \right) \tag{13}$$

In equation (13), the subscript i refers to the ith hydrolyzed species of a given corrosion product listed inTable 8; $D_{i,j}$ is the diffusion constant for the species in question, Sh_j is the Sherwood number for the jth section, and L_j is the characteristic length for that section. The wet area of the jth node is A_j, and C is an unit conversion factor to give the rate in mol s^{-1}. The temperature dependence of the diffusion coefficient constant is presumed to be of Arrhenius type. As the model considers only the activation by thermal neutrons, the rate of activation of the ith species in the jth node of the loop is given as:

$$ACT_{ij} = c_{b,isotope,i} \Phi_j \sigma_j \tag{14}$$

In this relation, $c_{b,isotope,i}$ is the volume concentration of isotopes present, Φ_j is the neutron flux in the jth section, and σ_i is the neutron capture cross-section. Table 9 lists the nuclear reactions that are considered in this model. These reactions were chosen based on the corrosion products dissolving into the system, a review of the isotopes modeled in existing codes and information about measurements taken by plant owners and operators.

Table 9 Nuclear Reactions considered in the model.

1	$^{54}Fe(n, \gamma)^{55}Fe$
2	$^{58}Fe(n, \gamma)^{59}Fe$
3	$^{50}Cr(n, \gamma)^{51}Cr$
4	$^{59}Co(n, \gamma)^{60}Co$
5	$^{94}Zr(n, \gamma)^{95}Zr$
6	$^{58}Ni(n, p)^{58}Co$
7	$^{58}Co(n, \gamma)^{59}Co$

The most critical set of physical values to this model are the Gibbs energies of formation for the full cell reactions that correspond to the reactions listed in Table 8. During the course of developing the model, the authors stated that not all of the values contained in the available databases are entirely accurate.

As an example of a calculation using the model, Figure 28 shows the calculated surface concentrations normalized in a fashion to show the trends of all the components. The values are the concentration for a node, minus the average concentration from around the loop of that element, with that difference being divided by the average. Clearly, an inverse solubility is predicted for nickel; the change in concentration of nickel is the most pronounced of the elements. This implies that as the bulk concentration of nickel rises, one may expect to see precipitation occur in larger amounts in the higher temperature areas, such as the

hot leg. Figure 29 shows a non-logarithm scale of the total accumulated activity in each node, after an operating period of eighteen months. Two distinct maxima occur at nodes 6 and 14, which are the hot and cold legs, respectively. Also of interest is the drop through the steam generator, although it becomes clear substantial accumulation will occur in the steam generator tubes.
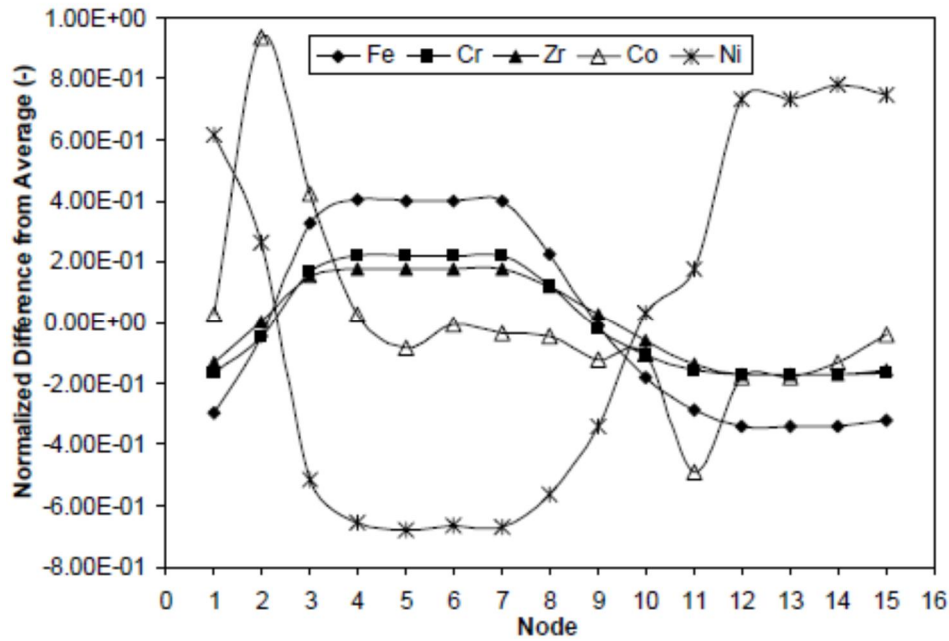

Figure 28 Surface concentration trends according to the model. Normal operating conditions, $[H_2]=25 \ cm^3 \ kg^{-1}$ (STP); $[O_2]=5$ ppb. The trends are given for each element as a whole, that is, the sum of all of the species of the same element.
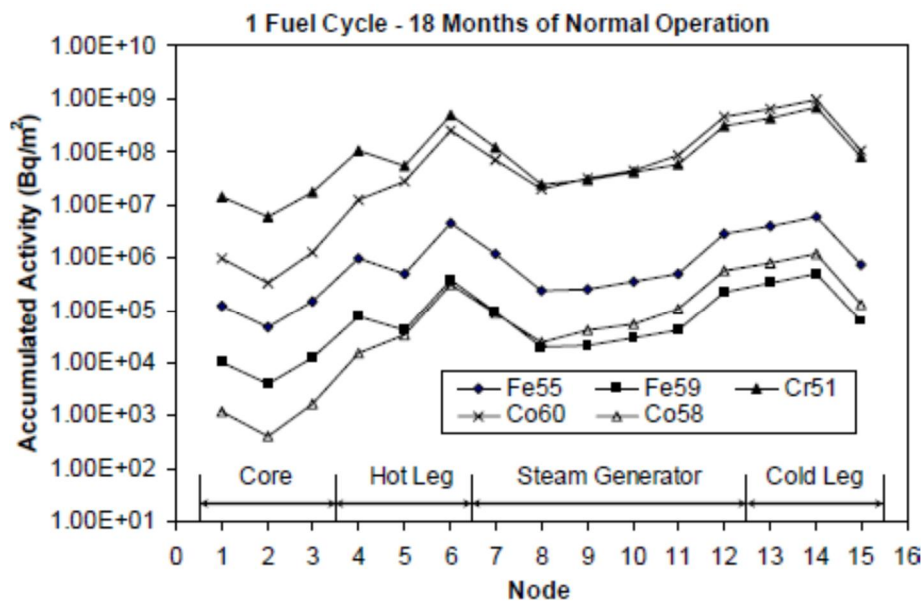

Figure 29 The accumulated activity in each node, by isotope, after 18 months of operation (a typical fuel cycle or a PWR). Nodes as in Fig. 27.

The model predicts cobalt and chromium are the dominating corrosion products in terms of activity transport in PWRs. Ultimately, by the sequence of the

calculations described above, the corrosion products with the greatest collective surface concentrations around the loop will produce the highest steady state concentration in the bulk coolant, and hence, the largest concentration of activated isotopes, assuming the physical constants are not abnormally large or small for this isotope. In the case of this model, Cr and Co routinely have the greatest local concentrations; with the iron and nickel having the next highest concentrations. The first conclusion we can draw from this is that if a material is causing an activity transport problem, it is paramount to reduce the surface concentrations as much as possible. Steps have already been taken in a range of plants to reduce the amount of cobalt in some plants by the replacement of materials. A second conclusion is that great care must be taken when calculating the surface concentrations of each ion. As said previously, these values determine the outcome of the entire model, and should certainly be studied to further improve its accuracy.

8.2.6 The model of Castelli

This very recently described model [72] is based on extensive work on quantifying the film formation and corrosion release rates of construction materials in PWRs by Ziemniak et al. [40,41,73,74] in the past decade. The mathematical expression to characterize the total oxide growth rate is the well-known parabolic expression considered to be a limiting case of Wagner's theory of film growth for thick layers

$$m_r = \left(k_p - k_r \right)^{1/2} \tag{15}$$

where k_r is the release rate coefficient usually stated as a percentage of the total growth rate. A more accurate description of this rate constant would be to call it the apparent release rate because it describes the mass of alloy that has been converted to an oxide phase that is not present in the residual chromite and ferrite sublayers usually formed on stainless steels and nickel-based alloys. In an ideal case, the corrosion rate of each different alloy would be described by a single rate constant (k_p) unique to that alloy under all conditions. As a first approach to the real situation, the model takes into account the empirically found dependences of the parabolic rate constant on temperature, initial surface condition and coolant additives such as Zn. Further, empirically determined ratios between the parabolic rate constant and corrosion release rate constant are used, such as for AISI 304 stainless steel [73]

$$\overline{k}_r = [k_p - 0.42 \left(k_p - k_r \right)] \tag{16}$$

 In addition, elemental speciation of the alloy corrosion growth and release rate is used, as exemplified in Table 10. Implicit in this speciation is the assumption that all Cr remains in the chromite sublayer.

All parts of the coolant loop were modeled as a simple pipe defined by a material, a hydraulic diameter (d_h), and a hydraulic length (l_h) if one knows the wetted surface area (A_s), the part volume (V), and the cross-sectional flow area (A_f) of the region. This assumption describes the entire circuit in the spatial domain as a length (X) that is subdivided into many smaller analytical cells of space and time. A schematic representation of a discrete analytical cell is given in Figure 30 together with the associated physico-chemical processes. The rate constants pertinent to these processes are collected in Table 11, whereas the nuclear

processes considered for the activation of corrosion products are shown in Table 12.

Table 10 Evaluated Corrosion Growth and Total Release rates (mg dm^{-2}-t$^{-1/2}$)

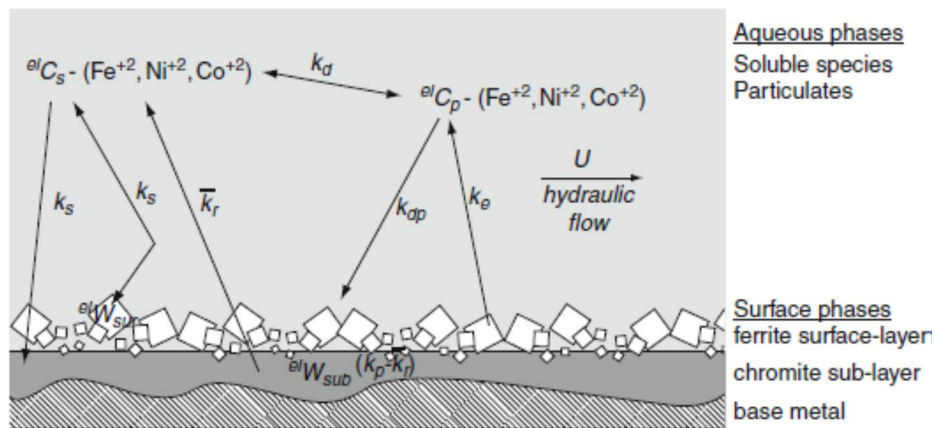| Element	$\bar{k}_p$	$\bar{k}_r$	$\bar{k}_p$	$\bar{k}_r$
	As Machined		Electropolished	
304 stainless steel				
Fe	0.8728	0.5950	0.2909	0.1983
Ni	0.0824	0.0524	0.0275	0.0175
Alloy 600				
Fe	0.0996	0.0527	0.0199	0.0105
Ni	0.0642	0.0294	0.0128	0.0059
Alloy 690				
Fe	0.0461	0.0354	0.0092	0.0071
Ni	0.0226	0.0182	0.0045	0.0036

Figure 30 Schematic of the dependent variables and physicochemical processes in a prototypical analytical cell according to the Castelli's model.

Table 11 Summary of Processes and Rate Constants pertinent to the physico-chemical processes taken into account in Castelli's model.

Process	Rate Constant	Sublayer	Surface Layer	Solubles	Particulates
Corrosion growth	$(k_p - \bar{k}_r)$	Source			
Corrosion release	$\bar{k}_r$			Source	
Hydrothermal crystallization dissolution	k_s	Source or loss	Source or loss	Source or loss	
Particulate deposition	k_{dp}		Source		Loss
Particulate erosion	k_e		Loss		Source
Particulate crystallization dissolution	k_d			Source or loss	Source or loss
Hydraulic flow	U			Source and loss	Source and loss

Table 12 Summary of the nuclear processes considered in the model.

Stable Precursor (% Abundance)	Production Reaction	Radionuclide Produced	Half-life	Thermal Production Cross Section (bn)	Resonance Integral Production Cross Section (bn)	Fast Production Cross Section (bn)
Co^{59} (100%)	(n,γ)	Co^{60}	5.271 yr	37	74	
Zn^{64} (48.63%)	(n,γ)	Zn^{65}	243.8 days	0.64	1.5	
Ni^{58} (68.08%)	(n,p)	Co^{58}	70.88 days			0.113
Fe^{58} (0.282%)	(n,γ)	Fe^{59}	44.5 days	1.3	1.2	

The source term to the soluble particles equations is a kinetic one, i.e. is derived on the basis of the rate constant for corrosion release

$$\frac{\partial c_s}{\partial t} = 4 \frac{\bar{k}_r}{d_h \sqrt{t}} \tag{17}$$

Particulate deposition and erosion (sometimes referred to as re-entrainment) are the processes that couple the ferrite layer surface solid phase with the particulate aqueous solid phase. To describe those, the model of Kushneriuk and Blair [76] is employed. The corresponding coolant equation is written as

$$\frac{\partial c_p}{\partial t} = 4 \frac{\left(k_e w - k_{dp} c_p\right)}{d_h} \tag{18}$$

where the deposition source term is proportional to the coolant concentration of particulates and the erosion loss term is proportional to the surface mass in the ferrite layer, *w*. At this point once again, the model uses an empirical relationship between the erosion constant and deposition velocity. Further, the building block equations for hydrothermal crystallization/dissolution processes are based on simple linear mass transfer correlations of the type

$$\frac{\partial c_s}{\partial t} = 4 k_s \frac{\left(c_s - c_{sat}\right)}{d_h} \tag{19}$$

where c_{sat} is the elemental saturated (or equilibrium) coolant concentration, and k_s is the turbulent mass transfer coefficient in units of centimeters per second derived from correlations of the Sherwood number. The equilibrium concentrations in the coolant are derived from solution equilibria which have been comprehensively documented recently e.g. in Ref.77.

An important feature of the model with regard to the modeling of CRUD deposition and AOA is the attempt to take into account the boiling-enhanced deposition in a two-phase medium. The following equation is suggested for the boiling enhanced hydrothermal crystallization of the "scale" (or equivalently, adherent CRUD layer):

$$\frac{\partial c_s}{\partial t} = -4 k_s \frac{H(Q, -\Delta c)\left(F_b(Q) c_s - c_{sat}\right)}{d_h} \tag{20}$$

where Q is termed the quality of the two-phase liquid, and F_b(Q), which is an enhancement factor based on the amount of boiling (Q) that acts to supersaturate

the solution and thus drive the mass to the scale surface. Another important feature of these equations is the Heaviside function, which only allows these fluxes to occur if there is boiling (i.e., Q > 0) and if the boiling is sufficient to cause super-saturation. In a similar manner, enhanced particulate deposition equations can be written in analogy to (18) but without the erosion term.

Even if containing some useful insights into the complexity of the system to be modeled, the approach of Castelli remains practically untested and extensive future work is required to evaluate its predictive abilities for the evolution of CRUD deposition and AOA phenomena.

8.2.7 The CRUD chemistry model (CCM)

A few years ago, Henshaw et al. [78,79] developed a one-dimensional (through-thickness) model that couples thermal hydraulics with the water chemistry. Postulating heat transfer through Wick boiling, they modeled to the downward flow of water soaking through the CRUD, evaporating into steam at the surface of the chimneys. A particular advance of the model was to investigate the various chemical reactions taking place within the porous deposits. This model is described in some detail below. It includes the following features:

- a Wick boiling model;
- radiolysis chemistry of water, taking into account the alpha dose from the 10B(n,α)7Li reaction;
- magnetite dissolution and iron hydrolysis reactions;
- Ni–Fe ferrite dissolution and nickel hydrolysis reactions;
- Ni metal and Ni oxide formation;
- boric acid chemistry and the precipitation of lithium borate;
- non-ideal solution thermodynamics;
- the effect of solute concentration on the saturation temperature and vaporisation enthalpy of water.

8.2.7.1 Thermal hydraulics

The thermal hydraulics model that is used is based on Cohen's one dimensional Wick boiling model [80]. This simulates water transport through the porous deposit and evaporation and steam transport within steam chimneys. The model is derived by considering the heat transfer in the deposit unit cell. Heat transfer is assumed to take place by conduction across the porous shell from the fuel pin towards the bulk coolant and by evaporation of steam at the surface of the chimney, as shown schematically in Figure 31. The temperature distribution is given by

$$\frac{d^2T}{dx^2} - \frac{2\pi r_c N_c h_c}{f k_c}\left(T - T_s\right) = 0 \tag{21}$$

where f is the fractional area of the porous shell, N_c is the area density of chimneys, r_c is the chimney radius, k_c is the thermal conductivity of the porous shell, h_e is the evaporative heat transfer coefficient and T_s is the saturation temperature.
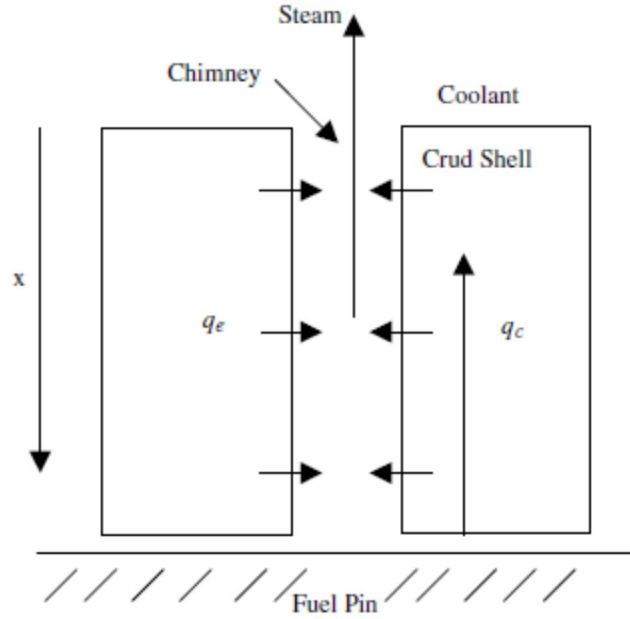
Figure 31 Schematic diagram of heat transport during Wick boiling: q_e is the evaporative heat flux and q_c the conductive heat flux.

Steady state mass conservation of water in the solution in the porous shell leads to the following equation for the liquid velocity

$$\frac{d\left(\rho_w u_l\right)}{dx} - \frac{2\pi r_c N_c h_c}{fH_v}\left(T - T_s\right) = 0 \tag{22}$$

where H_v is the vaporization enthalpy of water and ρ_w is the water density. The thermal hydraulics model implemented in this work differs though from the simple Cohen model [80] because T_s, H_v and h_e are all functions of the species concentrations in the water and are derived from fundamental thermodynamic relationships [79].

8.2.7.2 Transport

Dissolved species are transported by flow, by diffusion in their concentration gradient and, if they are charged, by drift in the electric potential gradient. For each species in the liquid phase (there is an equivalent equation for the corresponding vapor phase species) the model assumes

$$\frac{\partial c_i}{\partial t} = \left(\frac{\partial c_i}{\partial t}\right)_R + \left(\frac{\partial c_i}{\partial t}\right)_P - \frac{1}{\varepsilon}\frac{\partial J_1}{\partial x} \tag{23}$$

where c_i is the concentration in the liquid, and the first term on the right of the equation is due to changing species concentrations by chemical reaction (subscript R for reaction), the second term is due to liquid/steam partitioning (subscript P for partitioning) and the third term is due to transport. In equation (23), ε is the porosity of the deposit, which is the fraction of free space present per unit volume of CRUD. The superficial molecular flux J_l is given by the generalized Fick's law

$$J_1 = -D_1\frac{\partial c_1}{\partial x} - \frac{zFD_1 c_1}{RT}\frac{\partial \phi}{\partial x} + u_1 c_1 \tag{24}$$

where D_l is the diffusion coefficient, z is the charge number, F is the Faraday constant, and $\partial \phi / \partial x$ the potential gradient. To simplify the notation, subscripts are not appended to differentiate the species. The diffusion coefficient D_l in the porous shell is related to the diffusion coefficient in liquid water D_w by the following empirical equation

$$D_l = \frac{\varepsilon D_w}{\tau} \tag{25}$$

where τ is the tortuosity factor, representing an effective path length through the deposit. On the other hand, the potential gradient is obtained from a generalized Ohm's law equation involving the effective solution conductivity. The rate of loss of volatile species (hydrogen, radiolytically produced oxygen and boric acid) from the liquid to the vapor phase is given by

$$\left(\frac{\partial c_i}{\partial t} \right)_P = -\frac{2\pi r_c N_c h_c}{\varepsilon f} k_m \left(c_V^{eq} - c_V \right) \tag{26}$$
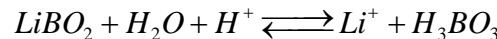
where k_m is the mass transfer rate for species passing between the gas and liquid phases and c_V^{eq} is the equilibrium concentration in the vapor phase, determined by the relevant partitioning constant.

8.2.7.3 CRUD chemistry

Chemical reactions are included in CCM in the form of first-order rate equations, which express the rate of change of species concentrations as equal to the product of a rate constant and the concentrations of the reactants and products, involving also corrections for the activity coefficients due to the large solution concentrations within the deposit. Ionisation of water, boric acid equilibria, metal ion hydrolysis reactions of the type

$$Ni^{2+} + 2Fe^{2+} + 4H_2O \rightleftharpoons NiFe_2O_4 + 6H^+ + H_2 \; ,$$

$$Ni^{2+} + H_2O \rightleftharpoons NiOH^+ + H^+$$
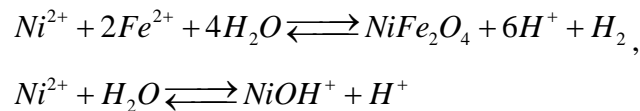
precipitation and/or dissolution reactions such as

$$LiBO_2 + H_2O + H^+ \rightleftharpoons Li^+ + H_3BO_3$$

as well as radiolysis of water, have been treated in this way.

The model provides credible explanations for many of the observed fuel CRUD /AOA phenomena. Calculated high temperatures in the CRUD and high pH at the end of cycle may explain the formation of bonaccordite in CRUDs greater than 100 μm. Predicted precipitation of $LiBO_2$ near 30μm explains why this is when AOA starts to be observed in most cores. The calculated pH changes associated with $LiBO_2$ precipitation suggests a possible explanation for the formation of a ZrO_2 layer in the CRUD. However, the lack of thermodynamic data on the Zr-system under the relevant conditions meant that this could not be modeled. The oxidizing condition predicted in thick CRUD explains why Cr is depleted in such CRUD, as it is more soluble under these conditions. The thermodynamics predict precipitation of NiO and Ni-ferrite onto the fuel. However, CCM predicts Ni-ferrite may convert to NiO within the CRUD if the demand for Fe deposition on the fuel "out strips" supply from the steam generators. This conversion tends to

occur at the CRUD/water interface. This explains why two forms of NiO are observed (from direct precipitation and from converted Ni-ferrite) and why the outer layer of the CRUD can be rich in NiO.

Further work is being carried out to try and understand the composition of the CRUD and in particular the relative amounts of Ni and Fe present [55,79]. Very recently, a more representative two-dimensional model was developed [81,82]. It couples mechanistically the processes which are in principle present; heat transfer through the wet CRUD, diffusive flow and boiling of the water at chimney surfaces to remove the heat, and the advection and diffusion of dissolved species. The 2D model also provides a framework within which the further, more sophisticated, physical chemistry analysis of Henshaw et al. [79] could in due course be incorporated.

8.2.8 The Boron-induced Offset Anomaly Risk Assessment Tool (BOA)

In 2003, EPRI teamed with Westinghouse Electric Company to co-develop an AOA risk assessment tool [83,84]. This software product, Boron-induced Offset Anomaly Risk Assessment Tool has since been revised several times [55].

The latest version of the BOA code, released in 2010, is version 3.0. This is a transient mass balance simulation that combines static system design features such as steam generator and loop piping materials and surface areas, fuel surface areas, and system flow rates into a computational framework that is used for analyzing the relative effects of time variant input such as core thermal hydraulics, system material general corrosion rates, sub-cooled nucleate boiling, and corrosion product deposition. The result is a complete model for the deposition of CRUD on the surfaces of the primary circuit and the concentration of boron within the thick CRUD that forms on the sub-cooled boiling surfaces of the upper fuel spans.

Version 3.0 includes several new features and improvements from the earlier versions of BOA, such as:
- Corrosion product release rates based on elemental releases of nickel and iron from steam generator tube alloys and stainless steel surfaces, respectively
- Release and deposition rates are calculated for multi-node steam generators and stainless steel surfaces.
- Addition of nickel/iron high temperature aqueous chemistry to the model.
- Precipitation of non-stoichiometric nickel ferrite, nickel oxide, and nickel metal.
- Inclusion of coupled particulate and soluble corrosion product deposition and release mechanisms.
- Fuel CRUD composition varies as a function of temperature and chemistry environment.
- Improved/extended Cohen boiling model in porous deposits.
- Improved lithium tetraborate deposition model.

An overview of the calculation assumptions of BOA 3.0 is given in Figure 32. The model requires a general description of the primary coolant system. Steam generator tubing materials are assumed to be Alloy 600, 690, or 800, and loop piping systems are stainless steel. The user inputs the system water mass, hot leg and cold leg temperatures, and the letdown removal flow rate, all of which are assumed constant throughout the cycle. Core thermal hydraulic parameters (heat

flux, temperature, pressure, mass flux and density) are taken from VIPRE simulation of the core design [19].
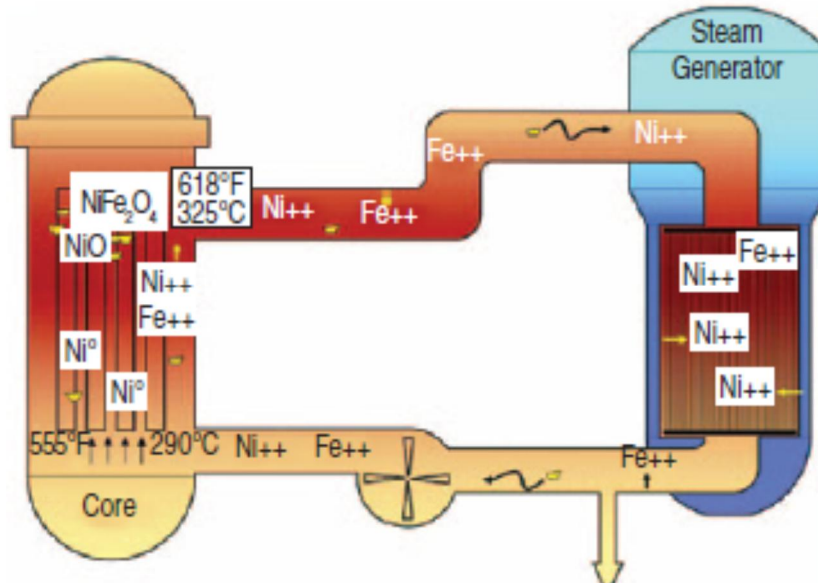

Figure 32 BOA mass balance model for coolant corrosion product concentration.

The steam generator tubing and stainless steel primary circuit materials continuously corrode at low rates releasing nickel and iron into solution in the coolant. A corrosion model originally developed by Robertson [85] is used to predict the amounts of nickel and iron released into the coolant per mass of metal corroded. This model also predicts the morphology and composition of the insoluble oxide film that grows on the corroding metal surface, which according to the developers compares quite well with experimental data.

The deposition of nickel and iron corrosion products around the primary circuit of a PWR is illustrated by the calculated example shown in Figure 33. The graph in the upper left part of the figure shows the corrosion product distribution at the end of a high duty cycle. This shows deposition concentrated on the boiling surface of the core, although its surface area is less than half of one percent of the total. The upper right graph shows the reduced deposition on the boiling surface when the release of particulate from the surfaces of the circuit is suppressed. The graph below shows the deposition during the following cycle when the boiling surface of the previous cycle becomes the ex-boiling surface of second cycle fuel. Although it started the second cycle with all the CRUD from the first cycle, it has lost 70% of it by the end of the cycle, with almost all of it transferred to the boiling surface. The mass of boron in the CRUD is obtained by first calculating the thickness of CRUD required to precipitate lithium tetraborate, reported to be more stable than lithium metaborate in the CRUD formation conditions [86]. It is then assumed that, for thicknesses greater than this, all the pores within the CRUD become filled with solid lithium tetraborate. In practice this occurs at a rate governed by the increase in CRUD thickness, rather than the influx of lithium and boron into the CRUD. For comparison with plant data for neutron absorption, it is the mass of ^{10}B within the CRUD rather than the total boron mass that is important. This is calculated in BOA 3.0 by taking into account its loss in the ^{10}B(n,α)^{7}Li reaction.
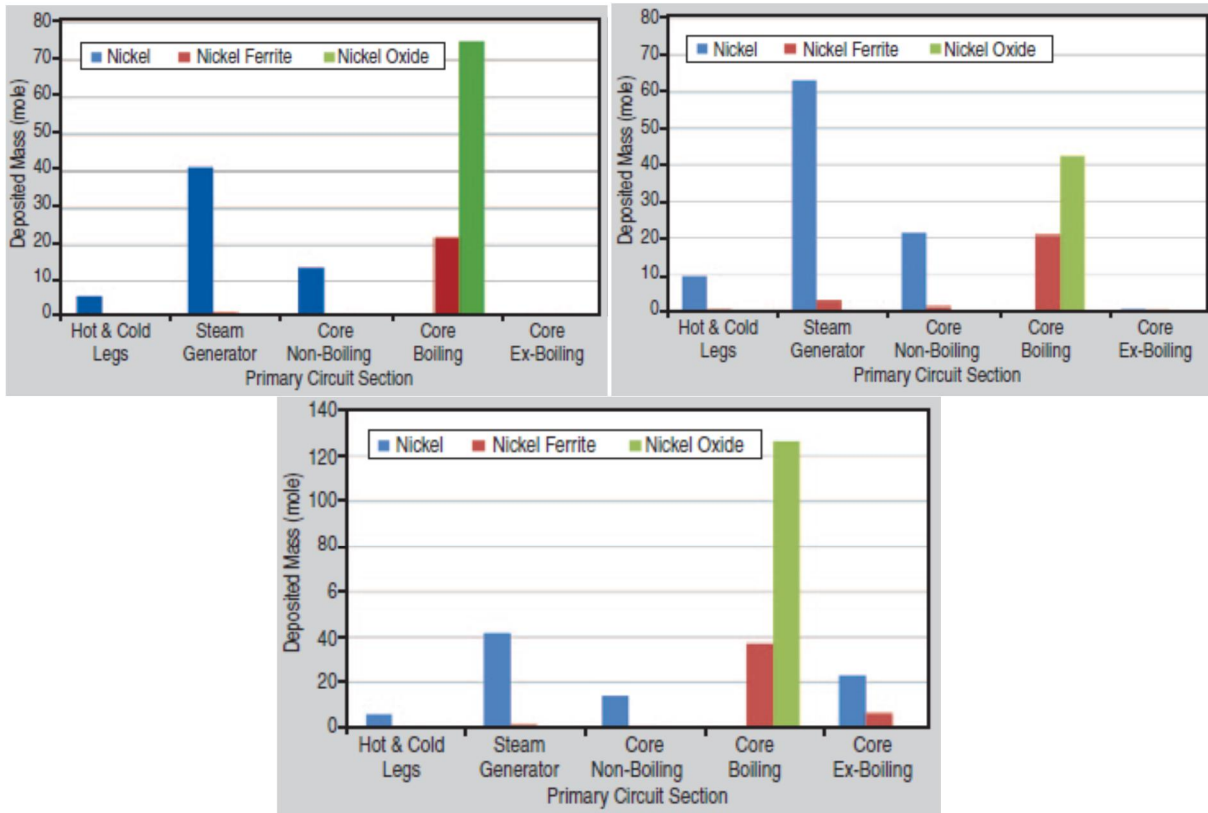
Figure 33 (above, left) Deposition of corrosion products around the primary circuit of a PWR at the end of a high duty cycle; (above, right) Deposition of corrosion products around the primary circuit of a PWR at the end of a high duty cycle with suppressed release of particulate material; (below) Deposition of corrosion products around the primary circuit of a PWR at the end of a second high duty cycle.

Figure 34 (above) shows the calculated temperature distribution within a 35 μm thick PWR fuel CRUD for a heat flux of 850 kW m^{-2}. The temperature increase up to a thickness of 18.4 μm occurs as a result of the increase in saturation temperature with increasing concentration of boric acid. The increase in temperature for thicknesses greater than this occurs by conduction in a deposit whose pores have become filled with lithium tetraborate. This suppresses Wick boiling in the bottom 6.6 mm of the deposit. The overall increase in temperature is 11 K. Figure 34 (below) shows the calculated increase in the concentrations of boric acid and lithium ions with depth in the deposit. This shows the concentrations of boric acid and lithium increasing by factors of ten and fifty respectively up to the depth where lithium tetraborate precipitates.

As a further development, it is expected that the CASL/MPO CRUD deposition model (MAMBA) will leverage off the existing capabilities of BOA and LANL's multi-phase chemical kinetics code (ChemPaC) to produce a higher-resolution and more extensive chemical kinetics model for CRUD deposition. The MAMBA model will also be integrated into CASL's virtual reactor environment which will enable an improved assessment of CIPS risk as well as the optimization of new cladding and other materials [55, 85].
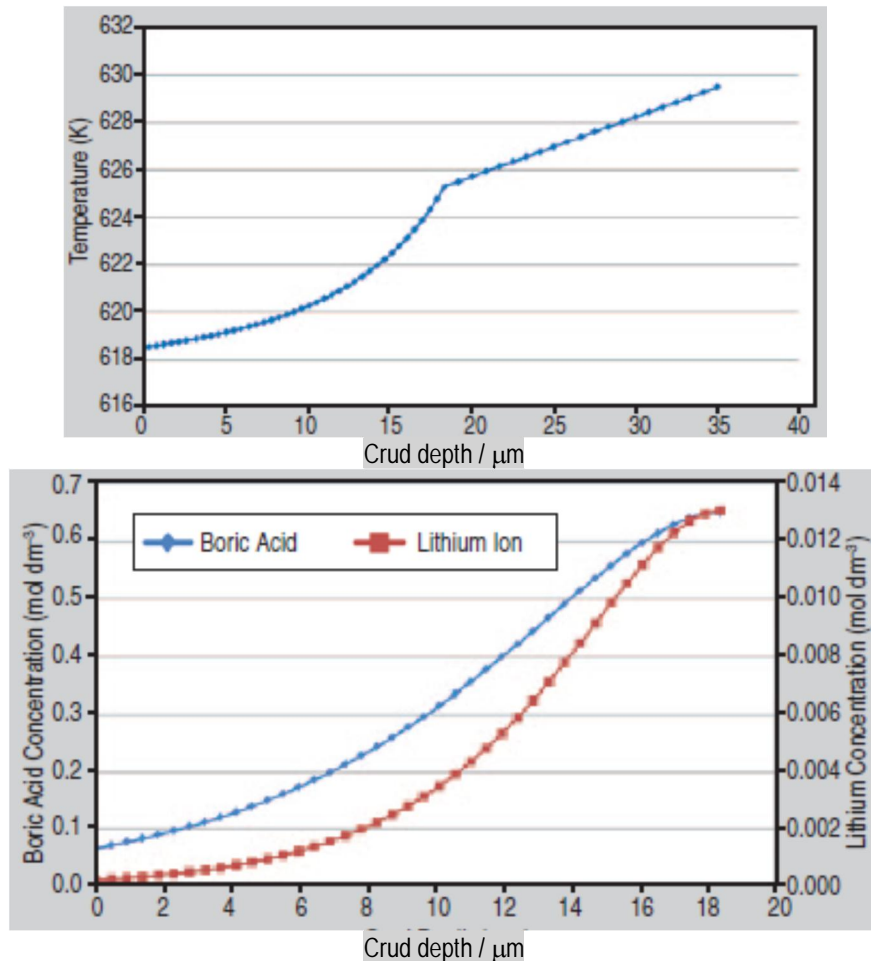
Figure 34(above) calculated temperature distribution in a 35 μm thick PWR fuel CRUD; (below) calculated concentrations of boric acid and lithium ions within a PWR fuel CRUD.

8.2.9 Micro-layer evaporation and dry-out (MED) model

The MED model, which was developed for predicting iron CRUD deposition on the boiling surface of Boiling Water Reactor (BWR) fuel rods [88,90], was very recently extended for application to metallic ion deposition, and modified to evaluate deposition of CRUD and metallic ions on sub-cooled boiling surface [91]. As an analogy to the unstable deposits on the BWR fuel rod surfaces such as NiO or CoO, which react with Fe_2O_3 to form nickel and cobalt ferrites, the major species in the PWR primary cooling water, boron and lithium, deposit as $Li_2B_4O_7$ on the fuel rod surface due to SNB (Figure 35). It is assumed that $Li_2B_4O_7$ does not accumulate on the fuel surface, but some of the released species react with NiO and $NiFe_2O_4$ to become quasi-stable Ni_2FeBO_5, which accumulates on the fuel surface and influences neutron absorption and then local power shift. However, the amount of quasi-stable Ni_2FeBO_5 deposited on the fuel rod surface is not sufficient to explain AOA. The deposition amount of unstable $Li_2B_4O_7$ under sub-cooled boiling conditions is larger than Ni_2FeBO_5 as a result of balancing deposition and release of $Li_2B_4O_7$. The equation of motion of bubbles under sub-cooled boiling conditions was obtained from a cavitation model [92]. A schematic diagram of bubble growth and collapse is shown in Figure 36.
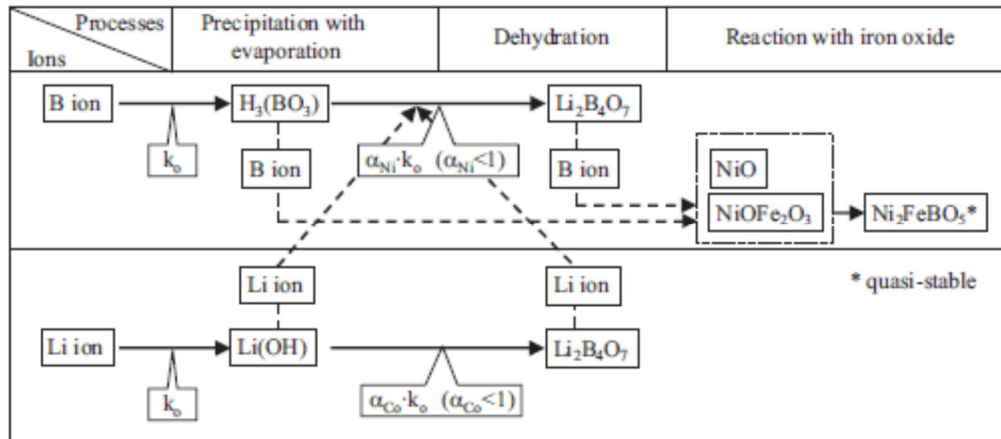
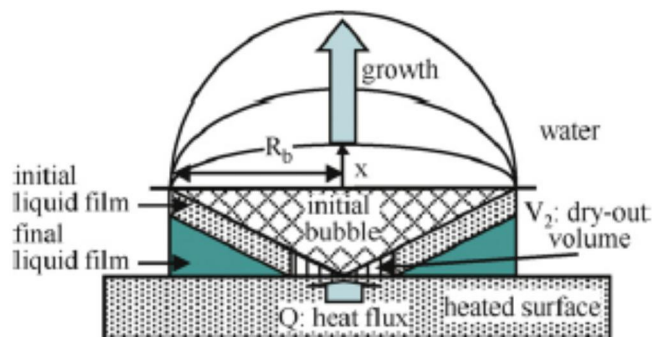Figure 35 Scheme of chemical change of deposited Ni and B.

Figure 36 Bubble growth and collapse model.

Concerning the chemical reactions of boron with nickel ferrite, it is assumed that at first, boron deposits on the fuel rod surface as $Li_2B_4O_7$, which is easily released into water and some of the ions react with nickel ferrite to become bonaccordite, Ni_2FeBO_5 [93], according to the respective mass balances. The effects of deposited B on the changes in reactor power were calculated by changing the concentrations of B, Ni and Li and exposure time. Measurable local reactivity change due to boron accumulation on sub-cooled boiling fuel was estimated as 15%, because boron depositing area was restricted to only the local upper part of the core region with sufficiently high power density (high heat flux). The core area with estimated boron accumulation exceeding 4 g m^{-2} was designated as the AOA risk region. This value was four to forty times larger than the measured value in the fuel deposit on the sub-cooled boiling fuels [52].

Calculated exposure time-dependent boron accumulation on the fuel rod surface is shown in Figure 37. Both lithium tetraborate and bonaccordite contents increased with exposure time. Total deposited amount of metastable species was much larger than that of quasi-stable ones, thus reactor activity might be determined by the unstable species. After plant shutdown, unstable species was released very quickly and soon disappeared, while quasi-stable species still remained on the fuel rod surface, and could be determined by PIE. However, the measured deposits might differ from the actual amount deposited under plant operation. The gap between the measured and the estimated values was expected to be bridged by in situ measurement of deposits under high temperature conditions. It can be concluded that in spite of the fact that the model was able to capture some of the

main trends leading to the occurrence of AOA, further development is needed in order to fully quantify its predictions.
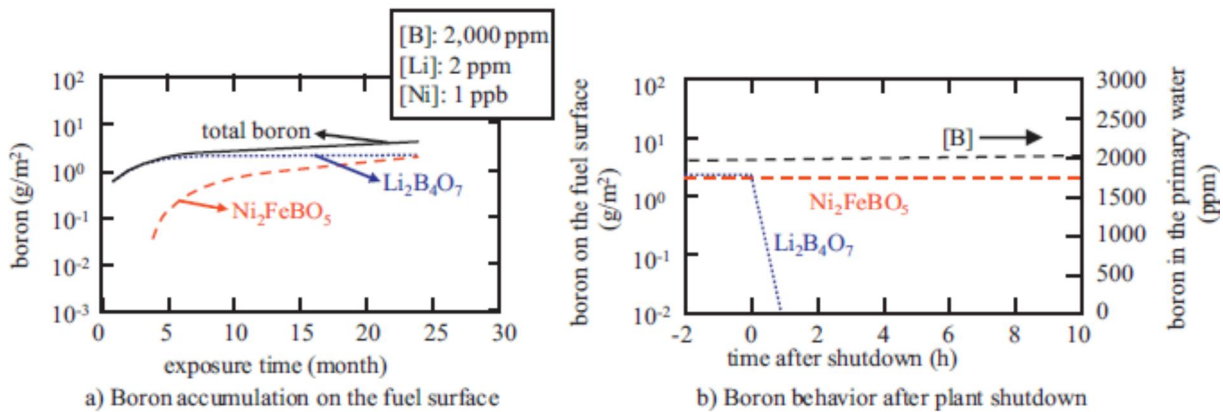

Figure 37 Schematic chart of boron accumulation: (a) Boron accumulation on the fuel surface and (b) boron behavior after plant shutdown.

8.3 Discussion and outlook

8.3.1 Source term modeling - ANTIOXI

Most part of the models briefly outlined in the previous sections treat the source term of activity build-up and CRUD formation on an empirical basis. To predict surface concentrations of relevant precursors to active species and CRUD deposited on fuel, the approaches chosen rely either on thermodynamic solubility and ECP calculations, or on empirical kinetic constants derived from somewhat outdated concepts for the growth and restructuring of oxide layers on construction materials in the primary circuit of PWRs. These features make the comparison between the predictive abilities of the models concerning the source term of activity build-up and CRUD deposition ambiguous at best.

From a kinetic standpoint, the main controlling factor of oxide film growth and metal dissolution rates on stainless steels and nickel-based alloys in PWRs, i.e. oxide thicknesses and corrosion release, are the solid state transport rates within the inner, also called barrier, oxide layer. Models for such transport have been developed for many years, but only recently has the modeling reached a sufficient sophistication to allow a reasonably good quantitative correlation between the calculated values and the growth rates of oxide films on structural materials in real PWR environments. Such a quantitative model, developed within the ANTIOXI project of the 6th Framework Programme of the European Commission, [94-97] is described to some detail in the present section of the report. An approach to the growth of the outer, deposited layer crystallites using diffusion formalism is also presented, and the coupling between the models for the compact and porous layers is discussed. To treat the exchange of material between the oxide and the coolant, an adsorption-surface complexation approach is added to the model.

8.3.1.1 Growth of the inner layer and dissolution of metal through that layer

The ANTIOXI approach to the growth of the inner layer is illustrated in Figure 38. Although it has been presumed that Cr and Ni are transported through the oxide via vacancies and Fe via interstitial cation sites, at this point the model does not

distinguish between the types of the defects via which the respective metallic constituent is transported through the inner layer of oxide.
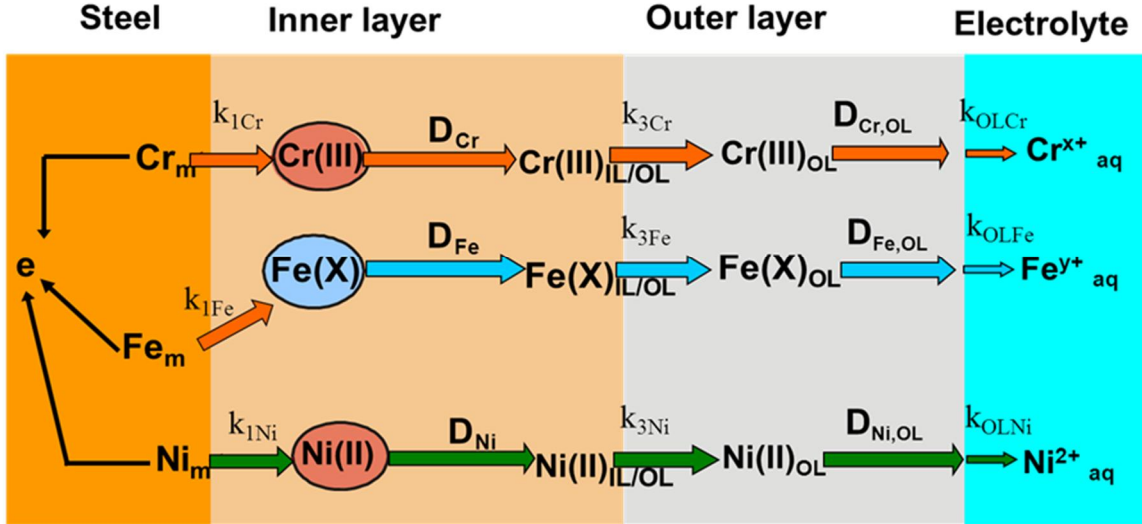

Figure 38 A simplified scheme of the growth of the inner and outer layers of the film formed on a structural material according to the ANTIOXI model. For details see text.

The depth profile of a metallic oxide constituent j = Fe, Cr,Ni, etc., can be expressed as the dependence of its molar fraction, $y_j = c_j V_{m,MO}$, on the distance within the inner layer, where c_j is its molar concentration and $V_{m,MO}$ the molar volume of the phase in the layer. The transient diffusion-migration equations for each component read as

$$\frac{\partial y_{Fe}}{\partial t} = D_{Fe}\frac{\partial^2 y_{Fe}}{\partial x^2} + \frac{XF\vec{E}D_{Fe}}{RT}\frac{\partial y_{Fe}}{\partial x}$$

$$\frac{\partial y_{Cr}}{\partial t} = D_{Cr}\frac{\partial^2 y_{Cr}}{\partial x^2} + \frac{3F\vec{E}D_{Cr}}{RT}\frac{\partial y_{Cr}}{\partial x} \qquad (27)$$

$$\frac{\partial y_{Ni}}{\partial t} = D_{Ni}\frac{\partial^2 y_{Ni}}{\partial x^2} + \frac{2F\vec{E}D_{Ni}}{RT}\frac{\partial y_{Ni}}{\partial x}$$

where X stands for the nominal valency of Fe in the oxide. The boundary conditions at the alloy/film and film/electrolyte interfaces, as well as the initial conditions can be written as

$$y_{Fe}(x,0) = y_{Fe,a},\, y_{Cr}(x,0) = y_{Cr,a},\, y_{Ni}(x,0) = y_{Ni,a}$$

$$y_{Fe}(0,t) = y_{Fe,a},\, y_{Cr}(0,t) = y_{Cr,a},\, y_{Ni}(0,t) = y_{Ni,a}$$

$$y_{Fe}(L_i,t) = \frac{k_{1Fe}y_{Fe,a}}{V_{m,MO}}\left[\frac{1}{k_{3Fe}} + \frac{RT}{XF\vec{E}D_{Fe}}\right],\, y_{Ni}(L_i,t) = \frac{k_{1Ni}y_{Ni,a}}{V_{m,MO}}\left[\frac{1}{k_{3Ni}} + \frac{RT}{2F\vec{E}D_{Ni}}\right] \quad (28)$$

$$y_{Cr}(L_i,t) = \frac{k_{1Cr}y_{Cr,a}}{V_{m,MO}}\left[\frac{1}{k_{3Cr}} + \frac{RT}{3F\vec{E}D_{Cr}}\right]$$

where $x = 0$ at the alloy/film interface and $x = L_i$ is the film/coolant or inner layer/outer layer interface, L_i being the inner layer thickness.

8.3.1.2 Outer layer growth and release kinetics

The outer layer is presumed to grow via the precipitation of material that is dissolved from the substrate through the inner layer of oxide. The growth of this layer is formally treated as a diffusion process in a matrix constituted of the outer layer crystals and the electrolyte in between. Since the outer layer is not continuous, the role of the potential gradient in this layer can be considered negligible with respect to the concentration gradient. Thus, to calculate the depth profile of a certain cation in the outer layer, the following system of equations has to be solved:

$$\frac{\partial y_{Fe,OL}}{\partial t} = D_{Fe,OL} \frac{\partial^2 y_{Fe,OL}}{\partial x^2}$$

$$\frac{\partial y_{Cr,OL}}{\partial t} = D_{Cr,OL} \frac{\partial^2 y_{Cr,OL}}{\partial x^2} \qquad (29)$$

$$\frac{\partial y_{Ni,OL}}{\partial t} = D_{Ni,OL} \frac{\partial^2 y_{Ni,OL}}{\partial x^2}$$

The boundary conditions at the inner interface of the outer oxide layer are identical to those used as outer boundary conditions at the inner layer / electrolyte interface (see eqn. (28)), which ensures the continuity of the composition of the whole film. At the outer layer/coolant interface, formal reaction rate constants are introduced: $k_{OL,i}$, (i=Fe,Cr, Ni etc.) and the respective boundary conditions at $x = L_o$, where L_o is the outer layer thickness, are defined as follows

$$y_{Fe}(L_o,t) = \frac{k_{3Fe} y_{Fe}(L_i,t)}{k_{OLFe}}$$

$$y_{Ni}(L_o,t) = \frac{k_{3Ni} y_{Ni}(L_i,t)}{k_{OLNi}} \qquad (30)$$

$$y_{Cr}(L_o,t) = \frac{k_{3Cr} y_{Cr}(L_i,t)}{k_{OLCr}}$$

These can be regarded as rate constants for release when the solubility limit of a respective cation is not reached, and rate constants for deposition if this solubility limit is exceeded.

8.3.1.3 Growth laws for the inner and outer layers of oxide

A successful model for the oxidation behavior should be able to predict the growth of the oxide with time of exposure. In the present approach, a growth law previously employed to predict oxide film growth on austenitic materials in nuclear power plant coolants at subcritical temperatures [94-96] has been adopted for the inner layer:

$$L_i(t) = L_i(t=0) + \frac{1}{b} \ln\left[1 + V_{m,MO}(k_{1,Cr} y_{Cr,a} + k_{1,Fe} y_{Fe,a} + k_{1,Ni} y_{Ni,a}) b e^{-bL_i(t=0)} t\right]$$

$$b = \frac{3\alpha_1 F \vec{E}}{RT} \qquad (31)$$

It is noteworthy that this equation is valid subject to the assumption that the transfer coefficients for all the reactions at the alloy / inner layer interface are equal to α_1.

For the outer layer, a parabolic law was derived starting from the hypothesis that its growth can be approximated by a linear diffusion-like mechanism, as outlined above. As a first approximation, it is proposed that the growth rate of this layer is proportional to the apparent diffusional flux of Fe, $J_{diff,Fe}$:

$$\frac{dL_o}{dt} = V_{m,MO}J_{diff,Fe} = V_{m,MO}D_{o,Fe}\frac{\Delta y_{Fe}}{V_{m,MO}L_o} = D_{o,Fe}\frac{\Delta y_{Fe}}{L_o} \tag{32}$$

Where

$$\Delta y_{Fe} = y_{Fe}(L_o,t) - y_{Fe}(L_i,t) = \left(\frac{k_{3Fe}}{k_{OLFe}} - 1\right)k_{1Fe}y_{Fe,a}V_{m,MO}\left(\frac{1}{k_{3Fe}} + \frac{RT}{XF\vec{E}D_{Fe}}\right)$$

Integrating equation (32) from 0 to t and from 0 to L_o, the growth law for the outer layer is obtained in the form

$$L_o(t) = \sqrt{2D_{o,Fe}t\left(\frac{k_{3Fe}}{k_{OLFe}} - 1\right)k_{1Fe}y_{Fe,a}V_{m,MO}\left(\frac{1}{k_{3Fe}} + \frac{RT}{XF\vec{E}D_{i,Fe}}\right)} \tag{33}$$

Thus the outer layer growth is expressed in terms of the rate constants and diffusion coefficients for Fe in the inner and outer layers, respectively [98].

8.3.1.4 Incorporation of solution-originating cations in the oxide

The individual steps of incorporation of coolant-originating species in the bi-layer oxide are schematically depicted in Figure 39. The first step in the interaction is assumed to be the adsorption on the outer surface of the oxide, which is treated using the surface complexation approach [95,96]. The surface hydrolysis of an oxide in PWR coolant conditions is described in terms of the 1-pK surface complexation model

$$\equiv \text{Fe-OH}^{1/2+} \Longrightarrow \equiv \text{Fe-O}^{1/2-} + \text{H}^+ \tag{34}$$
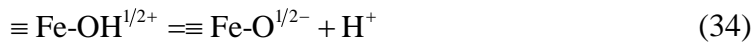
Correspondingly, the interaction of a coolant-originating cation, M^{2+}, with the oxide surface is written as

$$\equiv \text{Fe-OM}\left(\text{OH}\right)^{1/2+} + \tfrac{3}{2}\text{H}^+ \rightleftharpoons \equiv \text{Fe-OH}^0_{1/2} + M^{2+} + H_2O \tag{35}$$
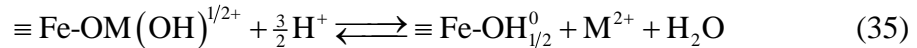
In order to predict quantitatively the depth profile of a solution-originating cation incorporated into the inner layer, the associated diffusion-migration equation for the non-steady state transport of that cation

$$\frac{\partial c_M}{\partial t} = D_M \frac{\partial^2 c_M}{\partial x^2} - \frac{2F\vec{E}D_M}{RT}\frac{\partial c_M}{\partial x} \tag{36}$$

is added to the system of equations (27) and the extended system is solved subject to the boundary conditions (28). The boundary condition at the inner layer/outer layer interface is given by the enrichment factor $K_{enr,M,i}$ defined as the ratio between the concentration of Zn at that interface and the Zn concentration in the water: $y_M(L_i,t) = K_{enr,M,i}c_M(sol)$. If the cation M is not present in the alloy substrate, a reflective boundary condition at the alloy / inner layer interface is used. If, in

addition, the solution-originating cation is present in the alloy substrate, such being the case with Co, Mn, etc., the boundary condition at the inner layer/electrolyte interface is written as

$$y_M(L_i, t) = K_{enr,M,i} c_M(sol) + \frac{k_{1M} y_{M,a}}{V_{mo}} \left[\frac{1}{k_{3M}} + \frac{RT}{2F\vec{E}D_M} \right]$$

Within the frames of the formal model for the outer layer growth, the depth profile of M in the outer layer is calculated by solving the system of equations (29) extended with:

$$\frac{\partial y_{M,OL}}{\partial t} = D_{M,OL} \frac{\partial^2 y_{M,OL}}{\partial x^2} \tag{37}$$

The boundary condition at the outer layer/water interface is set by the corresponding enrichment factor for the respective component at that interface:
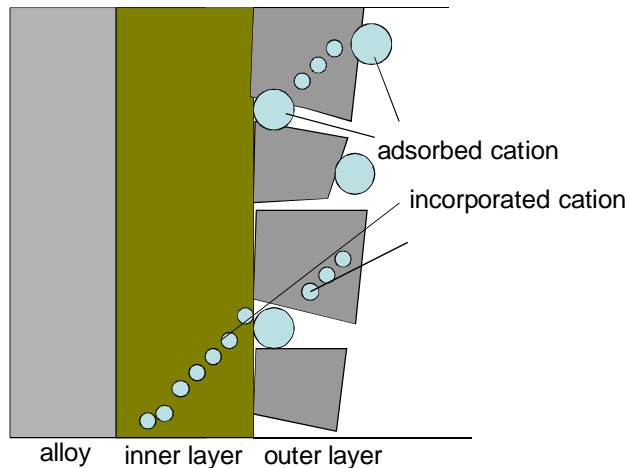$y_M(L_o, t) = K_{enr,M,o} c_M(sol)$.

Figure 39 Individual steps of the interaction of a coolant-originating cation with the bi-layer oxide on a construction material in the PWR primary circuit.

8.3.1.5 Incorporation of radioactive material in the oxide

The specific activity of the particles of a radioactive isotope that incorporates in the inner or outer oxide layers is defined by the expression

$$A_i = \lambda_i \frac{N_i}{S} \tag{38}$$

where λ_i is the rate constant of the decay of the respective nuclide (s^{-1}), and N_i is the number of particles of this nuclide per unit area of construction S (m^{-2}). Using the relationship between N, the oxide film thickness L and the volume concentration of active material $c_{R,i}$, we obtain

$$A_i = \lambda_i N_A c_{R,i} L \tag{39}$$

where N_A is Avogadro's number. The total concentration of active material is the sum of the concentration of all nuclides, i.e. the concentration of any nuclide can be represented as a molar fraction with respect to the total concentration of active material

$$y_{R,i} = \frac{c_{R,i}}{\sum_i c_{R,i}} \tag{40}$$

In other words, to calculate the specific surface activity of a nuclide, we can use equations analogous to (27) and (29) for incorporation in the inner or outer layers, taking into account the rate of radioactive decay

$$\frac{\partial A_i}{\partial t} = D_i \frac{\partial^2 A_i}{\partial x^2} - \frac{2F\vec{E}D_i}{RT} \frac{\partial A_i}{\partial x} - \lambda_i A_i \text{ inner layer}$$

$$\frac{\partial A_i}{\partial t} = D_i \frac{\partial^2 A_i}{\partial x^2} - \lambda_i A_i \text{ outer layer} \tag{41}$$

with the initial and boundary conditions as follows

$$A_i(0,t) = 0, A_i(x,0) = 0, A_i(L_i,t) = K_{enr,i,IL} A_i(sol)$$

$$A_i(0,t) = 0, A_i(x,0) = 0, A_i(L_o,t) = K_{enr,i,OL} A_i(sol) \tag{42}$$

where $A_i(sol)$ is the activity of the respective nuclide in the coolant. The enrichment factors for a given nuclide $K_{enr,i,IL}$ and $K_{enr,i,OL}$ are assumed equal to those for non-active particles of the corresponding chemical species, determined from the surface complexation theory.

8.3.2 Validation of the ANTIOXI model

8.3.2.1 Kinetic of oxide growth on PWR steam generator materials

Quantification of the oxidation processes on Ni alloys such as Alloy 600, 690 and 800, in a PWR coolant is of utmost importance since the radioactivity of the primary circuit is primarily due to cations released by corrosion of the steam generator tubes made mainly of these materials. A full treatment of both laboratory and in-reactor data to extract the full set of model parameters is given in the present section.

Figure 40 shows XPS depth profiles of the mass fractions of Ni, Cr and Fe in the oxides formed on Alloy 600 in simulated PWR water (2 ppm Li, 1200 ppm B, [H_2]=35 cm^{3}kg^{-1} STP) for 20 and 100 h at 325ºC [30,37,99,100] together with the corresponding profiles calculated by the model. XPS depth profiles for the oxides on Alloy 600 stemming from experiments involving much longer oxidation times in simulated PWR water at 260ºC [40] are presented in Figure 41, respectively. The diffusion coefficients for individual constituents in the inner and outer layers are collected in Figure 42. Further, XPS depth profiles of the mass fractions of Ni, Cr and Fe in the oxides formed on Alloy 690 in simulated PWR water for 20, 50 and 100 h at 325ºC are summarized in Figure 43. The calculated diffusion coefficients of individual constituents in the inner and outer layers are collected in Figure 44. The differences between parameters for oxides on Alloys 600 and 690 are not very significant, the only important difference being observed for the diffusion coefficients in the inner layer (Figure 44, left). In general it can be stated that the values of the parameters on Alloy 690 are somewhat larger and their time evolution more pronounced. The lower diffusion coefficients in the inner layer on Alloy 600 can be tentatively explained by the unavailability of Cr from the alloy layer underneath the oxide, which retards film growth, as suggested in Refs. 99,100. By examining the values of the diffusion coefficients of inner layer constituents of the oxide on nickel-based alloys, it can be concluded that the time of exposure has a significant influence on the values. In order to explain the effect of film aging on its properties, the effect of microstructure has to be considered.
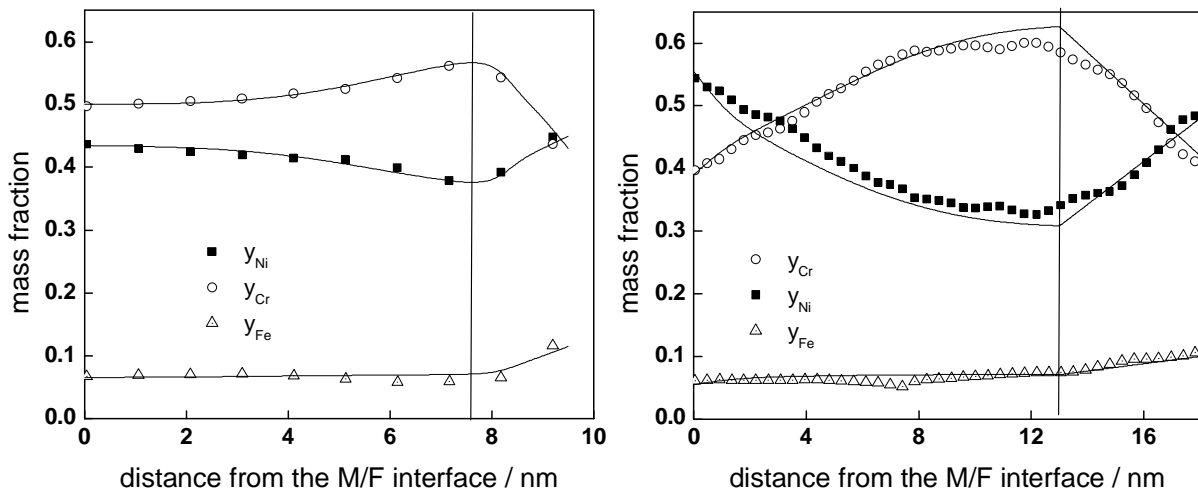
Figure 40 Experimental (points) and calculated (solid lines) depth profiles of the mass fractions of Fe, Cr, and Ni in the films formed on Alloy 600 in simulated PWR water for 20 h (left) and 100 h (right). The inner layer / outer layer boundary indicated with a vertical line.

Figure 41 Experimental (points) and calculated (solid lines) depth profiles of the mass fractions of Fe, Cr, and Ni in the films formed on Alloy 600 in simulated PWR water for 5000 h (left) and 10000 h (right). The inner layer / outer layer boundary indicated with a vertical line.

Figure 42 Dependence of the diffusion coefficients of inner layer constituents (left) and formal diffusion coefficients for the growth of the outer layer (right) on time of exposure of Alloy 600 to simulated PWR coolant.
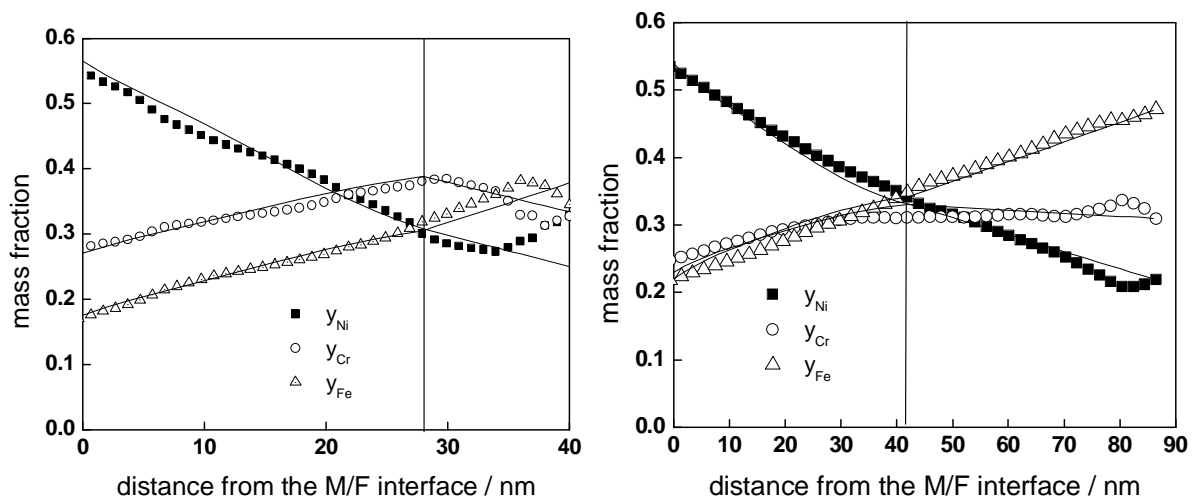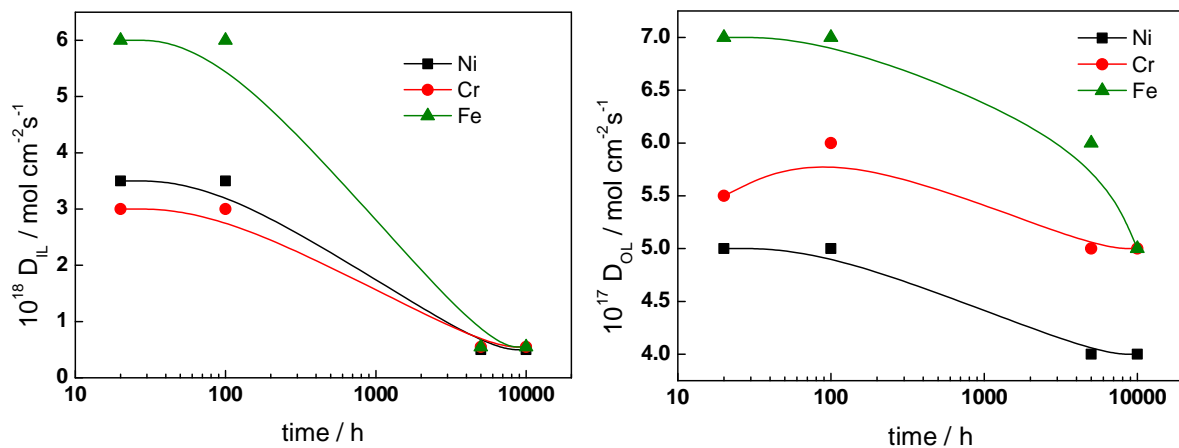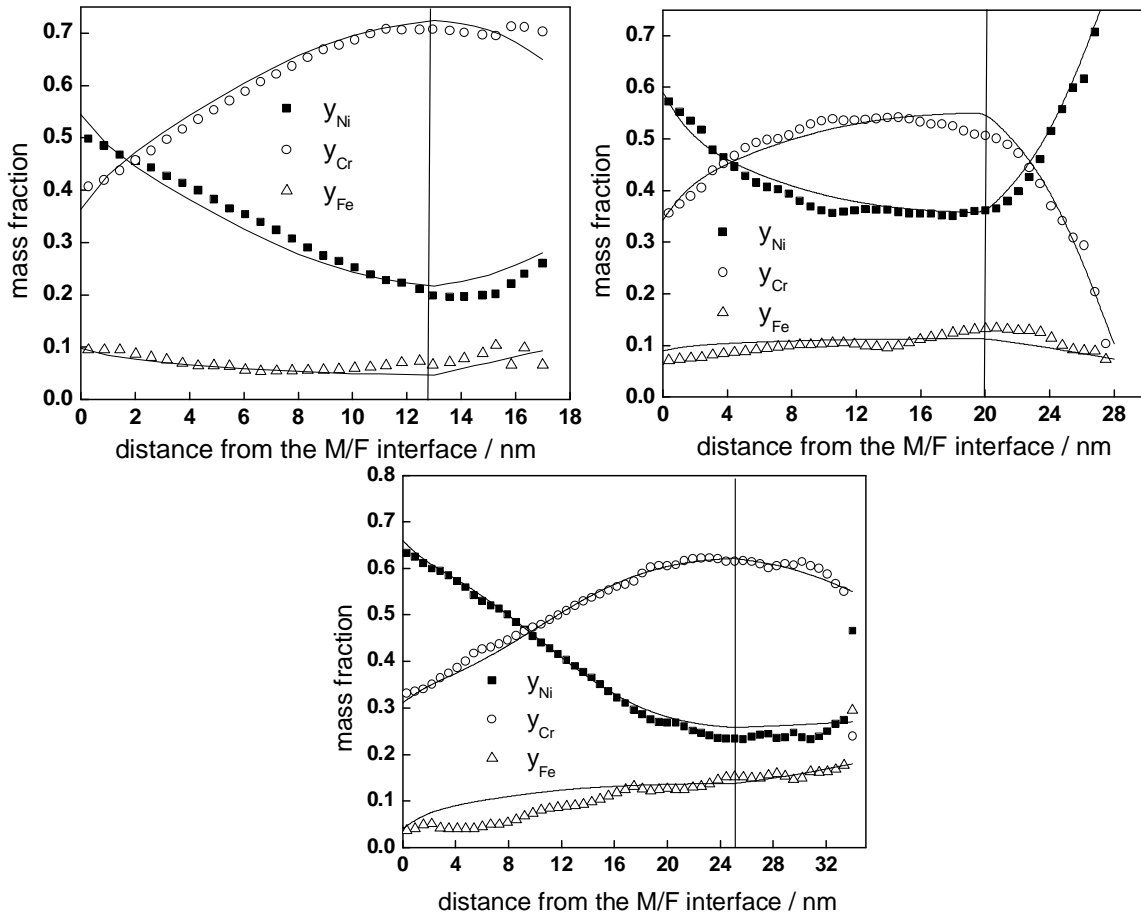
Figure 43 Experimental (points) and calculated (solid lines) depth profiles of the mass fractions of Fe, Cr, and Ni in the films formed on Alloy 690 in simulated PWR water at 325°C for 20 h (above, left), 50 h (above, right) and 100 h (below). The inner layer / outer layer boundary indicated with a vertical line.
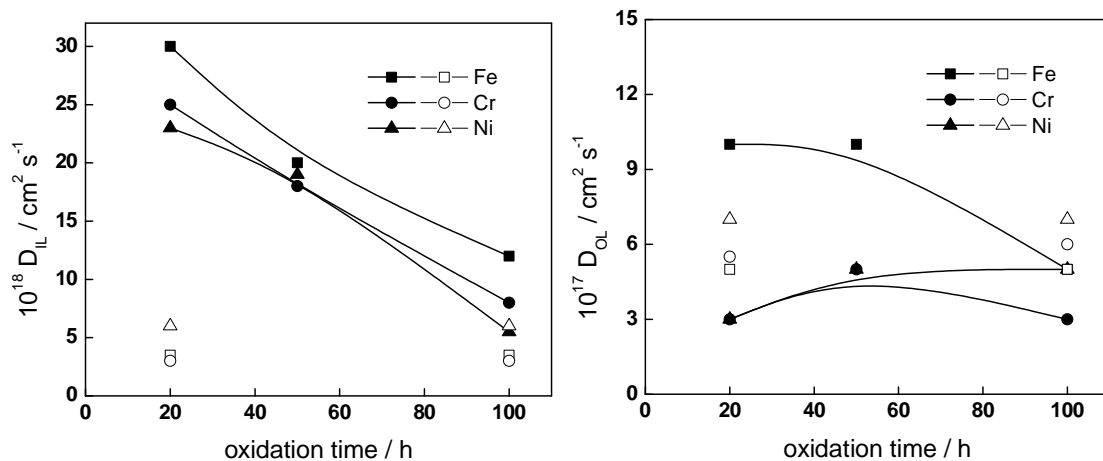
Figure 44 Dependence of the diffusion coefficients of inner layer constituents (left) and formal diffusion coefficients for the growth of the outer layer (right) on the time of exposure of Alloy 690 to simulated PWR water (full symbols). The values for the oxide on Alloy 600 are shown with open symbols for comparison.

In the simplest treatment (Figure 45), the effective diffusion coefficient can be expressed as a combination of the diffusion coefficients in the grain interior and at the grain boundary

$$D_{eff} = (1 - f_{gb})D_{gi} + f_{gb}D_{gb} \qquad (43)$$

where at first approximation, the following equation holds for the fraction of grain boundaries

$$f_{gb} \approx \frac{3\delta_{gb}}{\Phi} \qquad (44)$$

where δ_{gb} is the grain boundary width (of the order of 1 nm) and Φ is the grain size of the oxide in question. An additional explanation for enhanced conduction at boundaries is related to the formation of space charge regions in the grain areas adjacent to the boundaries. As charged species and defects tend to segregate to the grain boundaries to lower the strain and electrostatic energy of the system, the boundary charges are compensated by the formation of space charge in the adjoining grain areas. If a bulk defect with a high mobility is accumulated in the space charge region, the overall conductivity of the solid should increase. The width of the space charge region can be linked to the space charge screening length

$$L_D = \sqrt{\frac{\varepsilon\varepsilon_0 kT}{e^2 N}} \qquad (45)$$

Using typical values for $\varepsilon=20$, $T=573$ K and a bulk concentration of the high mobility carrier $N = 5 \times 10^{19}$ cm^{-3}, we arrive at $L_D = 5$ nm, which can be substituted for δ_{gb} in equation(44).
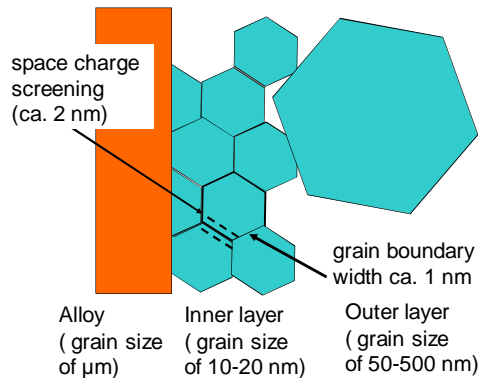

Figure 45 Approximation to take into account the layer microstructure.

If an increase of grain size of the oxide on Alloy 600 from 10 to 30 nm is adopted for oxidation between 20 and 5000 h [37,40], a corresponding decrease of the fraction of grain boundaries from 0.3 (at 20 h) to 0.1 (at 5000 h) is obtained from equations (44)-(45). Using the calculated value of the diffusion coefficient e.g. for Ni after 20 and 5000 h of oxidation (Figure 42), the grain interior diffusion coefficient is estimated to be of the order of 10^{-20} cm^2 s^{-1} in good agreement with an extrapolation of the diffusion coefficient of Ni for dry oxidation in the intermediate temperature range [101]. Although this can be considered as a proof for the validity of the present approach to the heterogeneity of the inner layer of oxide as a transport medium, the availability of grain size data for the inner

corrosion layers in high-temperature water is not sufficient to generalize this treatment for other structural materials.

A summary plot of the estimated values of the field strength in the inner layer of the oxide on Alloys 600 and 690 is given in Figure 46. If it is assumed that the space charge regions near grain boundaries determine the conduction through the oxide via a diffusion-migration mechanism, the decrease of the field strength in the inner layer with time of exposure can be tentatively attributed to the increase of the space charge screening length with time of exposure, which is tantamount of a decrease of the density of current carriers in the space charge regions.

The inner layer thicknesses for the oxides formed on Alloys 600, 690 and 800 in both simulated and in-reactor PWR water in the absence or presence of Zn in the water are compiled in Figure 47 as depending on exposure time. In the figure, the experimentally determined thickness values are compared with the thickness calculated according to equation(31). Once again a reasonable agreement is obtained without any further adjustment of parameters, which demonstrates the ability of the model to predict the kinetics of growth of the oxide on nickel-based alloys as well.
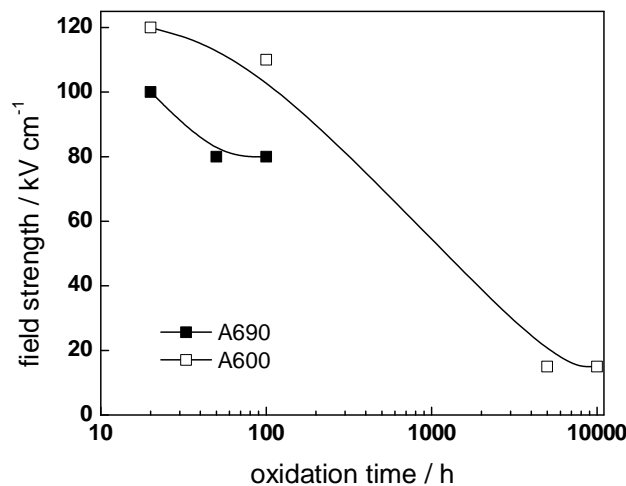

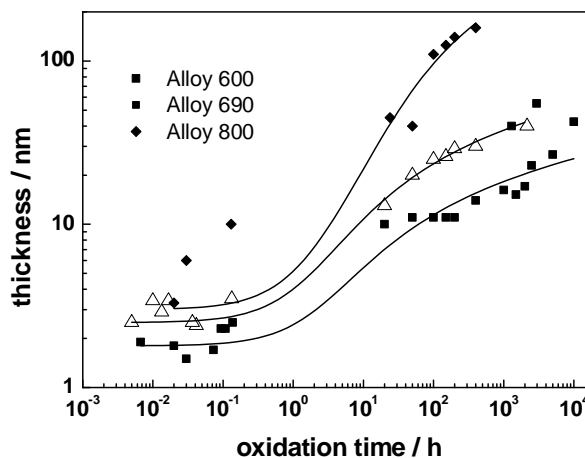*Figure 46 Summary of the calculated field strength values in the inner layer on Alloys 600 and 690.*

Figure 47 Inner layer thickness vs. time data for nickel-based alloys in simulated and in-reactor PWR water with or without Zn addition at 260-325°C (symbols) and calculated curves according to the model (solid lines).

8.3.2.2 Activity incorporation in the primary circuit

Very recently, calculations on the basis of the ANTIOXI model have been performed for 7 consecutive campaigns of Loviisa 1, 15th campaign of Kozloduy 5 and 14th campaign of Kozloduy 6 [102]. The obtained results are collected in Figure 48-Figure 49 as ratios between the mean surface activity of Co-58, Co6-0, Mn-54 and Sb-124 nuclides to the mean activity in the coolant for the respective campaign and nuclide.
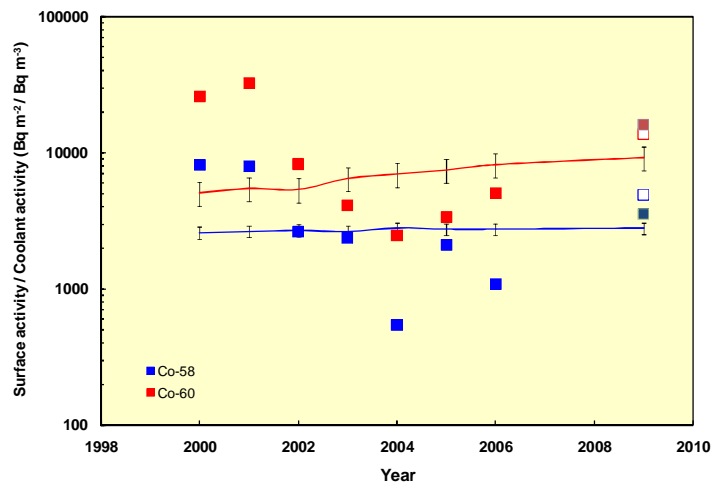
Figure 48 Ratio of the mean surface activity of Co-58, Co-60 to the mean activity in the coolant. 2000- 2006 data – Loviisa 1, 2009 data – Kozloduy 5 (open symbols) and Kozloduy 6 (closed symbols). ANTIOXI calculations are presented with solid lines.
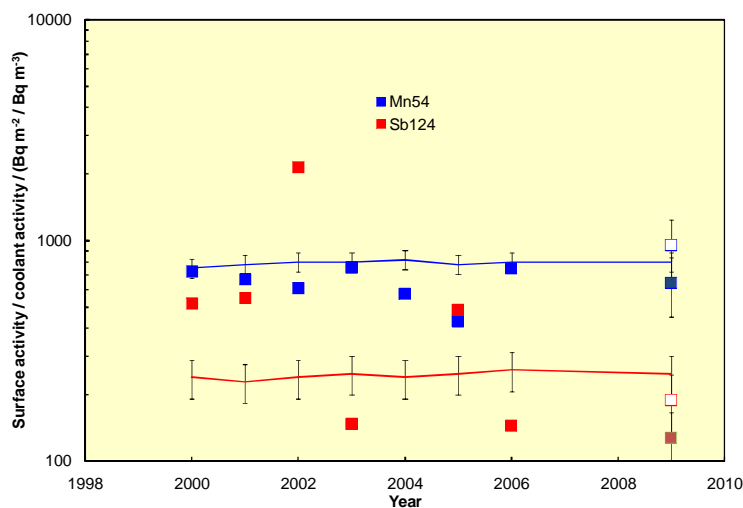
Figure 49 Ratio between the mean surface activity of Mn-54 and Sb-124 to the mean activity in the coolant. 2000- 2006 data – Loviisa 1, 2009 data – Kozloduy 5 (open symbols) and Kozloduy 6 (closed symbols ANTIOXI calculations are presented with solid lines.

On the basis of the calculated profiles of main and secondary constituents, as well as the enrichment factors at the inner layer/coolant boundary between outer layer crystallites and at the outer layer crystallite / coolant interface, the profiles of main long-life nuclides such as Co58, Co60 and Mn54 are successfully predicted. Via integration of the calculated profiles of the main long-life nuclides for several consecutive campaigns, predictions are made for the ratio of the surface activity to activity in the coolant for the next campaigns of Kozloduy reactors. More surface

activity data are needed in order to recalibrate the calculational procedure and obtain better accuracy in the case of Sb124 nuclide.

As a general conclusion, it can be stated that the ANTIOXI model represents a next step in the deterministic modeling of both oxide growth, restructuring on and corrosion release from PWR steam generator materials in normal operation conditions. It has been also demonstrated that the model can predict activity incorporation in primary circuit piping. However, further work is evidently necessary for the model to be able to handle transient situations such as those during shutdown and start-up of a PWR primary circuit. In order to simulate transients of temperature and coolant pH such as those during shutdown (see section 4.3), the temperature and pH dependence of the kinetic constants and diffusion coefficients associated with individual layer constituents have to be evaluated. Due to the lack of experimental data for a quantitative comparison with the model equations, such data are at the moment partly available only for AISI 316 steel in borate buffer solutions in the temperature range 150-300 °C [94] and in the range of high-temperature pHs between 7.1 and 8.0 [103]. Experimental data stemming from in-situ experiments during simulated shutdown and start-up [104] combined with corresponding characterization of oxides on typical steam generator materials (Alloys 600, 690 and 800) are needed in order to produce reliable values of kinetic and transport parameters in a wider range of transient conditions.

8.3.3   CRUD deposition

Three mechanisms may be involved in the deposition phenomena: deposition and release, precipitation-dissolution, and structural reorganization of the deposit. Deposition and release depend on flow characteristics, medium chemistry, and particles/wall properties. Deposition involves two steps: transport and attachment, the latter taking into account surface charges and interactions between the particle and the substrate. Precipitation- dissolution essentially depends on the solubility of the species. Regardless of whether deposit formation is a chemical or physical process (or both) it occurs in several stages including (1) adsorption, (2) incubation, (3) initiation, (4) growth, (5) growth limiting stage and (6) spalling and re-deposition (Figure 50) [103,106]. Later work introduced an additional step in the deposition process - ageing or consolidation, during which particles become chemically bonded to either the heat-transfer surface or to the pre-existing deposit. Consolidated CRUD is more strongly bound to the surface and is therefore not removed by the fluid at an appreciable rate. It has been demonstrated that the consolidation process involves the precipitation or recrystallization of solid material within the pores of the deposit [107].

In spite of the existence of several working approaches for activity accumulation that are able to capture the essential features of the conditions leading to AOA, several key factors of CRUD deposition could be further analyzed if a deterministic model of the process is developed and quantitatively compared to data from carefully designed experiments. Such a model could benefit from several features that have been already treated during the elaboration of the ANTIOXI model.

One such feature is adsorption and surface complexation, since the first step of deposition of CRUD on fuel cladding as a heterogeneous chemical reaction is an adsorption step. Adsorption of cations such as Li^+ and K^+ on monoclinic zirconia, as well as adsorption of boric acid on zirconia and nickel ferrite using high-

temperature titration experiments have been recently reported and analyzed [102-110]. Further, adsorption of ions and molecules on oxides is closely related to their surface charge which is in turn influenced by temperature, pH and adsorption processes [77,111]. Systematic point of zero charge and iso-electric point measurements at hydrothermal temperatures are, however, reported for a few relevant materials only, namely, zirconia and magnetite, a limited amount of data being available for trevorite [77,111].
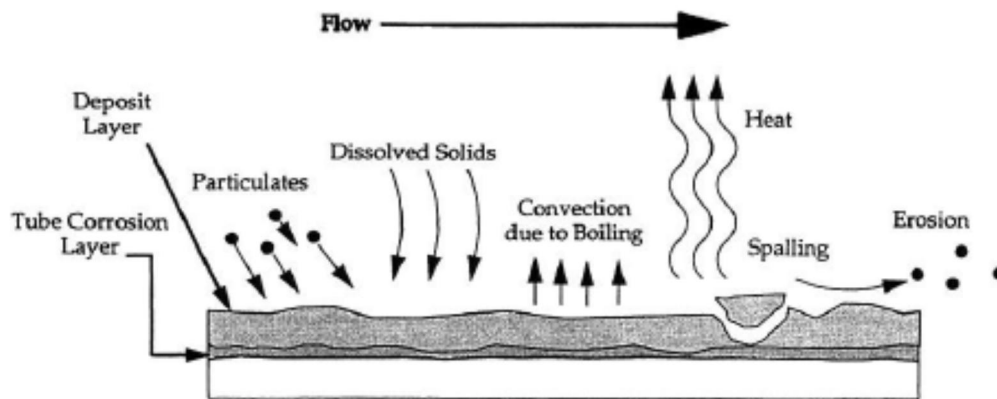

Figure 50 Schematic of the deposition and release mechanisms.

Another important point that would certainly merit further attention is the nature of precursor particles available for deposition on fuel cladding surfaces. The corrosion products in high-temperature aqueous environments, mainly metal oxides, are found not only in ionic, but also in colloidal form. The colloidal characteristics of suspended particles may have a decisive role in the mechanism of deposit formation. Thus, the initial step in the deposition process would in part depend on the electrostatic interaction between the fuel cladding wall surface and the suspended colloidal particles. A colloidal particle in an electrolyte solution bears surface charge due to adsorption of ions on its surface and/or due to the ionization of dissociable surface groups [112]. The water chemistry, especially the pH, has a strong effect on the surface charge of colloidal particles. At the pH of zero charge, i.e. at the pH at which the colloidal magnetite particles have no net surface charge the tendency for flocculation and following deposition by gravitational forces is high. The influence of adsorbed lithium and borate ions on the pH_{pzc} of magnetite and nickel ferrite has been recently estimated by potentiometric titrations even in high-temperature electrolytes with a suitable experimental setup [113]. The most common parameter used to describe the magnitude and sign of surface charge is the zeta-potential which indicates the degree of repulsion between adjacent, similarly charged particles in solution. Very recently, electrophoretic mobility measurements in a high-temperature setup have been used to estimate the zeta potential of magnetite particles [114].

Quantification and verification of high temperature experimental techniques for the measurement of deposition rate as a function of water chemistry, temperature and hydrodynamics is another key-element in the elaboration of a CRUD deposition model. For example, turbidimetry has been used to follow the evolution of particle concentration of a suspension in dynamic contact with the walls of a vessel. This method allows for qualitative results about the adhesion of metallic oxides particles on massive substrates to be obtained, and has been used already for iron oxides such as hematite [115]. A combination of X-ray fluorescence and Mössbauer

spectroscopic measurements [116,117] has also proven successful in determining both the speciation of iron oxides and oxy-hydroxides and the concentration of soluble (both ionic and suspended) iron in the secondary circuit. Another promising in-situ technique for the measurement of the first stages of deposition could be the diffuse reflection spectroscopy [118]. It has been recently used to to measure the coverage of samples by magnetite and hematite particles during formation of the first monolayer. The obtained spectra could be simulated from the fraction of surface covered by the particles, their sizes, and the absorption coefficients of the oxides. In addition, electrochemical techniques offer a dual possibility – to produce oxide nanoparticles with a well-defined size and distribution in order to study their electrical and colloidal properties, and also to characterise electrochemically (e.g. by voltammetry and electrochemical impedance spectroscopy [119]) arrays of such nanoparticles immobilized e.g. on inert supports such as carbon paste electrodes. Such measurements would allow a more detailed insight in the relationship between the kinetics of CRUD deposition, the composition, structure, electrical and electrochemical (particularly sorption) properties of the obtained deposit. In addition, such techniques are easier to implement in high-temperature water in comparison to measurements of electrical properties of colloidal dispersions prior to deposition, and at the same time can be regarded as complementary to such measurements.

9   Summary

Start-up and shutdown of nuclear power stations are the most crucial operations in which it is important to apply specific chemistry conditions. The associated transients may have an impact on the radiological condition related to maintenance for the following outage, the integrity of materials, the shutdown process duration, the radiochemistry during operation of the next cycle, the chemistry for layup condition during the next outage, etc. CRUD deposition on, and re-dissolution from the fuel cladding surface is an important problem in the primary circuit of light water reactors since it has a large impact on the activity build-up. Effects of fuel cladding material, water chemistry, hydrodynamic conditions and thermal gradients have to be taken into account in order to achieve CRUD control. In the present survey, a detailed description of the shutdown and start-up water chemistry transients and the associated interaction processes between coolant and oxide layers on construction materials is given. Particular attention is paid to the transformation of the corrosion layers and the rate of release of ions to the coolant. In addition, the relationships between CRUD composition, structure and morphology and the axial power anomalies (AOA/CIPS) are described. The main factors influencing AOA – sub-cooled boiling, CRUD formation and boron hideout – are outlined. A comprehensive review of the existing activity accumulation/transport and CRUD deposition/AOA models and associated codes is given, emphasizing the main assumptions, restrictions and predictive abilities. A deterministic model for the growth, restructuring of oxide layers and corrosion release (ANTIOXI) developed by the authors in recent years is presented as a further development of the modeling strategy concerning activity transport. Its application on steam generator construction materials (alloys 600, 690 and 800),as well as its predictive abilities with respect to activity build-up in the primary circuit are briefly outlined. Further steps towards an unified activity transport-CRUD deposition model are proposed.

References

1. Pressurized Water Reactor Primary Water Chemistry Guidelines: Volume 2, Revision 6. EPRI, Palo Alto, CA: 2007. 1014986.
2. Benchmarking Shutdown Chemistry Control Recommendations in the Pressurized Water Reactor Primary Water Chemistry Guidelines. EPRI, Palo Alto, CA: 2006. 1011780.
3. Pressurized Water Reactor Secondary Water Chemistry Guidelines – Revision 6. EPRI, Palo Alto, CA: 2004. 1008224.
4. Oxidation and Reduction of PWR Steam Generator Secondary Side Deposits: Experimental Data and Predictive Models, EPRI, Palo Alto, CA: 2002. 1003591.
5. Cycle Chemistry Guidelines for Shutdown, Layup and Startup of Combined Cycle Units with Heat Recovery Steam Generators, EPRI, Palo Alto, CA: 2006. 1010437.
6. Nordmann F., Odar S., Venz H., Kysela J., Ruehle W., Riess R. 2010. ANT international chemistry update and best practices. Proc. NPC2010, Quebec City, Canada, paper 9.02.
7. Fruzzetti, K.P., Frattini, P.L. Blok, J. 2004. A Review of the EPRI PWR Water Chemistry Guidelines. Proc. Int.Conf. Water Chem. Nucl. Power Plants, San Francisco, CA, USA, p.447.
8. Kim,K., Fruzzetti, K., Garcia, S., Eaker, R., Giannelli, J., Tangen, J., Gorman, J., Marks, C., Sawochka, S. 2010. Assessment of EPRI water chemistry guidelines for new nuclear power plants. Proc. NPC2010, Quebec City, Canada, paper 11.07P.
9. Mailand, I., Venz, H., 2007. Optimized Shutdown Chemistry instead of Decontamination to Reduce the Dose Rate during Outages, Power Plant Chem. 9, 42-50.
10. Mailand, I., Venz, H. 2008. Shutdown Chemistry – an approved method to reduce dose rate, Proc. Int. Conf. Water Chem. Nuclear Reactors Syst., Berlin, Germany, paper L06-1.
11. Mailand, I., Franz, P. 2010. Dose rate and contribution of the nuclides on the primary components during shutdown chemistry in Beznau NPP. Proc. NPC2010, Quebec City, Canada, paper 1.04.
12. Taunier, S., Varry, P., Tigeras, A., Bachet, M., Guinard, L., Bretelle, J.L., Rocher, A. 2008. New Primary Shutdown and Startup Chemistry guidelines recently developed for EDF PWRs, Proc. Int. Conf. Water Chem. Nuclear Reactors Syst., Berlin, Germany, paper L06-4.
13. Neder, H., Jürgensen, M., Wolter, D., Staudt, U., Odar, S., Schneider, V. 2006. VGB Primary and Secondary Side Water Chemistry Guidelines for PWR Plants. Proc. Int. Conf. Water Chem. Nuclear Reactors, Jeju, Korea, paper 1.3.
14. Fujiwara, K., Domae, M. 2004. Thermodynamic Evaluation of Nickel Solubility Depending on Redox Environment during Shutdown in PWR Primary Systems. Proc. 14th Int.Conf. Properties of Water and Steam, Kyoto, Japan, paper 581.
15. Ziemniak, S.E., Guilmette, P.A., Turcotte , R.A., Tunison, H.M. 2008. Oxidative dissolution of nickel metal in hydrogenated hydrothermal solutions. Corros. Sci. 50, 449-462.
16. Plancque, G., You, D., Mertens,V., Blanchard, E. 2008. Experimental study and modeling of the corrosion product dissolution. Applications to PWR conditions (nominal operating and cold shutdowns conditions). Proc. Int. Conf. Water Chem. Nuclear Reactors Syst., Berlin, Germany, paper P1-09.

17. PWR Shutdown Chemistry Practices, 1998 through 2001, EPRI, Palo Alto, CA: 2002. 1007307.

18. Ishida, K., Wada, Y., Tachibana, M., Aizawa, M., Fuse, M.. Kadoi, E. 2006. Hydrazine and Hydrogen Co-injection to Mitigate Stress Corrosion Cracking of Structural Materials in Boiling Water Reactors, (I) Temperature Dependence of Hydrazine Reactions. J. Nucl.Sci. Technol. 43, 65-76.

19. PWR Axial Offset Anomaly (AOA) Guidelines, Revision 1, EPRI, Palo Alto, CA: 2004. 1008102.

20. Lister, D. 2004. Some Aspects of Corrosion in Cooling Water Systems and Their Effects on Corrosion Product Transport, Keynote Lecture, Eurocorr 2003, The European Corrosion Congress, Budapest, Hungary, September 28 – October 2, 2003, paper No.

21. Source Term Reduction: Impact of Plant Design and Chemistry on PWR Shutdown Releases and Dose Rates. EPRI, Palo Alto, CA: 2006. 1013507.

22. Combrade, P.; Foucault, M.; Vancon, D.; Marcus, P.; Grimal, J.-M.; Gelpi, A. 1989. In Proc. 4th Int.l Symp. on Environmental Degradation of Materials in Nuclear Power Systems - Water Reactors, NACE International, Houston, 5-79 - 5-94.

23. Szklarska-Smialowska, Z.; Lai, W.-K.; Xia, Z. 1990. Corrosion 46, 853-860.

24. Angeliu, T.M.; Was, G.S. 1993. J. Electrochem.Soc. 140, 1877-1883.

25. Byers, W.A.; Jacko, R.J. 1993. In Proceedings of the 6th Int. Symp. on Environmental Degradation of Materials in Nuclear Power Systems - Water Reactors, The Minerals, Metals and Materials Society, 837-844.

26. Noel, D.; Guinard, L.; Kerrec, O.; Le Bec, P.; Schwoehrer, P. 1994. In Proc. Int. Symp. Activity Transport in Water Cooled Nuclear Power Reactors, Ottawa, Canada, AECL, 1-12.

27. Guinard, L.; Kerrec, O.; Gardey, S.; Noel, D. 1998. In Proceedings of the JAIF International Conference on Water Chemistry of Nuclear Reactor Systems, Kashiwazaki, Japan, 483-489.

28. Soustelle, C.; Foucault, M.; Combrade, P.; Wolski, K.; Magnin, T. 1999. In Proceedings of the Ninth International Symposium on Environmental Degradation of Materials in Nuclear Power Systems - Water Reactors, F.P. Ford, S.M. Bruemmer and G.S.Was, Eds., The Minerals, Metals and Materials Society, 105-113.

29. Guinard, L.; Carette, F.; Pieraggi, B.; Kerrec, O. 2000. In Water Chemistry of Nuclear Reactor Systems 8, Bournemouth, United Kingdom, 250-252.

30. Machet, A.; Galtayries, A.; Marcus, P.; Combrade, P.; Jolivet, P.; Scott, P. 2002. Surf. Interf. Anal.34, 197-200.

31. Carette, F.; Lafont, M.C.; Chatainier, G.; Guinard, L.; Pieraggi, B. 2002. Surf. Interf. Anal.34, 135-138.

32. Carette, F.; Guinard, L.; Pieraggi, B. 2002. In Proc. International Conference Water Chemistry in Nuclear Reactor Systems, Avignon, France, SFEN, French Nuclear Energy Society (CD-ROM publication).

33. Panter, J.; Foucault, M.; Cloue, J.-M.; Combrade, P.; Viguier, B.; Andrieu, E. 2002. In CORROSION'2002, NACE International, Houston, paper No. 02519.

34. Kim, J.H.; Hwang, I.S. 2003. In Proceedings of the 11th International Symposium on Environmental Degradation of Materials in Nuclear Power Systems - Water Reactors,Stevenson, WA, 51-62.

35. Caron, D.; Daret, J.; Lefevre, Y.; Santarini, G.; Mazille, H.; Benoit, R.; Erre, R.; Cassagne, T. 2000. In EUROCORR 2000, Institute of Materials, London.

36. Alvarez, M.G.; Olmedo, A.M.; Villegas, M. 1996.J. Nucl. Mater. 229, 93-101.

37. Machet, A. 2004. Étude des premiers stades d'oxydation d'alliages inoxydables dans l'eau à haute température. PhD Thesis, Paris, p.189.

38. Ziemniak, S.E., Castelli, R.A.2003. Immiscibility in the Fe_3O_4-$FeCr_2O_4$ spinel binary. J. Phys. Chem. Solids 64, 2081–2091.

39. Ziemniak, S.E., Gaddipati, A.R., Sander, P.C. 2005. Immiscibility in the $NiFe_2O_4$-$NiCr_2O_4$ spinel binary. J. Phys. Chem. Solids 66, 1112–1121.

40. Ziemniak, S.E., Hanson, M. 2006. Corrosion behavior of NiCrFe alloy 600 in high temperature, hydrogenated water. Corros. Sci. 48, 498–521.

41. Ziemniak, S.E., Hanson, M. 2006. Zinc treatment effects on corrosion behavior of alloy 600 in high temperature hydrogenated water. Corros. Sci. 48, 3330–3348.

42. Marchetti, L., Perrin, S., Raquet, O., Pijolat, M. 2008. Corrosion mechanisms of Ni-base alloys in pressurized water reactor primary conditions Mater. Sci. Forum 595-598, 529-537.

43. Sennour, M., Marchetti, L., Frantz, M., Perrin, S.,Molins, R. Pijolat, M. 2010. A detailed TEM and SEM study of Ni-base alloys oxide scales formed in primary conditions of pressurized water reactor. J. Nucl. Mater. 402, 147-156.

44. Huang, J., Wu, X., Han, E.-H. 2010. Electrochemical properties and growth mechanism of passive films on Alloy 690 in high-temperature alkaline environments. Corros. Sci. 52, 3444-3452.

45. Huang, J., Liu, X., Han, E.-H., Wu, X. 2011. Influence of Zn on oxide films on Alloy 690 in borated and lithiated high temperature water. Corros. Sci. 53, 3254-3261.

46. Effect of Boron Concentration on Alloy-690 Corrosion Product Release Rates - Results at 325°C and 285°C, EPRI, Palo Alto, CA : 2001. 1011744.

47. EPRI Pressurized Water Reactor Zinc Application Guidelines, EPRI, Palo Alto, CA; 2006, 1013420.

48. Fuel Reliability Guidelines: PWR Fuel Cladding Corrosion and Crud. EPRI 1015499, Palo Alto, CA 2008.

49. Solubility of Zinc Silicate and Zinc Ferrite in Aqueous Solution at Light Water Reactor Temperatures. EPRI 1015035, Palo Alto, CA: 2007.

50. Palmer, D.A., Anovitz, L. M., Wilson, L. L. 2008. Solubility of Zinc Silicate and Zinc Ferrite in Aqueous Solution to High Temperatures, Proc. 15th International Conference on the Properties of Water and Steam, Berlin, Germany, paper 5-04.

51. Byers, W. A., Deshon, J., Gary, G. P., Small, J. F., Mcinvale, J. B.2006. Crud Metamorphosis at the Callaway Plant. Proc. Int. Conf. Water Chem. Nuclear Reactors, Jeju, Korea, paper 7.3.

52. Sawicki, J.A. 2008. Evidence of Ni_2FeBO_5 and m-ZrO_2 precipitates in fuel rod deposits in AOA-affected high boiling duty PWR core. J. Nucl. Mater. 374, 248-269.

53. Sawicki, J.A. 2010. Analyses of CRUD deposits on fuel rods in PWRs using Mössbauer spectroscopy. J. Nucl. Mater. 402, 124-129.

54. Sawicki, J.A. 2011. Hydrothermal synthesis of Ni_2FeBO_5 in near-supercritical PWR coolant and possible effects of neutron-induced 10B fission in fuel CRUD. J. Nucl. Mater. 415, 179-188.

55. Deshon, J., Hussey, D., Kendrick, B., McGurk, J., Secker, J., Short, M. 2011. Pressurized Water Reactor Fuel Crud and Corrosion Modeling. JOM, 63, 65-72.

56. Macdonald, D.D., Urquidi-Macdonald, M., Mahaffy, J.H., Jain, A., Kim, S.H., Gupta, V., Pitt, J. 2006. Electrochemistry of Water-Cooled Nuclear Reactors. Final Technical Progress Report, Grant No. DE-FG07-021D14334.

57. Mirza, N.M., Rafique, M., Hyder, M.J., Mirza, S.M. 2003. Computer simulation of corrosion product activity in primary coolants of a typical PWR under flow

rate transients and linearly accelerating corrosion, Annals of Nuclear Energy 30, 831-851

58. Deeba, F., Mirza, A.M., Mirza, N.M., 1999. Modeling and simulation of corrosion product activity in pressurized water reactors under power perturbations, Annals of Nuclear Energy 26, 561-578.

59. Mirza, A.M., Mirza, N.M., Mir, I. 1998. Simulation of corrosion product activity in pressurized water reactors under flow rate transients, Annals of Nuclear Energy 25, 331-345.

60. Mirza, N.M., Rafique, M., Mirza, S.M., Hyder, M.J. 2005. Simulation of corrosion product activity for nonlinearly rising corrosion on inner surfaces of primary coolant pipes of a typical PWR under flow rate transients. Appl. Radiation Isotopes, 62, 681-692.

61. Mirza, S.M., Rafique, M., Ahmad, F., Mirza, N.M. 2010. Static and dynamic sensitivity analysis of corrosion product activity in primary coolant circuits of pressurized water reactors. Progr. Nuclear Energy 52, 648-654.

62. Kasahara, K., Nishimura, T. 1993. Advanced Evaluation Code for CRUD behavior in PWR. Proc. Annual Meeting of the Atomic Energy Society of Japan, Kobe, Japan, p. 578.

63. Burrill, K., Menut, P. 2001. A description of activity transport codes in the IAEA benchmarking exercise. Proc. Water Chemistry of Nuclear Reactor Systems 8, BNES, 519-525.

64. Dinov, K. et al., 2000. Modeling of VVER Light Water Reactors Activity Buildup, Proc. 8th International Conference on Nuclear Engineering, Baltimore, U.S., Paper ICONE-8229.

65. Dinov, K. 1991. A Model of Crud Particle/Wall Interaction and Deposition in a Pressurized Water Reactor Primary system. Nuclear Technology, 94, 281-285.

66. Marchetto, C. , Tarabelli, D., You, D., Andrieu, C., Long, A., Zeitoun, D. 2000. PACTOLE V3: a new code version to predict corrosion product contamination. Proc. Water Chemistry of Nuclear Reactor Systems 8, Bournemouth, UK, BNES, p. 224-229.

67. Di Pace, L., Dacquait, F., Nguyen, F., Larat, B. 2005. Development of PACTITER code and its application to safety analyses of ITER Primary Cooling Water System. In Proc. EUROCORR 2005, Lisbon, Portugal.

68. Carrette, F., Guinard, L., Pieraggi, B. 2002. Kinetics of Corrosion Products Release from Nickel-Base Alloys corroding in Primary Water Conditions: a New Modelling of Release, Proc. Of the International Conference on Water Chemistry in Nuclear Reactors Systems, Avignon,France, paper 146.

69. Nguyen, F., Marteau, H., Dacquait, F., Perot, N., Ranchoux, G., Guinard, L., Long, A.2004. First numerical simulations of contamination of the PWR primary circuit by activated corrosion products with the PACTOLE V3.0 code. Proceedings of the International conference on Water chemistry in nuclear reactors systems, San Francisco USA, 1922-1932.

70. Urquidi-Macdonald, M., Jacesko, S. L., Macdonald, D.D., Salter-Williams, M. 2002. Importance of ECP in the Prediction of Radiation Fields in PWR and VVER Primary Circuits. Power Plant Chem. 4(7).

71. Macdonald, D.D., Urquidi-Macdonald, M. 2007. The Electrochemistry of Nuclear Reactor Coolant Circuits. Ch.9 in Encyclopedia of Electrochemistry, Vol. 5, Electrochemical Engineering, Macdonald, D.D., Schmuki, P., Eds.Wiley-VCH, Weinheim, 663-725.

72. Castelli, R. 2009. Nuclear Corrosion Modeling – the nature of CRUD. Elsevier. 195 p.

73. Ziemniak, S.E., Hanson, M. 2002. Corrosion behavior of 304 stainless steel in high temperature, hydrogenated water, Corros. Sci. 44, 2209–2230.

74. Ziemniak, S.E., Hanson, M. 2006. Zinc treatment effects on corrosion behavior of 304 stainless steel in high temperature hydrogenated water, Corros. Sci. 48, 2525–2546.

75. Ziemniak, S.E., Hanson, M., Sander, P.C. 2008. Electropolishing effects on corrosion behavior of 304 stainless steel in high temperature, hydrogenated water. Corros. Sci. 50, 2465-2477.

76. Kushneriuk, S.A., Blair, J.M. 1976.Deposition of radioactive materials by a flowing fluid in a pipe Nucl. Sci. Eng. 60, 87–105.

77. Wesolowski, D.J., Ziemniak, S.E., Anovitz, M., Machesky, M.L., Benezeth, P., Palmerm D.A. 2004. Solubility and surface adsorption characteristics of metal oxides. Ch.14 in Aqueous Systems at Elevated Temperatures and Pressures, Palmer, D.A., Fernandez-Prini, R., Harvey, A.H., Eds. Elsevier, 493–595.

78. Modeling PWR Fuel Corrosion Product Deposition and Growth Processes: Final Report. EPRI, Palo Alto, CA: 2005. 1011743.

79. Henshaw, J., McGurk, J.C., Sims, H. E., Tuson, A., Dickinson, S., Deshon, J. 2006. A model of chemistry and thermal hydraulics in PWR fuel CRUD deposits. J. Nucl. Mater. 353, 1-11.

80. Cohen, P., 1974. Heat and mass transfer for boiling in porous deposits with chimneys. AICHE Symposium Series 70, 71–80.

81. Haq, I., Cinosi, N., Bluck, M., Hewitt, G., Walker, S.2011. Modelling heat transfer and dissolved species concentrations within PWR CRUD. Nucl. Eng. Des. 241, 155-162.

82. Cinosi, N., Haq, I., Bluck, M., Walker, S.P. 2011. The effective thermal conductivity of CRUD and heat transfer from CRUD-coated PWR fuel. Nucl. Eng Des. 241, 792-798.

83. Boron-Induced Offset Anomaly (BOA) Risk Assessment Tool, Version 1.0 (Palo Alto, CA: EPRI, 2003) 1003211.

84. Bosma, J.R., Deshon, J., Epperson, K.R., Kennamore, P., Secker, J.R., Young, M.Y. 2004. A Comprehensive Method for Assessing Fuel Performance Risks Due to Crud Deposition, Proc. 2004 International Meeting on LWR Fuel Performance, Orlando, Florida (CD-ROM).

85. Robertson, J. 1991. The mechanism of high-temperature aqueous corrosion of stainless steels. Corros. Sci. 32, 443-465.

86. Abdel-Khalik, S.I., 2005. Experimental Investigation of the Root Cause Mechanism and Effectiveness of Mitigating Actions for Axial Offset Anomaly in Pressurized Water Reactors. Final Technical Report, DE-FG07-02ID14324.

87. Rashid, J. Y.R., Yagnik, S.K., Montgomery, R. O.2011. Light Water Reactor Fuel Performance Modeling and Multi-Dimensional Simulation. JOM,63, 81-88.

88. Fujimori, H., Asakura, Y., Suzuki, K., Uchida, S., 1988. In situ thickness measurement of nickel ion deposits on heated surface in water by thermal wave method. J. Nucl. Sci. Technol. 25, 158-164.

89. Uchida, S., Asakura, Y., Ohsumi, K., Miki, M., Aizawa, M., Matsushima, Y., Yonezawa, K., 1987. Chemical composition of CRUD depositing on BWR fuel surfaces. J. Nucl. Sci.Technol. 24, 385-392.

90. Nishino, Y., Asakura, Y., Sawa, T., Uchida, S., Ohsumi, K., Yoshikawa, S., Amano, O., 1989. Deposition of nickel and cobalt ions on heated stainless steel under nucleate boiling condition. J. Nucl. Sci. Technol. 26, 1112-1120.

91. Uchida, S., Asakura, Y., Suzuki, H. 2011. Deposition of boron on fuel rod surface under sub-cooled boiling conditions—an approach toward understanding AOA occurrence. Nucl. Eng.Des. 241, 2398-2410.

92. Holl, J.W., Kornhauser, A.L., 1970. Thermodynamic effects on desinent cavitation on hemispherical nosed bodies in water of temperatures from 80 degrees F to 260 degrees F. J. Basic Engineering, Trans. ASME Ser. D 92-1, 44-58.

93. Kawamura, H., Furuya, M., 2008. Effect of pH and Ni/Fe ration on CRUD deposition behavior on heated Zircaloy-4 surfaces in simulated PWR primary water. In Proc. International Conference on Water Chemistry of Nuclear Reactor Systems, Berlin, Germany, paper P2-04.

94. Betova, I., Bojinov, M., Kinnunen, P., Lundgren, K., Saario, T. 2008. A Mixed-Conduction Model for the Oxidation of Stainless Steel in a High-temperature Electrolyte. Estimation of kinetic parameters of individual inner layer constituents J. Electrochem. Soc. 155, C81-C92.

95. Betova, I.; Bojinov, M.; Kinnunen, P.; Saario, T. 2008. ANTIOXI - Development and testing of an integrated corrosion and activity build-up model. VTT Research Report VTT-R-10525-08. 47 p.

96. Betova, I., Bojinov, M., Kinnunen, P., Lundgren, K., Saario, T.2009. A kinetic model of the oxide growth and restructuring on structural materials in nuclear power plants. Chapter 3 in Structural Materials and Engineering, F. Nagy, Ed., Nova Publishers, 2009, 91-133.

97. Eek, W.2009. ANTIOXI - Development of oxide model for activity buildup in LWRs – Validation of model. VTT Research Report VTT-R-04208-09. 57 p.

98. Penttilä, S., Betova, I., Bojinov, M., Kinnunen, P., Toivonen, A. 2011. Estimation of kinetic parameters of the corrosion layer constituents on steels in supercritical water coolant conditions. Corros. Sci. 53, 4193-4203.

99. Machet, A., Galtayries, A., Zanna, S., Klein, L., Maurice, V., Jolivet. P., Foucault, M., Combrade, P., Scott, P., Marcus, P. 2004. XPS and STM study of the growth and structure of passive films in high temperature water on a nickel-base alloy. Electrochim. Acta 49, 3957-3964.

100. Bojinov, M., Galtayries, A., Kinnunen, P., Machet, A., Marcus, P. 2007. Estimation of the parameters of oxide film growth on nickel-based alloys in high-temperature water electrolytes. Electrochim. Acta 52, 7475-7483.

101. Chevalier, S., Desserey, F., Larpin, J.P. 2005. Oxid. Met. 64, 219-234.

102. Betova, I., Bojinov, M., Minkova, K. 2010. Validation And Verification Of A Deterministic Model For Corrosion And Activity Incorporation Using Operational Data From Kozloduy NPP. Proc. NPC2010, Quebec City, Canada, paper 5.10P.

103. Betova, I., Bojinov, M., Kinnunen, P., Lundgren, K., Saario, T.2009. Influence of Zn on the oxide layer on AISI 316L(NG) stainless steel in simulated pressurised water reactor coolant. Electrochim. Acta 54, 1056-1069.

104. Bojinov, M., Buddas, T., Halin, M., Laitinen, T., Mäkelä, K., Mäkelä, M., Saario, T., Sirkiä, P., Tompuri, K. 2000. Stability of oxide films on stainless steel during simulated PWR shutdown and start-up conditions. in Proc. Int. Conf. Water Chemistry of Nuclear Reactor Systems 8, Bournemouth, UK, Vol.1, p.73-78.

105. Charlesworth, D. H. 1970. The Deposition of Corrosion Products in Boiling Water Systems. A1CHE Chem. Eng. Prog. Symp. Set. 66(104), 21-30.

106. Somerscales, E.F. C. 1997. Fundamentals of corrosion fouling. Exp.Therm. Fluid Science 14, 355-366.

107. Beverskog, B. 2006. AOA Fuel Crud: a Theoretical Approach. Proc. Int. Conf. Water Chem. Nuclear Reactors, Jeju, Korea, paper 7.2.

108. Adsorption of Ions on Zirconium Oxide Surfaces from Aqueous Solutions at High Temperatures, EPRI, Palo Alto, CA: 2003. 1007855.

109. Palmer, D.A., Machesky, M.L., Bénézeth, P., Wesolowski, D.J., Anovitz, L.M., Deshon, J.C. 2009. Adsorption of Ions on Zirconium Oxide Surfaces from Aqueous Solutions at High Temperatures, J. Solution Chem. 38, 907-924.

110. Adsorption of Boric Acid on Synthetic Fuel Crud Oxides, EPRI, Palo Alto, CA: 2002. 1003384.

111. Machesky, M.L., Wesolowski, D.J.,Palmer, D.A., Ridley, M.K., Bénézeth, P., Lvov, S.N., Fedkin, M.V. 2006. Ion adsorption in the hydrothermal regime: experimental and modeling approaches. Ch.12 in Surface Complexation Modeling, J. Lutzenkirchen, Ed., Elsevier, pp.324-358.

112. Barale, M., Mansour, C., Carrette, F., Pavageau, E.,M. Catalette, H., Lefèvre, G., Fédoroff, M., Cote, G.2008. Characterisation of the surface charge of oxide particles of PWR primary water circuits from 5 to 320 °C. J. Nucl. Mater. 381, 302-308.

113. Barale, M., Lefèvre, G., Carrette, F., E.,M. Catalette, H., Fédoroff, M., Cote, G. 2008. Effect of the adsorption of lithium and borate species on the zeta potential of particles of cobalt ferrite, nickel ferrite, and magnetite. J. Colloid. Interface Sci. 328, 34-40.

114. Vidojkovic, S., Rodriguez-Santiago, V., Fedkin, M.V., Wesolowski, D. J. Lvov, S.N. 2011. Electrophoretic mobility of magnetite particles in high temperature water. Chem.Eng.Sci. 66, 4029-4035.

115. Lefèvre, G., Hamza, A., Fédoroff, M., Carrette, F., Cordier, H. 2006. A turbidimetric method to measure isoelectric points and particles deposition onto massive substrates. Colloids Surfaces A:Physicochem.Eng.Aspects 280, 32-38.

116. Sawicki, J.A., Molander, A., Stutzmann, A. 2010. Precipitation and transformation of iron species in the presence of oxygen and hydrazine in a simulated stainless steel feed water system, Chapter 14 in Corrosion Monitoring in Nuclear Power Systems: Research and Applications, Ritter, S. Molander A., Ed., Maney Publishing, pp. 221–238.

117. Sawicki, J. A., Sawicka, B. D., Price, J.E. 2010. A method of examining iron oxides speciation and transport to steam generators during nuclear power reactor startups. J. Nucl. Mater. 407, 157-164.

118. Dégardin, O., Benfarah, M. , Lefèvre, G. 2009. Diffuse reflection spectroscopy as a tool to measure low surface coverage of metal substrates by metallic oxide particles. Colloids Surfaces A:Physicochem.Eng.Aspects 345, 219-223.

119. Rodríguez-López, A., Torres-Torres, D., Mojica-Gomez, J. Estrada-Arteaga, C., Antano-López, R. 2011. Characterization by electrochemical impedance spectroscopy of magnetite nanoparticles supported on carbon paste electrode. Electrochim.Acta, 56, 8078–8084.